



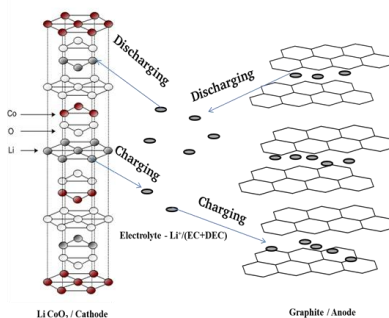
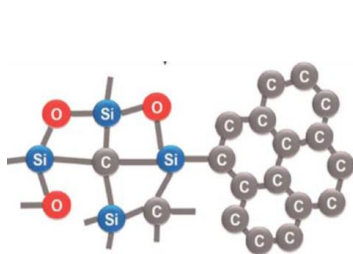
Doctoral School in Materials Science and Engineering

Study of Silicon Oxycarbide (SiOC) as Anode Materials for Li-ion Batteries

V.S. Pradeep

Advisor: Prof. Gian Domenico Soraru

Co-Advisor: Dr.-Ing. Magdalena Graczyk-Zajac



December 2013

Study of Silicon Oxycarbide (SiOC) as Anode Materials for Li-ion Batteries

Vallachira Warriam Sasikumar Pradeep
(V.S. Pradeep)

E-mail: pradeep.vallachira@ing.unitn.it

Approved by:

Prof. Gian Domenico Soraru,
Advisor
Department of Industrial
Engineering
University of Trento, Italy

Ph.D. Commission:

Prof. Vincenzo M. Sglavo,
Department of Industrial
Engineering
University of Trento, Italy.

Dott. Federico Smeacetto,
Department of Applied Science
and Technology
Politecnico di Torino, Italy.

Dott. Raul Bermejo,
Institut Für Struktur- und
Funktionskeramik
Montanuniversität Leoben, Austria.

University of Trento,
Department of Industrial Engineering

December 2013

University of Trento - Department of Industrial Engineering

Doctoral Thesis

**Vallachira Warriam Sasikumar Pradeep - 2013
Published in Trento (Italy) – by University of Trento**

ISBN:

To My Parents

Contents

| | |
|---|------------|
| Abstract | x |
| Thesis Overview | xii |
| Chapter 1. State of The Art - Lithium ion Batteries - Current Perspectives | 1 |
| 1.1 Electrochemical Power Sources..... | 1 |
| 1.2 Battery Characteristics..... | 3 |
| 1.3 Lithium ion Batteries..... | 6 |
| 1.3.1 Components of Lithium ion Batteries..... | 10 |
| 1.3.1.1 Cathodes..... | 10 |
| 1.3.1.2 Electrolytes..... | 12 |
| 1.3.1.3. Separators..... | 12 |
| 1.3.1.4. Anode Materials..... | 13 |
| 1.4 Carbon Based Anode Materials..... | 14 |
| 1.5 Polymer Derived Ceramics as Anodes in Lithium-ion Batteries..... | 20 |
| References..... | 21 |
| Chapter 2. Polymer Derived Silicon Oxycarbide Ceramics (SiOC) | 27 |
| 2.1 Polymer Derived Ceramics (PDCs) - General Overview..... | 27 |
| 2.2 Silicon Oxycarbide (SiOC) Glass Ceramics..... | 28 |
| 2.3 Synthesis of SiOC Ceramics..... | 31 |
| 2.3.1 Sol-gel Techniques..... | 31 |
| 2.3.2 Hydrosilylation..... | 33 |
| 2.3.3 Polymer to Ceramic Conversion..... | 34 |
| 2.4 Structure of SiOCs..... | 36 |
| 2.4.1 Nanodomain Model of SiOC..... | 39 |

| | |
|---|-----------|
| 2.5 Polymer Derived Silicon Oxycarbides as Anodes in Lithium ion Batteries | 43 |
| References | 51 |
| Chapter 3. Experimental Setup - Synthesis and Characterization of SiOC Glass Networks..... | 56 |
| 3.1 Synthesis of SiOC Ceramics | 56 |
| 3.1.1 Hydrosilylation | 56 |
| 3.1.2 Sol-gel..... | 59 |
| 3.1.3 Effect of Heat Treatment..... | 62 |
| 3.1.4 Effect of Pyrolysis Gas Atmosphere | 63 |
| 3.2 Structural Characterization | 63 |
| 3.2.1 Thermogravimetric (TG/DTA) Studies | 63 |
| 3.2.2 Elemental Analysis | 64 |
| 3.2.3 X-ray Diffraction Studies | 64 |
| 3.2.4 NMR..... | 65 |
| 3.2.5 Electron Paramagnetic Resonance (EPR)..... | 67 |
| 3.2.6 Raman Spectra..... | 69 |
| 3.3 Electrochemical Characterization | 70 |
| 3.3.1 Electrode Preparation | 70 |
| 3.3.2 Cell Assembly | 71 |
| 3.3.3 Galvanostatic Charging/Discharging..... | 72 |
| 3.3.4 Cyclic Voltammetry | 74 |
| References | 76 |
| Chapter 4. Searching Insights in to the Lithium Storage Mechanism in Polymer Derived SiOC Anode Materials..... | 79 |

| | |
|---|------------|
| 4.1 Understanding Lithium Storage Mechanism in Polymer Derived SiOC Anode Materials | 80 |
| 4.1.1 Introduction..... | 80 |
| 4.1.2 Experimental Part..... | 81 |
| 4.1.2.1 Materials Synthesis..... | 81 |
| 4.1.2.2 Preparation of Electrodes and Cells | 82 |
| 4.1.2.3 Characterization Techniques | 83 |
| 4.1.3 Results and Discussion | 85 |
| 4.1.3.1 Structural Characterization | 85 |
| 4.1.3.2 Electrochemical Characterization | 94 |
| 4.1.3.2.1 First insertion/extraction Behavior..... | 94 |
| 4.1.3.2.2 Rate Capability Studies..... | 102 |
| 4.1.4 Conclusions..... | 106 |
| 4.2 Influence of Pyrolysis Atmosphere on the Lithium Storage Properties of Carbon-Rich SiOC Anodes | 108 |
| 4.2.1 Introduction | 108 |
| 4.2.2 Experimental Part | 109 |
| 4.2.2.1 Sample Preparation | 109 |
| 4.2.2.2 Characterization..... | 110 |
| 4.2.3 Results and Discussion..... | 111 |
| 4.2.4 Conclusions..... | 121 |
| References | 122 |
| Chapter 5. Li Storage Properties of Dense and Porous SiOC ceramics | 128 |
| 5.1 Introduction..... | 129 |
| 5.2. Experimental | 131 |

| | |
|---|------------|
| 5.2.1. Materials Synthesis..... | 131 |
| 5.2.2. Preparation of Electrodes and Cells | 132 |
| 5.2.3. Characterization Techniques | 133 |
| 5.3. Results | 134 |
| 5.3.1. Structural Characterization | 134 |
| 5.3.1.1. Chemical Analysis | 134 |
| 5.3.1.2. Powder XRD and Raman Spectroscopy Analysis of the Studied Silicon Oxycarbide Materials..... | 135 |
| 5.3.1.3. N ₂ Adsorption Analysis | 137 |
| 5.3.1.4. Transmission Electron Microscopy (TEM) Characterization..... | 140 |
| 5.3.2. Electrochemical Investigation | 142 |
| 5.4. Discussion..... | 146 |
| 5.5. Conclusions..... | 151 |
| References..... | 153 |
| Chapter 6. Thesis Conclusions..... | 158 |
| Future Outlook | 160 |
| Acknowledgements..... | 162 |
| Curriculum Vitae | 164 |

Abstract

The principal object of this thesis is the investigation of silicon oxycarbide (SiOC) ceramics as anode material for Li-ion batteries. The investigated materials are prepared by cross linking commercial polymer siloxanes via hydrosilylation reactions or hybrid alkoxide precursors via sol-gel. The cross linked polymer networks are then converted in to ceramic materials by a pyrolysis process in controlled argon atmosphere at 800-1300 °C.

In details the influence of carbon content on lithium storage properties is addressed for SiOC with the same O/Si atomic ratio of about 1. Detailed structural characterization studies are performed using complementary techniques which aim correlating the electrochemical behavior with the microstructure of the SiOC anodes. Results suggest that SiOC anodes behave as a composite material consisting of a disordered silicon oxycarbide phase having a very high first insertion capacity of ca 1300 mAh g⁻¹ and a free C phase. However, the charge irreversibly trapped into the amorphous silicon oxycarbide network is also high. In consequence the maximum reversible lithium storage capacity of 650 mAh g⁻¹ is measured on high-C content SiOCs with the ratio between amorphous silicon oxycarbide and the free C phase of ~ 1:1. The high carbon content SiOC shows also an excellent cycling stability and performance at high charging/discharging rate with the stable capacity at 2C rate being around 200 mAh g⁻¹.

Increasing the pyrolysis temperature has an opposite effect on the low-C and high-C materials: for the latter one the reversible capacity decreases following a known trend while the former shows an increase of

the reversible capacity which has never been observed before for similar materials.

The influence of pyrolysis atmosphere on lithium storage capacity is investigated as well. It is found that pyrolysis in Ar/H₂ mixtures, compared to the treatment under pure Ar, results into a decrease of the concentration of C dangling bonds as revealed by electron spin resonance (ESR) measurements. The sample prepared under Ar/H₂ mixture shows an excellent cycling stability with an increase in the specific capacity of about 150 mAh g⁻¹ compared to its analogues pyrolysed in pure argon atmosphere.

In order to study the role of porosity towards the lithium storage properties, a comparison of dense and porous materials obtained using same starting precursors is made. Porous SiOC ceramics are prepared by HF etching of the SiOC ceramics. HF etching removes a part of the amorphous silica phase from SiOC nanostructure leaving a porous structure. Porous ceramics with surface areas up to 640 m² g⁻¹ is obtained. The electrochemical charging/discharging results indicate that the porosity can help to increase the lithium storage capacity and it also leads to an enhanced cycling stability.

This work demonstrates clearly that silicon oxycarbide (SiOC) ceramics present excellent electrochemical properties to be applied as a promising anode material for lithium storage applications.

Thesis Overview

In this section, a brief outline of the whole thesis is presented. The purpose of this thesis is to synthesize silicon oxycarbide (SiOC) ceramics and study the Li-intercalation mechanism of the SiOC anodes which is already proved to be a promising anode material for Li-ion batteries as evident from various literature reports. The thesis starts with a short chapter (**Chapter 1**) introducing lithium ion batteries and current trends and developments in battery research based on literature survey. The first chapter (**Chapter 1**) addresses general concepts of batteries focusing on Li-ion batteries with its importance in the energy storage needs of future. The discussion continues with the current developments on materials used in Li-ion batteries for vehicular applications and portable devices. The following chapter (**Chapter 2**) is about polymer derived ceramics (PDCs) with a focus on silicon oxycarbide ceramics (SiOC) presenting a general overview starting from different synthesis approaches, materials used, structure and properties. **Chapter 3** gives the experimental details of synthesis of SiOC ceramics, heat treatments, experimental setup, structural characterizations performed and electrochemical measurements to analyze the lithium storage properties and different correlative studies performed during this PhD program. The **Chapter 4**, which is the core part of this thesis work, addresses detailed studies correlating both electrochemical and structural features of SiOC ceramics of controlled compositions with the help of conventional techniques. Different characterization methods have been used to analyze the SiOC anode materials in order to understand the Li-intercalation mechanism. Finally, **Chapter 5** presents another phase of the

study with a comparison of dense and porous SiOCs. The thesis is completed with a short chapter presenting the main conclusions of this PhD work and outlook of the proposed future research activity.

Chapter 1. State of the Art - Lithium ion Batteries - Current Perspectives

1.1 Electrochemical Power Sources

Electrochemical power sources are systems which can transform chemical energy in to electrical energy directly. An electrochemical cell is capable of storing energy by using a reversible chemical reaction which allows the direct conversion of chemical energy in to electrical energy. History of electrochemical power systems starts with the inventions of Italian scientist Alessandro Volta in 1801[1, 2]. Volta constructed a voltaic pile with zinc and silver electrodes separated by a brine soaked felt which is considered to be the first electrochemical battery ever produced. After this great invention many studies were performed to develop electrochemical systems with different electrodes using various combinations of materials. Requirements of consumer electronics have fueled the research for developing efficient energy storage systems. Current technologies for energy production from coal, natural gas, oil products etc. had raised the issue of pollution and it is becoming a critical problem for environment. Issues on global warming and recent climate changes associated with high toxic emissions from different sources had forced the researchers to focus more on sustainable technologies for energy production such as energy from wind and solar power as an alternative to the polluting oil resources[3-6]. Development of different technologies for energy production including use of renewable energy sources such as wind and solar needs a good support

from the energy storage systems to have an efficient back up of this produced energy [5, 6].

Batteries are promising electrochemical energy storage technologies to meet the current energy storage requirements owing to their excellent features such as, long cycle life, high efficiency, low maintenance etc. Different battery technologies can be classified in to [7]

- Portable batteries: To be applied in portable devices such as mobile phones, laptops etc.
- Transport batteries: To be used in starting, lighting and ignition (SLI) for cars or in electrical vehicles (e.g., in e - scooters and hybrid electrical vehicles).
- Stationary batteries: To be used for stand-by power, computer backup, telecommunications, etc.

Rechargeable secondary batteries are considered as one of the best choices for the energy storage. A battery is a collective ensemble of electrochemical cells connected in parallel or series to provide required voltage and capacity. Electrochemical rechargeable batteries are best suited for storing energy from the sustainable sources which can convert stored chemical energy in to electricity with high efficiency and without any toxic emissions [5]. Many types of rechargeable batteries are currently used for energy storage; which includes mainly Lead –acid, Ni-Cd, Ni-MH, and Li-ion batteries[7]. From these battery systems Li-ion batteries are one of the best promising candidates for using in applications ranging from small portable gadgets to electric vehicles (HEV) including applications in biomedical devices[5, 8-10]. Li-ion batteries are one of the excellent choices for the energy storage owing to its light weight, greater energy density and longer

life span. Different battery technologies in terms of their energy densities are represented in Figure 1.1. The performance of batteries are expressed in terms of unit of weight (Wh Kg^{-1}) or per unit volume (Wh l^{-1}), that a battery is able to deliver and this is a function of the cell potential (V) and capacity AhKg^{-1} [9].

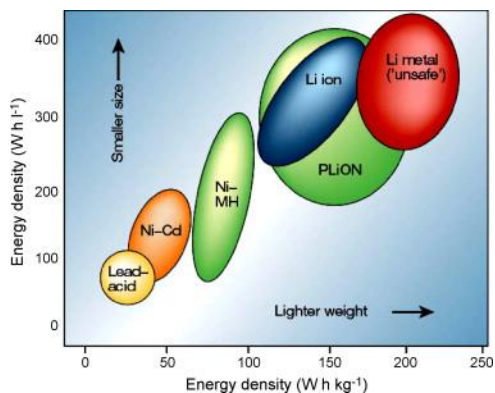


Figure 1.1 Comparison of different battery technologies [9]

1.2 Battery Characteristics

Generally a battery assembly is composed of one or more electrochemical cells connected in parallel or series to store a required energy. Total available energy of a battery depends on how much electricity it can deliver and it is directly related to their size. The Ampere-Hour (Ah) capacity of a battery is the most important unit for explaining the

performance of a battery. It is defined as the amount of current that a battery can deliver for one hour before the battery voltage reaches the end-of life point. Charge and discharge currents are generally expressed in terms of fractions or multiples of C-rate. The C rate is the rate of current that is numerically equal to the Ah rating of the cell. A current of 1C rate means the battery can be charged / discharged in a time of one hour. The cells are characterized in terms of available capacity, available energy and power it can deliver. [2, 7, 8]

Theoretical charge capacity of a cell is the total amount of a charge obtained from a cell and can be derived from faradays equation,

$$Q = \int_{t1}^{t2} I(t)dt = mnF \quad (\text{eq. 1.1})$$

Where, n = number of moles of electrons exchanged

F= Faradays constant ($\approx 96500C \text{ mol}^{-1}$)

Number of moles of electrons flowing through the external circuit corresponds to number of moles of electro active ions diffusing through the electrolyte in to the respective electrodes while charging/ discharging. So the total theoretical capacity is proportional to the number of moles of lithium inserting/ extracting.

Practical capacity is the actual number of Coulombs or “Ah” it delivers.

$$Q_p = I * t \quad (\text{eq. 1.2})$$

Where, I = current (A) and t = time (h)

Coulombic efficiency of a cell is the ratio of practical capacity to the theoretical one (Q_p/Q_t)

Specific capacity of a cell is the capacity per mass of cell or half-cell. In order to quantify the amount of capacity with respect to the mass of the material and in that way allow the comparison of various cells and half-cell, the capacity is usually expressed in Ah/g.

The specific energy of a cell (E) is explained as

$$E = \frac{nF\Delta E^\circ}{\sum_i m_i} \quad (\text{eq. 1.3})$$

Energy is generally explained in units of Watt hour (Wh).

Energy density can be expressed based on their size/ weight

$$E_v = \frac{nF\Delta E^\circ}{\sum_i V_i} \quad (\text{eq. 1.4})$$

Volumetric Energy density = Wh/L

Gravimetric energy density = Wh/Kg

The specific power (P) of a battery is represented by

$$P = \frac{I\Delta E^\circ}{\sum_i mi} \quad (\text{eq. 1.5})$$

Specific power is explained in the units of W/Kg

The power density, P_v (W dm^{-3}), is the power divided by the volume of the cell

$$P_v = \frac{I\Delta E^\circ}{\sum_i V_i} \quad (\text{eq. 1.6})$$

1.3 Lithium ion Batteries

Lithium ion batteries (LIB) are state of art technologies for portable electronic applications because of their compactness, light weight, high efficiency and longer life span compared to other rechargeable battery types[2, 11-13]. The main advantage for lithium ion batteries lies on electrochemical properties of lithium metal such as its low molecular weight, small ionic radius, and low redox potential of -3.04 V vs SHE (Standard Hydrogen Electrode)[4, 7]. These properties make the LIBs light weight which accounts for their high energy densities. LIBs are one of the greatest achievements of electrochemistry with specific energies of 150 Wh Kg^{-1} (gravimetric) and 400 Wh l^{-1} (Volumetric) representing smaller size and light weight[9, 11]. LIBs were first commercialized by Sony in 1991 using a layered lithium transition metal oxide cathode ($(LiT^M O_2, T^M = \text{Transition metal})$) and graphite anode ($Li_x C$) with a gravimetric energy density of around 180 Wh Kg^{-1} [11, 14]. Major part of the present studies on LIBs is focused on developing suitable electrode and electrolyte materials with

improved intrinsic properties to meet present day requirements including commercial applications in hybrid electric vehicles (HEV). The developments in batteries are based on increasing the power and energy densities, while minimizing the size and weight of systems. It is important to improve the energy densities, life span and charging rate to realize the commercialization of batteries for transportation purposes, e.g. hybrid electric vehicles. Billions of lithium ion batteries are produced for portable applications. The lithium ion battery productions per year are reported by B. Scrosati, et al. in 2010, which shows the growing needs of energy efficient lithium ion batteries[13]. A schematic representation of a cylindrical lithium ion battery system is given in Figure 1.2, showing the arrangement of number of electrochemical cells in an ordered way to make a final battery of required voltage and power.

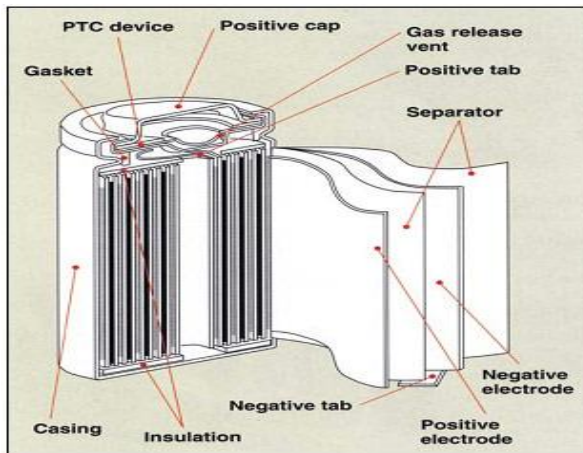
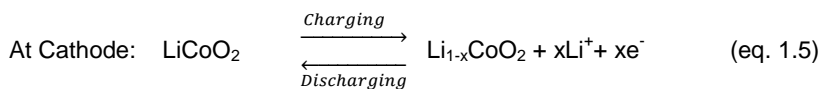
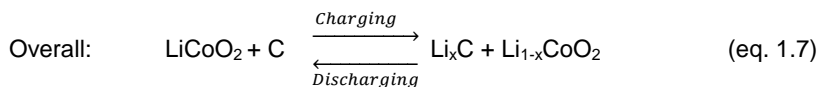
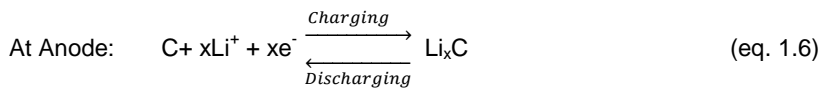


Figure 1.2 Representation of a cylindrical lithium ion battery system (Courtesy Sanyo)

Lithium ion batteries are different from so called lithium batteries. In contrast to lithium batteries, which contain metallic lithium as negative electrode and present severe security issues during recharging, lithium ion batteries contain no metallic lithium. Lithium is found only in ionic form in electrolytes and in atomic scale in oxide cathode materials and when intercalated in to carbon anodes[3]. The main working principle of lithium ion batteries is the reversible electrochemical reaction leading to insertion/extraction of lithium ions in the electrode materials along with parallel electron addition/removal which flows through the external circuit. Main objection to rechargeable batteries are based on safety considerations due to side reactions and thermal runaways in the case of shorts/leakage. The challenge is to produce lithium ion batteries that are safer, cheaper and have great energy density. The structure of a conventional lithium ion battery consists of a cathode, mainly lithium transition metal oxide, a carbon based anode, an electrolyte consisting of a solution of a lithium salt in a mixed organic solvent (eg. LiPF_6 in a mixture of ethylene carbonate and dimethyl carbonate) and a separator soaked in electrolyte to avoid electrical contact between the electrodes. A typical lithium ion battery configuration is represented in Figure 1.3. The battery voltage is derived from the electrochemical potential difference between the cathode and anode. The performance of lithium ion batteries depends on the intrinsic properties of the materials used for the cell assembly. A general reaction scheme during charging/discharging of a conventional lithium ion battery with LiCoO_2 cathode and graphite anode is represented below[7].





General reactions scheme representing working of a conventional lithium ion

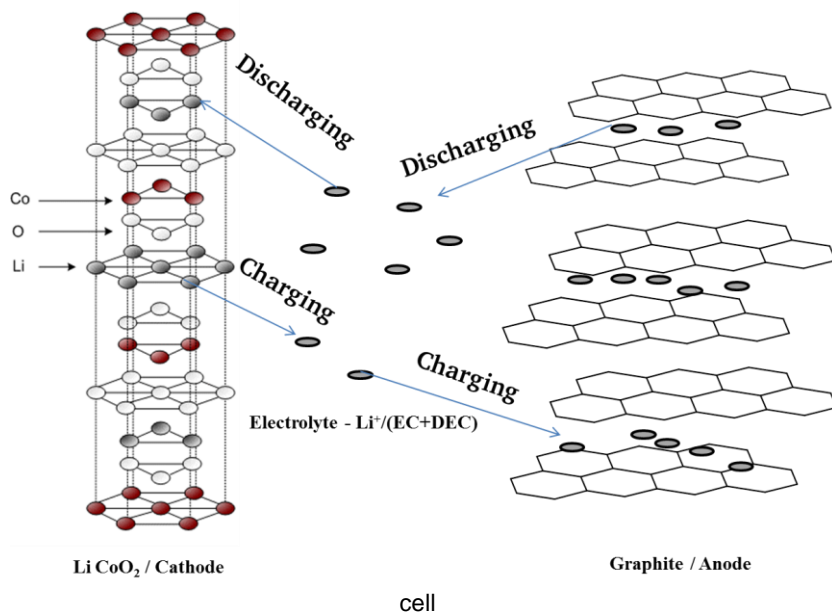


Figure 1.3 Structure of a conventional lithium ion cell assembly

Figure 1.3. demonstrates a scheme of a functioning of conventional lithium ion batteries. The cathode material is made from a lithium transition metal oxide ($LiT^M O_2$, T^M = Transition metal) coated on an aluminium current collector using a binder. Anode material is a carbon coated on a copper current collector in presence of a binder and conducting medium. Both the electrodes are separated by a separator soaked in an electrolyte solution of lithium salt. The separator acts as an insulator between both the electrodes with ion permeable properties. During charging of a battery by connecting an external load, lithium ions from the cathode diffuse in to the intercalation sites between graphene layers in anodes through the electrolyte. Discharging is performed by connecting a negative load and the lithium intercalated in the anodes diffuse back to the cathode. Electrons always flow in parallel through the external circuit connecting both the electrodes.

1.3.1 Components of Lithium ion Batteries

1.3.1.1 Cathodes

Cathodes or positive electrodes in lithium ion batteries are made up of materials capable of reversible lithium insertion from electrolytes during battery operation [14][15]. Many intercalation materials have been proposed as cathodes in commercial LiBs. Mostly used cathode materials are based on lithium transition metal oxides like, $LiCoO_2$, $LiMn_2O_4$, $LiFePO_4$ etc. [15]. $LiCoO_2$ is the easily available and mostly used cathode material with a theoretical capacity of 145 mAh g^{-1} . Structure of $LiCoO_2$ materials are in space group $R\bar{3}m$, with Li ions and Co ions occupying octahedral sites, respectively. Oxygen ions form a cubic close packing. The structure of $LiCoO_2$ is a layered arrangement with alternating lithium – cation sheets and

CoO_2^- anion sheets[9, 16]. Studies are going on to develop materials with superior capacities, high voltage and extended stability to match the current requirements[7]. Due to safety issues (and capacity as well) $LiCoO_2$ is replaced by mixed oxides. These are all layered structures. Moreover, from the point of view of fast diffusion, tridimensional cathode materials are of interest, i.e. $LiFePO_4$, $LiMnO_4$ etc.

A capacity vs potential graph of some of the common cathode materials are presented in Figure 1.4 (Adapted from Ref. 15)

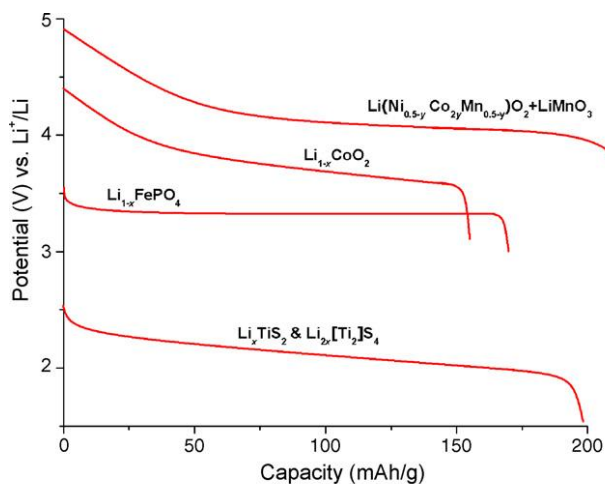


Figure 1.4 Discharge characteristics of different cathode insertion materials (Adapted from Ref. 15)

1.3.1.2 Electrolytes

The term electrolyte in lithium ion batteries refers to an ion-conducting solution comprising solvent and a salt. General electrolytes for lithium ion batteries include lithium salts in a mixture of organic solvents. The ideal properties of non-aqueous electrolytes for practical batteries includes high conductivity over a wide temperature range, large electrochemical window, low temperature coefficient of viscosity, good solvating properties for ions, low toxicity etc.[8]. Stability of electrolyte is an important factor determining the irreversible capacity loss by means of passive film formation due to electrolyte decomposition at the surface of the electrode. Mostly used liquid electrolyte is 1M solution of lithium hexafluorophosphate, $LiPF_6$ in a mixture of organic carbonates (propylene, ethylene, diethyl etc). Electrolytes based on propylene carbonate solvents can cause the problem of solvent co-intercalation leading to exfoliation of the anode [12]. The study on electrolytes has now moved in to solid state polymer electrolyte which can offer better safety standards for lithium ion batteries. Polymer electrolytes helps to develop the concept of solid state batteries and these electrolytes can function at slightly higher electrochemical potentials up to 5.5 V vs Li/Li^+ compared to the organic electrolytes which decomposes at this voltage[17, 18]. The commonly used polymer electrolyte is poly (ethylene oxide) -salt complex.

1.3.1.3. Separators

Separators have been used as spacers to prevent electronic contact but to allow ion transport between the cathode and anode. Most of the lithium ion cells use micro porous polyolefin separators. They are mostly made from polyethylene or polypropylene. A good separator should be an

electronic insulator with good ion permeability. The research on separators ranges from micro porous films to complex multilayer structures to meet the requirements of high energy batteries. Development of new solid state lithium ion batteries started studying polymer electrolytes which can act also as an active separator[7].

1.3.1.4. Anode Materials

Research on anode materials addresses to a wide variety of compounds, able to support the reversible storage of lithium without any changes in host structure/nanostructures. Lithium metal itself has been applied as an anode material, but problem of dendrite formation on the electrode surface and volume changes after couple of electrochemical cycling led to safety issues and cell failure. The mainly studied negative electrodes include Lithium metal alloys, e.g. lithium–silicon(*Li-Si*), lithium–tin(*Li-Sn*), alloys, etc.[19-22] The obstacles for these materials are the volume changes associated with lithium intake while charging and they have a large volume expansion which leads to reduced life time and damage of anode structure. Also there are materials like lithium titanium oxide, $Li_4Ti_5O_{12}$ (LTO) which are safe materials of high rate capability and no volume changes but having disadvantage such as low capacity of 160 mAh g^{-1} and higher operating voltage. For comparison, lithium silicon alloy in its fully lithiated composition $Li_{4.4}Si$ has a theoretical specific capacity of 4200 mAh g^{-1} compared to 372 mAh g^{-1} of graphite, but unfortunately this large intake of lithium is accompanied by a large volume expansion of around 300 % [20, 23]. This leads to the cracking of the electrode and in consequence to failure of the cells. Studies are going on to increase the capacity retention with battery cycling by using different structural forms of materials such as *Si*

nanowires, nanoparticle as a composite by embedding *Si* in carbon etc. *Si/C* composites are reported to offer capacities of more than 800 mAh g⁻¹ for the initial cycles with an improved cyclability compared to silicon[24-26]. The discovery of Li-intercalation / deintercalation process in carbonaceous materials in presence of selective electrolytes boosted the research on LIB anodes. Carbonaceous materials have been proposed to be one of the most promising anode materials in terms of safety and longer cell life.

1.4 Carbon Based Anode Materials

In contrast to most of the lithium alloy-based electrodes, carbonaceous materials such as graphite experience small volume changes (~10%) during alloying and de alloying with lithium ions and due to their structural stability, they show excellent stability towards multiple electrochemical insertion/extraction cycles[8, 27, 28]. Electrodes based on graphite were the conventionally used anodes in prototypes of the commercial lithium ion batteries. But the theoretical capacity of graphite is limited to 372 mAh g⁻¹ with the formation of *LiC₆*, hosting one lithium atom per every 6 carbon atoms [7, 8, 27, 29, 30].

General reaction scheme of lithium insertion in to carbon host structure is given by



During charging lithium ions penetrate into interlayer space between the carbon layers, while the reduction of graphite undergoes with the electron flowing through the external circuit. The stoichiometric formula for graphite intercalation compound is LiC_6 . This reaction process is termed as an intercalation process and during intercalation the carbon host structure remains unchanged. During extraction by applying a negative load the lithium ions release back from the interlayer space between graphene layers. This shows that the structural morphology of host carbon species is an important factor in deciding the reversible lithium storage capacity.

Carbon structures can be classified in to two, graphitic and non-graphitic (disordered) carbons. Graphitic carbons are carbonaceous materials having layered arrangement of sp^2 graphene layers with a long range order and have a specific stacking sequence. Whereas non-graphitic or disordered carbon structures have carbon atoms arranged in planar hexagonal layers with a short range order[7, 8, 30].

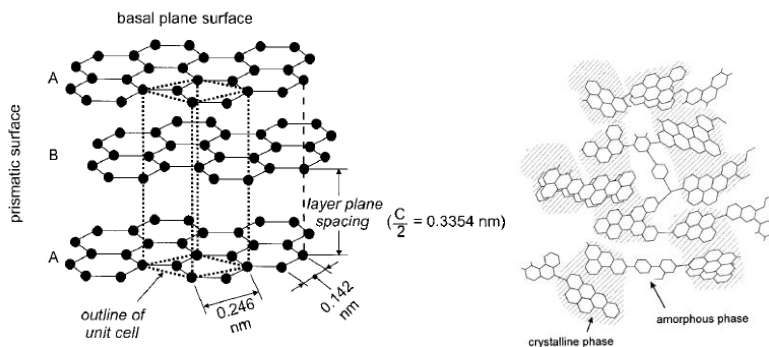


Figure 1.5 Schematic representation of a) Graphite and b) Non-graphitic disordered carbon structures[30]

Graphite electrodes have some drawbacks including intercalation of solvated lithium in between graphene layers during charging; as the solvated lithium ions are larger in size, it elongate the space between graphene layers leading to exfoliation of the surface and also to the cracking of electrode surface[24, 30-32].

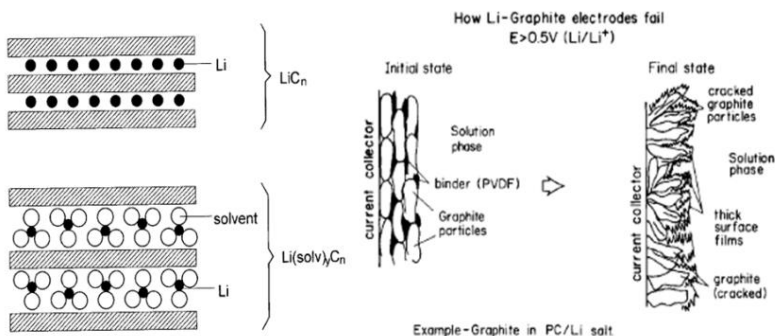


Fig. 9. Schematic drawing of binary (LiC_n) and ternary $[Li(solvent)_n C_n]$ lithium-graphite intercalation compounds. Modified and redrawn from [63].

Figure 1.6 Failure probe of graphite electrode [24, 30-32]

Disordered carbons are reported to store significantly large amount of lithium compared to graphite. When there is a disorder in the form of defects, non-uniform arrangement of graphene layers leading to stacking fault etc, the structures are called non-graphitic or disordered carbon structures. Disordered carbons are formed during pyrolysis of organic polymers at higher temperatures. The advantages of disordered carbons over graphite structure are (i) prevents intercalation of solvated lithium ions, which can lead to exfoliation of the layered electrode structure (ii) provides

additional sites for lithium storage with a stoichiometry of $x > 1$ in $Li_x C_6$. (iii) possible to store lithium ions in edges and surfaces of graphene layers in addition to normal intercalation between layers. Compounds with disordered carbon structures are found to be a promising anode material for future lithium ion batteries [28, 30, 36].

Hundreds of carbonaceous materials have been then analyzed as potential alternative anode materials to graphite for lithium ion batteries and the research still continues to realize the commercial applications in advanced technologies[8, 27, 28, 30, 36-42]. In the Sony battery produced in 1991, the thermal decomposition product of polyfurfuryl alcohol resin (PFA) was used as the carbon anode[14]. Since then, many kinds of carbonaceous materials, from crystalline to strongly disordered carbon, have been tested as anodes in lithium-ion batteries. In order to tackle the challenges there should be detailed studies on different carbon morphologies to have a compromise in volume changes during lithium insertion in host materials. Anodes based on disordered carbon materials have reported to overcome these problems. These materials are found to be promising anode materials with reversible capacities of more than 700 mAh g^{-1} compared to the conventional graphite anode with a theoretical capacity of 372 mAh g^{-1} [8]. Dahn et al. have reported detailed studies on electrochemical behavior of carbonaceous materials of different morphologies. It was reported [36] that disordered carbon materials can host twice more lithium ions to form Li_2C_6 compared to graphite. Capacity can also be increased with the presence of hetero atoms such as residual hydrogen by lithium binding on hydrogen terminated edges.

The intercalation process during charging is associated with the formation of a protecting layer of solid electrolyte interface (SEI) on the

electrode surface which prevents further solvent reduction and acts as a passive layer allowing only the transport of lithium ions[8, 34, 35, 43]. This SEI layer acts as a protective film on the anode surface. This layer has to be not only a good ionic conductor for lithium diffusion but also should be an electronic insulator. The formation of SEI layer adds to a part of irreversible capacity during first cycle of charging/ discharging of lithium ion cells[33], but from the second cycle the efficiency of charging/discharging reaches 99%.

A typical charge/discharge profile of a graphite anode (Capacity vs Voltage) is represented in Figure 1.7 with voltage (V) on Y axis and specific capacity (mAh g⁻¹) on X axis. The graphite electrodes for this measurement were produced following the general procedures and characterized using a half-cell approach with lithium metal as the counter/ reference electrode. The graphite anodes are characterized by assembling a half cell with lithium metal as the anode and a 1M LiPF₆ in a mixture of EC/DEC solvents as electrolyte. The initial voltage drop from 3 V to 1 V is mainly because of the internal polarization inside the system and from 1 to 0.3 V corresponds to the formation of SEI (Solid Electrolyte Interface) layer, there is also a minor chance for the intercalation of solvated lithium ions in the interlayer spaces but in most of the cases the intercalation of these solvated ions are prevented by SEI layer. The reversible intercalation of lithium ions in graphite starts only below 0.3 V as observed by a long plateau below this region. Largest part of specific capacity is falls below this region.

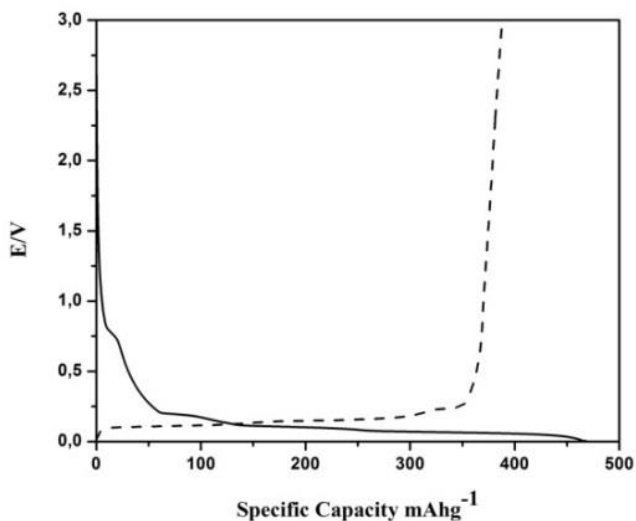


Figure 1.7 First cycle charging/discharging of graphite anode: Straight line represents charging and dashed lines represent discharging

The charging and discharging was performed at a same rate of C/20. The rate is assigned based on theoretical capacity of graphite (372 mAh g⁻¹). The charging capacity 465 mAh g⁻¹ is well above the theoretical limit associated with the formation of SEI and due to metallic lithium plating during first lithium insertion. The discharge capacity is 396 mAh g⁻¹ almost similar to the theoretical capacity. The efficiency of the cell is 86% and from second cycle the efficiency reaches 99% without any loss in capacity.

1.5 Polymer Derived Ceramics as Anodes in Lithium-ion Batteries

Research based on silicon/carbon composite anodes and different carbon structures have led to the studies on applicability of polymer derived ceramics as promising anode materials. Different forms of PDC ceramics such as SiOC, SiCN etc. has been analyzed in detail for lithium storage applications [44-51]. Among different members of PDC group silicon oxycarbide materials got more attention as an alternative to graphite/ silicon anodes. Silicon Oxycarbide Ceramics (SiOC) derived from polymer precursors have gained much more attention for the past two decades as a promising anode material for lithium ion batteries [25, 26, 46, 49, 52-56]. It has been already reported that SiOCs are capable to deliver a specific capacity as high as 800 mAh g⁻¹ with enhanced life span. The excellent electrochemical features displayed by this class of materials are attributed to their complex nanostructure with amorphous SiOC tetrahedral phase along with a network of disordered free carbon layers. SiOCs with different elemental compositions have been thoroughly studied to understand the lithium intercalation mechanism in their amorphous networks. A clear idea about the intercalation mechanism is necessary to modify the drawbacks like irreversible capacity loss, hysteresis between insertion/extraction generally associated with these materials. Tailoring the structural and electrochemical features of SiOCs with selective precursors and synthesis route may help to overcome the barriers for realizing their commercial applications. Anode features of SiOC glass ceramics are discussed in detail in chapter 2 along with current developments.

References

- [1] B. Scrosati, "Charging towards the superbattery". *Nature*, 473 (2011) 448-449.
- [2] B. Scrosati, C.A.Vincent, "Modern Batteries" 1997: Elsevier.
- [3] R.J. Brodd et al., "Batteries", 1977 to 2002. *J. the Electrochem. Soc.*, 151(3)(2004) K1.
- [4] K. Brandt, "Historical development of secondary lithium batteries" *Solid State Ionic's*, 69 (1994) 173-183.
- [5] J.M. Tarascon, M.Armand, "Building better batteries", *Nature*, 451 (2008)
- [6] J.B. Goodenough and Y. Kim, "Challenges for Rechargeable Li Batteries", *Chem. Mater.*, 22 (3) (2010) 587-603.
- [7] *Handbook of battery materials*, ed. J.O. Besenhard. 1999: Wiley-VCH.
- [8] *Industrial chemistry library*, ed. G. Pistoia. Vol. 5. 1994: Elsevier.
- [9] M. Armand and J.M. Tarascon, "Issues and challenges facing rechargeable lithium batteries" *NATURE*, 414 (2001) 359-367.
- [10] B. Dunn, H. Kamath, and J.M. Tarascon, "Electrical energy storage for the grid: a battery of choices", *Science*, 334 (6058) (2011) 928-35.
- [11] Y. Nishi, "Lithium ion secondary batteries; past 10 years and the future" *J. Power Sources*, 100 (2001)
- [12] G. Pistoia, "Batteries for Portable Devices" 2005: Elsevier.
- [13] B. Scrosati and J. Garche, "Lithium batteries: Status, prospects and future", *J. Power Sources*, 195(9) (2010) 2419-2430.

-
- [14] T. Nagaura and K. Tozawa, "Lithium ion rechargeable batteries", Progress in Batteries and Solarcells, 9, 1990
- [15] J.B. Goodenough and Y. Kim, "Challenges for rechargeable batteries" J. Power Sources, 196 (16) (2011) 6688-6694.
- [16] O.I. Velikokhatnyi, J. P. Maranchi, I. Kim, M. K. Datta, P. N. Kumta, "Ceramic Materials for Lithium-Ion Battery Applications", 2005 Taylor & Francis Group, LLC.
- [17] D. Guyomard and J.M.Tarascon, "High voltage stable liquid electrolytes for $\text{Li}_{1+x}\text{Mn}_2\text{O}_4$ /Carbon rocking-chair lithium batteries", J. Power Sources, 54 (1995)
- [18] M. Armand, "The history of polymer electrolytes", Solid State Ionics, 69, (1994)
- [19] D. Fauteux and R. Koksang, "Rechargeable lithium battery anodes: alternatives to metallic lithium", J. APPL. ELECTROCHEM., 23 (1993)
- [20] M.N. Obrovac and L. Christensen, "Structural Changes in Silicon Anodes during Lithium Insertion/Extraction", Electrochem. and Solid-State Letters, 7(5) (2004) A93
- [21] Y. Idota, T. Kubota, A. Matsufuji, Y. Maekawa and T. Miyasaka, "Tin-based Amorphous Oxide: A High Capacity Lithium-ion Storage Material". Science, 276 (1997)
- [22] M. Winter and J.O. Besenhard, "Electrochemical lithiation of tin and tin-based intermetallics and composites", Electrochim. acta, 45 (1999)
- [23] J.H. Ryu, et al., "Failure Modes of Silicon Powder Negative Electrode in Lithium Secondary Batteries" Electrochem. and Solid-State Letters, 7(10) (2004) A306.

-
- [24] C.K. Chan, C.K., et al., "High-performance lithium battery anodes using silicon nanowires", *Nat. Nanotechnol.*, 3(1) (2008) 31-5.
- [25] D. Ahn and R. Raj, "Cyclic stability and C-rate performance of amorphous silicon and carbon based anodes for electrochemical storage of lithium", *J. Power Sources*, 196 (4) (2011) 2179-2186.
- [26] A.M. Wilson, G.Zank, K. Eguchi, W. Xing and J.R. Dahn, "Pyrolysed silicon-containing polymers as high capacity anodes for lithium-ion batteries", *J. Power Sources*, 68 (1997) 195-200.
- [27] D.A. Stevens and J.R. Dahn, "The Mechanisms of Lithium and Sodium Insertion in Carbon Materials", *J. the Electrochem. Soc.*, 148(8) (2001) A803.
- [28] T. Zheng, Y.Liu, E.W. Fuller, S. Tseng, U. Von Sacken and J.R. Dahn, "Lithium insertion in high capacity carbonaceous materials", *J. Electrochem. Soc.*, 142, (1995)
- [29] T. Zheng, "Lithium Insertion in High Capacity Carbonaceous Materials", *J. the Electrochem. Soc.*, 142(8) (1995) 2581.
- [30] M. Winter, J.O. Besenhard, M.E. Spahr and P. Novak, "Insertion electrode materials for rechargeable batteries", *Advanced Materials*, 10(10) (1998) 725-763.
- [31] J.L. Tirado, "Inorganic Materials for the Negative Electrode of Lithium-ion Batteries". *Nat. Nanotech.*, 3 (2003)
- [32] J.O. Besenhard, M. Winter, J. Yang and W. Biberacher, "Filming mechanism of lithium-carbon anodes in organic and inorganic electrolytes". *J. Power Sources*, 54 (1995)
- [33] P. Verma, T. Sasaki, and P. Novák, "Chemical surface treatments for decreasing irreversible charge loss and preventing exfoliation of graphite in Li-ion batteries", *Electrochim. Acta*, 82 (2012) 233-242.

-
- [34] P. Verma, P. Maire, and P. Novák, "A review of the features and analyses of the solid electrolyte interphase in Li-ion batteries", *Electrochim. Acta*, 55 (22) (2010) 6332-6341.
- [35] E. Paled, "The Electrochemical Behavior of Alkali and Alkaline Earth Metals in Nonaqueous Battery Systems-The Solid Electrolyte Interphase Model", *J. Electrochem. Soc.*, 1979.
- [36] S. Wang, T.K., H. Matsui and Y. Matsumura, "Mechanism of Lithium Insertion in to Disordered Carbon", *Synthetic Metals*, 103 (1999) 2523-2524.
- [37] T. Zheng, "Hysteresis during Lithium Insertion in Hydrogen-Containing Carbons", *J. The Electrochem. Soc.*, 143 (7) (1996) 2137.
- [38] X.H. Zhaoxiang Wang, X. Rongjian and C. Liquan, "A new possible mechanism of lithium insertion and extraction in low-temperature pyrolytic carbon electrode", *Carbon*, 37 (1999) 685-692.
- [39] P. Papanek, M.Radosavljevic and J.E.Fischer., "Lithium Insertion in Disordered Carbon-Hydrogen Alloys: Intercalation vs Covalent Bindin", *Chem. Mater.*, 8 (1996) 1519-1526.
- [40] E. Buiel, A.E.George and J. R. Dahn, "On the Reduction of Lithium Insertion Capacity in Hard-Carbon Anode Materials with Increasing Heat-Treatment Temperature", *J. Electrochem. Soc.*, 145 (7) (1998) 2252-2257.
- [41] W. Xing and J.R. Dahn, "Study of Irreversible Capacities for Li Insertion in Hard and Graphitic Carbons", *J. Electrochem. Soc.*, 144(4) (1997)
- [42] F. Béguin et al., "A better understanding of the irreversible lithium insertion mechanisms in disordered carbons", *J. Phys. and Chem. Solids*, 65 (2-3) (2004) 211-217.

-
- [43] M. Winter, W.K.Appel, B. Evers, T. Hodel, K. Moller, I. Schneider, M. Wachtler, M.R. Wagner, G.H. Wroldnigg and J.O. Besenhard, "Studies of anode/electrolyte interface in lithium ion batteries", *Monatshefte fur chemie*, 132 (2001)
- [44] M. Graczyk-Zajac, G. Mera, J. Kaspar and R. Riedel "Electrochemical studies of carbon-rich polymer-derived SiCN ceramics as anode materials for lithium-ion batteries", *J. Eur. Ceram. Soc.*, 30 (15) (2010) 3235-3243.
- [45] M. Graczyk-Zajac, C. Fasel and R. Riedel, "Polymer-derived-SiCN ceramic/graphite composite as anode material with enhanced rate capability for lithium ion batteries", *J. Power Sources*, 196 (15) (2011) 6412-6418.
- [46] J. Shen and R. Raj, "Silicon-oxycarbide based thin film anodes for lithium ion batteries", *J. Power Sources*, (196(14) 2011) 5945-5950.
- [47] X. Liu, M.-C. Zheng and K. Xie, "Mechanism of lithium storage in Si-O-C composite anodes", *J. Power Sources*, 196 (24) (2011) 10667-10672.
- [48] H. Konno, et al., "Si-C-O glass-like compound/exfoliated graphite composites for negative electrode of lithium ion battery", *Carbon*, 45(3) (2007) 477-483.
- [49] J. Kaspar, M. Graczyk-Zajac and R. Riedel, "Carbon-rich SiOC anodes for lithium-ion batteries: Part II. Role of thermal cross-linking", *Solid State Ionics*, 225 (2012) 527-531.
- [50] M. Graczyk-Zajac, L. Toma, C. Fasel and R. Riedel, "Carbon-rich SiOC anodes for lithium-ion batteries: Part I. Influence of material UV-pre-treatment on high power properties", *Solid State Ionics*, 225 (2012) 522-526.

-
- [51] R. Bhandavat and G. Singh, "Improved electrochemical capacity of precursor-derived Si(B)CN-carbon nanotube composite as Li-ion battery anode", *ACS Appl. Mater. Interfaces*, 4(10) (2012) 5092-7.
- [52] P.E. Sanchez-Jimenez and R. Raj, "Lithium Insertion in Polymer-Derived Silicon Oxycarbide Ceramics", *J. Amer. Ceram. Soc.*, 93(4) (2010) 1127-1135.
- [53] D. Ahn and R. Raj, "Thermodynamic measurements pertaining to the hysteretic intercalation of lithium in polymer-derived silicon oxycarbide", *J. Power Sources*, 195(12) (2010) 3900-3906.
- [54] H. Fukui, H. Ohsuka, T. Hino and K. Kanamura, "Polysilane/Acenaphthylene Blends Toward Si-O-C Composite Anodes for Rechargeable Lithium-Ion Batteries", *J. Electrochem. Soc.*, 158 (5) (2011) A550.
- [55] H. Fukui, H. Ohsuka, T. Hino and K. Kanamura, "Preparation of Microporous Si-O-C Composite Material and Its Lithium Storage Capability", *Chem. Letters*, 38(1) (2009) 86-87.
- [56] H. Fukui, H. Ohsuka, T. Hino and K. Kanamura, "A Si-O-C composite anode: high capability and proposed mechanism of lithium storage associated with microstructural characteristics", *ACS Appl. Mater. Interfaces*, 2(4) (2010) 998-1008.

Chapter 2. Polymer Derived Silicon Oxycarbide Ceramics (SiOC)

2.1 Polymer Derived Ceramics (PDCs) - General Overview

Synthesis of glass ceramics from cross-linked polymer precursors has gained interest over conventional powder processing route for the past couple of decades[1]. Polymer Derived Ceramics (PDCs) is a broad class of ceramics prepared by the pyrolysis of polymer precursors in a controlled atmosphere. These are novel multifunctional materials synthesized using different cross linking approaches and requiring lower sintering temperatures compared to the conventional methods. The studies on PDCs got momentum with the findings of Verbeek et al explaining the polymer to ceramic transformation in polyorganosilicon polymers in 1970s[2]. Later, in same period, Yajima et al. successfully synthesized the SiC ceramic fibers with high thermal stability by thermolysis of polycarbosilanes[3]. These findings had fuelled studies on synthesis of ceramic networks by low temperature pyrolysis of preceramic polymers.

PDCs are generally classified according to their basic structural networks. Main starting precursors of polymer derived ceramics are based on different organosilicon polymers. The main members of PDC group includes secondary systems such as SiC, Si₃N₄, BN etc. , ternary systems such as SiOC, SiCN and BCN, and quaternary SiBOC, SiOCN, SiBCN [4]. Excellent properties of these materials such as high thermo-chemical stabilities, hardness and high young's modulus along with oxidation stability had made them potential candidates for wide variety of applications at higher temperatures and in different chemical environments[5-11]. PDCs can also be processed in different structural forms as fibers, coatings, thin films etc.

depending on application requirement. A detailed flow chart of the organo silicon polymer precursors and final ceramic structures is presented in Figure 2.1 with precursors for synthesis of many classes of PDCs having silicon, nitrogen, carbon, boron etc. in their networks as reported by P. Colombo [11] and P. Greil [4]. The composition of the final ceramic depends on the amount, nature and chemistry of starting precursors. Parent precursors and structures of final silicon based polymer derived ceramics are also represented in Figure 2.1 along with the flow chart.

As per the main interest of this proposed research activity the discussions about PDCs are limited to SiOC based ceramics. Silicon oxycarbide with different structure, compositions and properties has been subjected to numerous studies and applications in detail during past couple of decades.

2.2 Silicon Oxycarbide (SiOC) Glass Ceramics

Silicon oxycarbides are ceramics having chemical structures with silicon bonded to both oxygen and carbon simultaneously. These are one of the best alternatives to overcome the limitations of pure silica glasses [12-16]. The concept of SiOC came after different trials for incorporating carbon in to silica in order to improve their properties such as crystallization resistance, thermal properties, mechanical properties and electrical properties [17]. Attempt for carbon incorporation in to silica started with physical addition of carbon in to molten silica followed by vigorous stirring. This method had problems with decomposition of carbon at high temperature required for melting silica and also carbon has a limited solubility in silica. The following studies to add carbon in to silica leads to the sol-gel synthesis of SiOC from hybrid alkoxides with terminal organic groups

[7, 12, 15, 16, 18]. Later it is identified that SiOC can also be produced via polymeric route using polymer precursors. The pyrolysis process of cross linked gels obtained from polymer precursors results in carbon incorporation to SiO₂ in larger amount to form SiOC ceramics. The carbon incorporation is by replacing 2 coordinated O by four coordinated C. During heat treatment the Si-C bonds in polymer networks remain stable up to a high temperature of more than 900 °C while cleavages of C-H bonds from organic moieties are observed at a temperature greater than 800 °C with evolution of hydrogen leading to the formation of randomly distributed free carbon networks in the amorphous SiOC network. The SiOCs formed after pyrolysis at high temperatures generally appear as a shiny, black and amorphous material due to the presence of elemental carbon in the form of disordered free carbon networks along with SiOC mixed tetrahedral units.

Silicon oxycarbide glass has exceptional high temperature strength and chemical stability compared to vitreous silica. Structure of SiOCs consists of three solid phases; amorphous silica, carbon and SiC with carbon bonded either to silicon or another carbon. Each oxygen atom bonds to two silicon atoms and there is no evidence for existence of carbon-oxygen bonds [5]. The role and nature of free carbon content has studied in detail using conventional structural characterization techniques such as Raman, NMR, Elemental analysis etc. Pyrolysis temperature is a key factor in determining mechanical and thermo-chemical properties of SiOC ceramics. With increased pyrolysis temperature phase separation in to oxygen rich and carbon rich species starts along with ordering of carbon networks

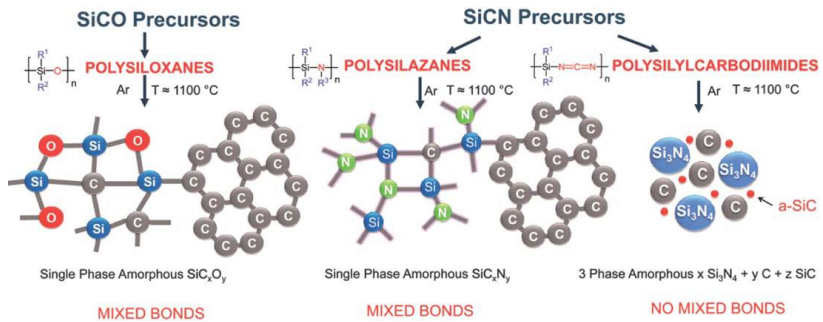
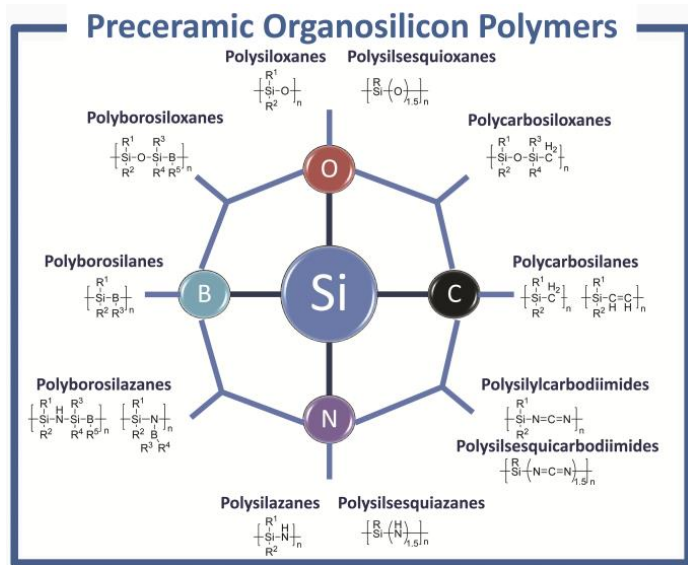


Figure 2.1 Flow chart representing different organosilicon polymer precursors and structures of final ceramics [4, 36]

2.3 Synthesis of SiOC Ceramics

Silicon oxycarbide glass ceramics are generally obtained by the pyrolysis of cross linked silicon resins. The synthesis of crosslinked silicon resins can be achieved either via sol-gel starting from organic modified silicon alkoxides or from commercial silicon based polymers. Cross linking of Si-based polymers can be achieved by hydrosilylation of polymers containing $Si-H$ or $C=C$ units or by thermal curing. The main methods for crosslinking polymer precursors are explained in detail in the following sections.

2.3.1 Sol-gel Techniques

Sol-gel process helps for the synthesis of homogeneous glass networks (precursors) at low temperatures. General sol-gel procedure starts with dissolving the starting material via hydrolysis/condensation process to form a colloidal dispersion called a sol and this sol is then dehydrated to eliminate the water followed by polymerization process to obtain a well cross linked gel of polymer networks. This gel is then aged / cured by drying for an optimum period and calcined at higher temperatures to form the final ceramic glass network. The carbon incorporation in SiO₂ glasses were first made successful by sol-gel method using alkoxides with terminal hydrocarbons. The sol-gel approach enabled the low-temperature synthesis of SiOC glasses without the problems of decomposition and oxidation during melting. The main starting precursors are alkyl substituted alkoxides of general formula $R'_n-Si(OR)_{4-n}$ ($R = CH_3, C_2H_5, C_3H_7, C_6H_6$ etc.). The structure of ceramics can be easily tailored by selectively choosing different alkoxide precursors. The $Si-C$ bond of the precursor is preserved during hydrolysis condensation and drying. Pyrolysis of dried gels then creates

amorphous silicon oxycarbide networks having $Si - C$, $Si - O$ and $C - C$ bonds in their network back bones. Structure and properties of the final ceramic are greatly influenced by the chain length and nature of alkyl group present in starting precursors. Different sol-gel mechanisms are represented in eq. 2.1 to 2.3 and a crosslinked polymer network obtained from methyl triethoxysilane (MTES) precursor before pyrolysis is represented in Figure 2.2.

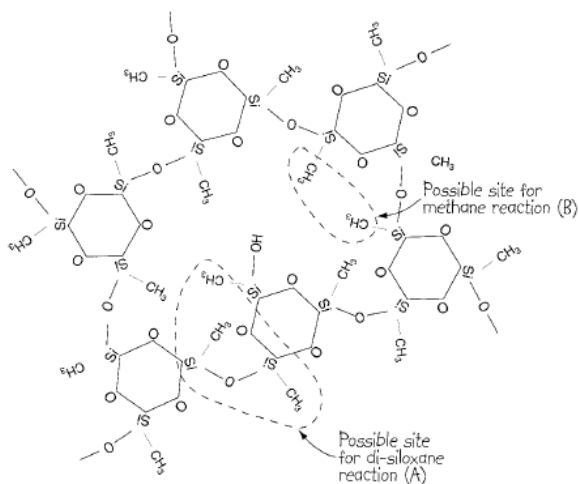
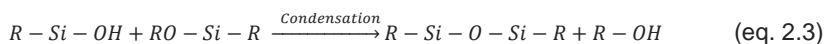
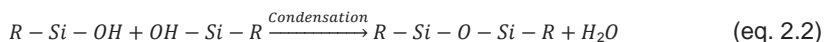
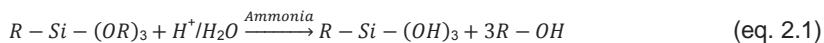


Figure 2.2 Representation of a crosslinked polymer network before pyrolysis [18]

A typical sol-gel method starts from an alkoxy silane and the silanes were hydrolysed using acidic water (Dilute HCl) according to the ratio of alkoxy group ($-OC_2H_5$) attached to each silicon atoms. Acidic water of optimum pH (H^+/HCl) acts as a catalyst to hydrolyze the alkoxy groups by changing $Si - OR$ groups in to $Si - OH$ groups (eq.2.1). During the entire hydrolysis process $R - Si$ bonds remains stable. Hydrolysis is followed by adding specific amount of ammonia solution to promote condensation which results in gelation (eq.2.2). Gelation time may vary from a period of couple of hours to several days. After condensation $Si - OH$ bonds are found to be replaced by $Si - O - Si$ linkages maintaining the $R - Si$ bond intact (eq. 2.2 and 2.3). This structural modification is confirmed using ^{29}Si MAS NMR [15]. Dried gels can be processed in to ceramics by heat treatment at temperatures above 800 °C.

2.3.2 Hydrosilylation

Hydrosilylation is another important technique for cross linking polymer precursors to produce covalent ceramics from different polysiloxane compounds having $Si - H$ and $C = C$ (Vinyl terminated compounds) moieties. Crosslinking can be achieved either by a transition metal catalyzed addition or by a free radical initiation technique. Hydrosilylation reaction proceeds via breakage of $Si - H$ bonds and formation of $Si - C$ bonds. Platinum based catalysts are used to initiate the reaction for most of the hydrosilylation reactions. The hydrosilylation mechanism is generally represented with the redistribution reaction between $Si - H$ bonds and $C = C$ bonds in the presence of a platinum catalyst to form $Si - C$ crosslinked networks. Cross linking process in polysiloxanes using hydrosilylation is represented in following eqn (eq.2.4).

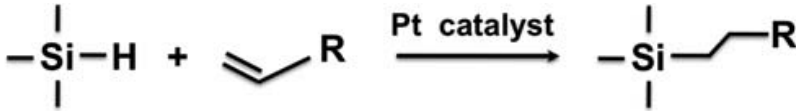
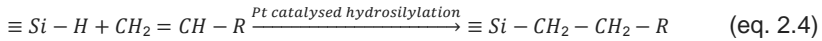


Figure 2.3 Scheme of hydrosilylation reaction [33]

Platinum catalyst acts as an excellent medium to initiate the reaction. Invention of hydrosilylation process was a key step to develop ceramic materials with tailored structural features starting from selective polymer precursors.

2.3.3 Polymer to Ceramic Conversion

The final step in the synthesis of SiOC ceramics are polymer to ceramic transition from crosslinked networks containing $Si - O$ and $Si - C$ bonds and this is achieved by thermal curing followed by pyrolysis at high temperatures of more than 800 °C in an inert atmosphere of Ar, He or in vacuum. Curing/crosslinking of the preceramic gels can be performed at a lower temperature of 150-200 °C prior to pyrolysis. Different pathways during polymer to ceramic conversion can be observed in the TG-DTA weight loss profile. A major weight loss can be observed in 400-800 °C temperature range accounting for the ceramic formation with the evolution of volatile gases such as CH_4 , hydrogen etc. from the preceramic crosslinked networks. A typical weight loss pattern is represented in Figure 2.4. A small weight loss of less than 5% is observed at up to 400 °C associated with condensation reactions, release of residual DVB, ethanol from sol-gel etc. Organic to

inorganic transition starts above 400 °C with a series of radical reactions resulting in the cleavage of chemical bonds such as $Si - C, C - H$ bonds with rearrangement and release of hydrocarbons such as CH_4, C_2H_6 etc. At this temperature range there also occur redistribution reactions around Si atoms in between $Si - O$ and $Si - C$ bonds' leading to the evolution of volatile organosilicon compounds and this is greatly influenced by the O/Si ratio of starting precursors [12]. The ceramic formation is achieved at a temperature of 800 °C with a total weight loss from 5 to 30% depending on the precursors used. From 800 to 1000 °C the polymer to ceramic conversion is achieved. Different reactions occurring during heat treatment are represented from eq. 2.5 to 2.9.



From 1000 to 1400 °C there is no observed weight loss and the concentration of Si, C and O remains constant with structural changes in the mixed oxycarbide concentrations as evidenced by ^{29}Si MAS NMR. Heat treatment to temperatures above 1500 °C leads to onset of carbothermal reduction reaction with formation of SiC_4 species by consuming mixed SiC_xO_y units. Further increase in pyrolysis temperature results in larger weight loss with removal of SiO/CO leaving only SiC/C . The possible carbothermal reduction proceeds via the following eqns.



A typical weightloss pattern of SiOC ceramics is represented below which shows thermal evolution pattern with increasing pyrolysis temperature .

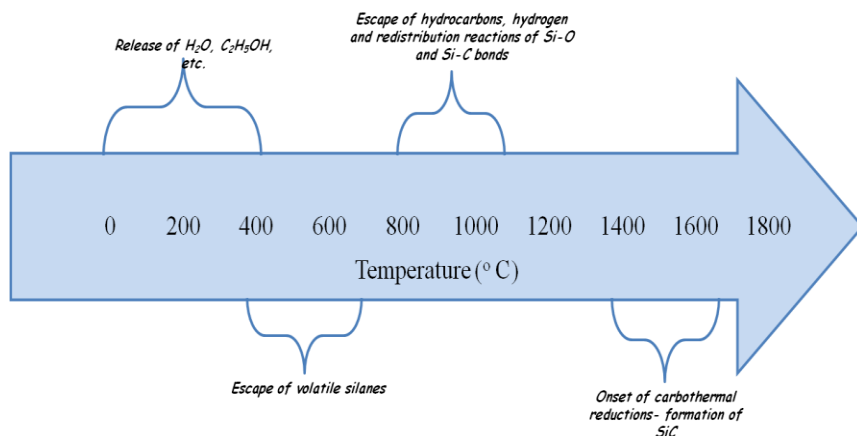


Figure 2.4 Polymer to ceramic conversion during heat treatment

2.4 Structure of SiOCs

Amorphous SiOC networks have a complicated structure. Structure of SiOC is still a controversial issue with different arguments between scientific communities. Basic structure of SiOCs formed at 1000 °C generally

consists of mixed SiC_xO_{4-x} species ($0 \leq x \leq 4$) along with a network of disordered free carbon. The structure of SiOC glasses have been explained in detail with the help of conventional techniques such as FTIR, Raman, NMR, SEM, TEM etc. The presence of a network of disordered free carbons distributed in the amorphous SiOC matrix gives the black shiny appearance to the pyrolysed SiOC glasses. Existence of free carbon networks in the structure is well confirmed by Raman spectra, NMR etc. It is also possible to synthesize stoichiometric SiOC networks without free carbon in the structure by making use of selective precursors such as TREOS. Different structures are proposed for SiOC ceramics in various literatures.

Based on the NMR and HRTEM studies Pantano et al [15] proposed a structure of SiOC as represented in Figure 2.5. Heat treatment at 1000 °C yields a small ratio of residual hydrogen as well as free carbon. Temperature above 1300 °C leads to phase separation in to oxygen rich SiO_2 and carbon rich SiC phases. The phase separation of stoichiometric SiOC composition is represented in eq. 2.12.



The below structure (Figure 2.5) clearly explains the existence of different bondings such as $Si - C$, $Si - O$ and $C - C$ bonds in the networks. There are no $C - O$ linkages observed in the amorphous structure with carbon bonds only to silicon or another carbon itself.

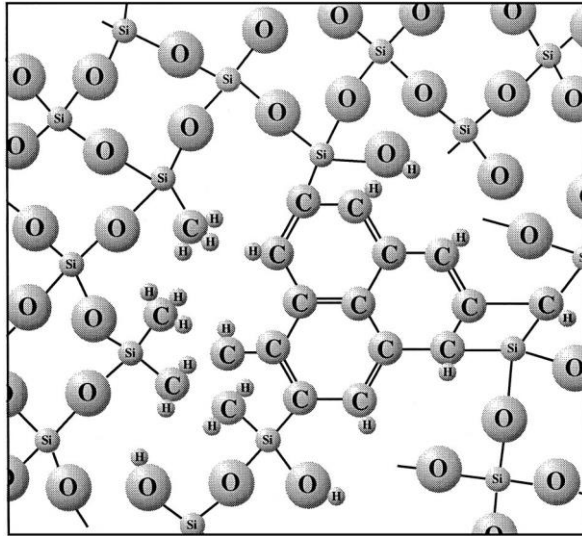


Figure 2.5 SiOC representations by C.G. Pantano et al[15]

In 2005 Scarmi et al had proposed an interesting observation of viscoelastic behavior in carbon rich SiOC ceramic materials[6]. Later a new model for SiOC ceramic structure has been proposed supporting this interesting property by Kleebe[19] et al explaining viscoelastic property observed on continuous loading/ unloading of the carbon rich SiOC glasses. The first model is with carbon embedded in the silica matrix and a second model with graphene encapsulating silica Figure 2.6. The second model was found to be in more agreement with the viscoelastic behavior of SiOC and this model has been supported by the studies on carbon enriched SiOCs. The viscoelastic behavior is connected with the proposed model using the following assumption; with the application of an external stress, the graphene networks deforms and while removing the stress it return back to

its initial state with encapsulating silica inside their networks. This is a time dependent recovery of elasticity without creating any permanent deformation. The viscoelasticity of SiOCs will be accounted in more detail while explaining the lithium storage mechanism of carbon rich SiOCs connecting the breathing of SiOC networks during the process of lithium insertion/ extraction.

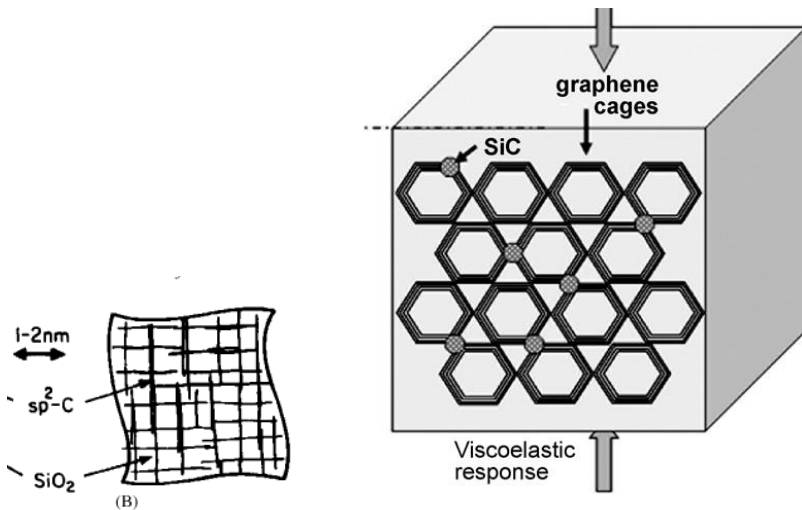


Figure 2.6 Structural distribution in SiOC ceramics proposed to explain the observed viscoelastic properties [6,19]

2.4.1 Nanodomain Model of SiOC

The proposal for the nanodomain concept was motivated from the findings of A. Scarmi et al on their studies about the viscoelastic behavior of SiOC glasses. This model is explained in detail by A. Saha et al with the help of a nanodomain representation of SiOC structure citing unusual properties associated with these materials[20]. The most suitable structure

for explaining the viscoelastic behavior and long term resistance to creep consists of SiO_2 tetrahedra en-caged in cells created by interconnected graphene networks. The cage like cells created by graphene networks will stand as the main attraction of this model. The mixed SiCO bonds exist in the interface between the SiO_2 tetrahedra and graphene networks.

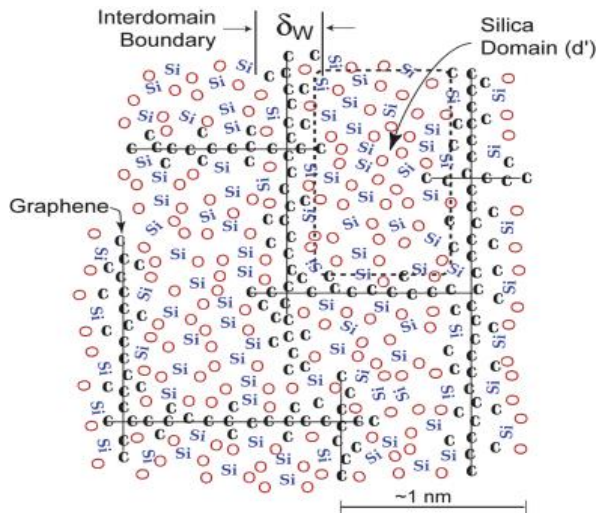


Figure 2.7 Nanodomain model of SiOC ceramic [20]

The nanodomain model is represented in Figure 2.7. The nanodomain model is composed of mainly three components: Cluster of SiO_2 tetrahedra in the center of domains which is surrounded by a monolayer of $\text{SiC}_x\text{O}_{4-x}$, $0 \leq x \leq 4$ mixed bond layer and cage-like networks formed by sp^2 graphene layers. The nanodomain model proposed by A. Saha[20] et al is in well agreement with the NMR and SAXS data. This

model is widely used to explain different properties including the high temperature behavior of SiOC ceramics.

A computational study of SiOC amorphous network has been proposed for SiOCs by P. Kroll in 2003 and an extended version in 2010 by using a computer assisted modeling approach using different stoichiometric compositions of SiOC[21-23]. Different models of stoichiometric silicon oxycarbide glasses had been proposed using theoretical approaches. The modeling is explained by generating continuous random networks of SiOC systems with $Si-C$ and $Si-O$ bonds and then these structures are investigated with density functional theory. This approach was able to predict the critical limit for maintaining a perfect network and onset of defects. These modelings also focus on different aspects of structure, energy and properties using separate models with different elemental inclusions. As an outcome of this study it's found that the lowest energy structures are associated with carbon segregated in extended graphene layers and not bonded to glass matrix. The proposed results showed that beyond a critical limit of carbon concentration network structure is disrupted and it starts to develop structural defects. This limit is explained to coincide with $Si-C$ bond percolation leading to a discontinuous behavior.

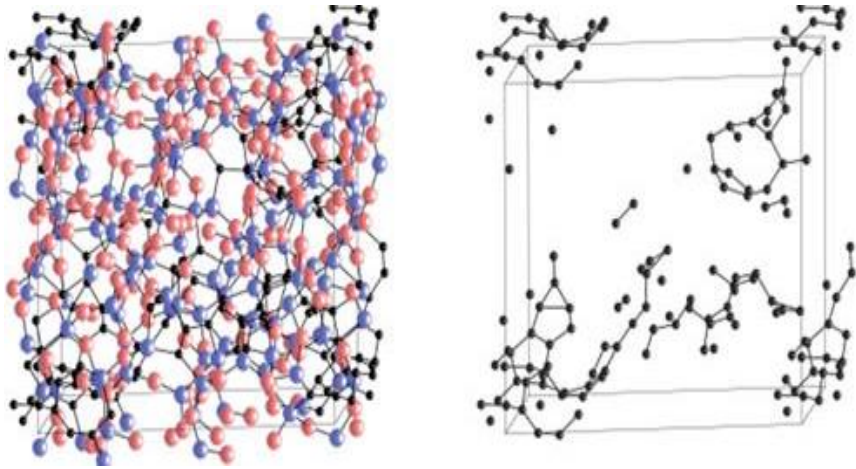


Figure 2.8 An example to show the simulated model of a-SiCO : Cf with excess carbon. The composition is $\text{Si}_{88}\text{C}_{24}\text{O}_{128}\text{C}_{56}$. On the left side the structure is shown as a ball and stick model. Blue, red, and black balls represent Si, O, and C. The right side shows only the carbon atoms in the structure. “Isolated” carbon atoms are part of the SiCO glass [21-23].

The composition of SiOCs can be presented using a ternary Si-C-O diagram with separations into stoichiometric line and region with excess free carbon/ silicon. The stoichiometric SiOC composition is represented by a tie line connecting SiC-SiO₂ compositions. The compositions falling above this tie line have excess free carbon and the one below this line will have excess free silicon. Every part in SiC-SiO₂ tie line corresponds to a specific value of domain size. A ternary representation is presented in Figure 2.9.

insertion through irreversible capacity loss (ICL). These are some of the disadvantages limiting developments of anodes based on SiOC glasses. The main lithium intercalation mechanisms along with potential electrochemically active sites are under investigation and are one of the controversial issues between different scientific communities. There are already some proposed mechanisms and active sites for the reversible lithium storage [25-31] based on different experimental supports.

The highest reversible lithium storage capacity reported for SiOC anodes is 920 mAh g^{-1} with a good rate capability[31]. Xing et al had made a detailed study using different stoichiometric compositions of Silicon oxycarbide ceramics. The capacities of each composition are then presented in a Si-C-O ternary representation. Capacities with different Si-C-O compositions are presented in Figure 2.10. The nature and amount of free carbon is reported to be an important factor in determining the lithium storage properties of SiOC glasses. Recently it has been observed that the mixed bond composition is also actively taking part in the process of lithium intake.

After the initial reports about the possible applications of these materials in lithium ion batteries, studies had carried out widely with SiOCs having different structural and electrochemical features. Structure of Si-O-C networks has been tailored using different synthesis approach using selective polymer precursors. Studies performed up to now points to the possibility of commercial application of these materials in lithium ion batteries. The enhanced specific capacities of SiOCs are accompanied with an extended cycling stability and rate capability. Many research outcomes are there to prove the promising performances for this class of materials.

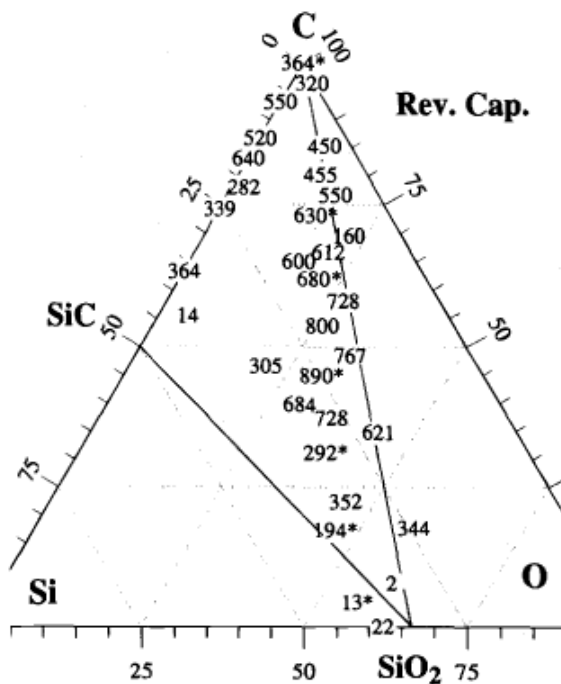


Fig. 3. Reversible specific capacities (in units of mAh/g) of electrochemical test cells for the selected samples shown in Fig. 2.

Figure 2.10 Si-O-C ternary diagram showing different SiOC samples with the delivered Li storage capacity [31]

There exists still a debate between different research groups regarding the active sites for reversible lithium storage. Exact knowledge about different storage sites in this SiOC matrix is necessary to overcome various disadvantages associated with these materials. The main electrochemically active sites in an amorphous SiOC structure includes

SiOC mixed tetrahedral phase, micro pores in amorphous networks, disordered free carbon layers which can store lithium in between sp² graphene layers and also in their edges. The structural and electrochemical features are well correlated and reported in numerous research activities.

The disordered free carbon content is believed to play a crucial role in determining the reversible lithium storage capacity. It has been observed that SiOCs with a considerable amount of free carbon, which lies well above the SiC-SiO₂ tie line, can perform far better compared to stoichiometric SiOCs without any free carbon content. Lithium storage capacity increases with the carbon content up to a particular elemental composition and above this limit capacity starts fading. This shows that there should be a well agreement between different structural phases in amorphous SiOC matrix. A minimum amount of disordered free carbon content is also necessary to ensure the electronic conductivity of these materials to have better lithium diffusion.

The main disadvantage of this type of materials in the form of larger irreversible capacity during first cycle of charging/discharging can be attributed to many possibilities. Presence of micropores in the structure may act as a trap for lithium ions during initial charging. Presence of defects in the structure, mainly dangling bonds in the form of carbon radicals or silicon radicals which are formed due to release of organic moieties and hydrogen during high temperature treatment can form various traps resulting in irreversible lithium storage. The dangling bonds are already reported to be acting as a trap for any potential electronic applications because of their reactive nature. Presence of oxygen content is also sometimes blamed to be one of the reasons for irreversible lithium storage in the form of *Li₂O*, which once formed is found to be irreversible (Wilson et al). These problems lead to loss of a specific amount of capacity during initial cycling of a battery.

Generally, Formation of SEI film, lithium storage in micro pores inside materials, irreversible lithium trap on oxygen etc. are responsible for the irreversible capacity loss (ICL). Studies are going on to overcome these problems to realize the applications of these materials in commercial batteries. Another important disadvantage of SiOC anode is the existence of significant hysteresis between lithium insertion and extraction process. There exists a significant hysteresis leading to a capacity loss during discharging. The hysteresis found to be higher in case of samples with substantial amount of hydrogen content. Presence of hydrogen in SiOC matrix results in a much higher hysteresis because of changes in hybridization state of free carbon during lithium intake and extraction.

Characterization of anode materials after lithium storage, i.e., the analysis of lithiated electrodes is an important step to understand clearly the different possible intercalation mechanisms in these materials. It is a really difficult task to achieve an external characterization of the lithiated SiOC materials as these materials are very sensitive to ambient atmosphere and are more reactive than lithium metal. Lithiated electrodes should be treated with high care to avoid the decomposition. Possible characterization techniques for studying lithiated anodes include Raman spectroscopy, NMR, ESR, SEM etc. The availability of any in situ measurement facilities avoiding direct contact of lithiated samples with external environment will be more suitable to understand the clear reaction profiles. Suitable techniques for analyzing lithiated anode materials includes ^{29}Si and ^7Li MAS NMR which can provide information about the environment of both silicon and lithium atoms. Lithium NMR studies of disordered carbon materials had been already reported by Wang et al.[32] showing different active sites for lithium ion storage.

^7Li MAS NMR studies on SiOCs anodes carried out by Fukui et al. reported different possible environments for lithium in the lithiated anode materials. It has been reported that lithium ions are occupying not only the place between carbon layers but also at the edges of these layers.

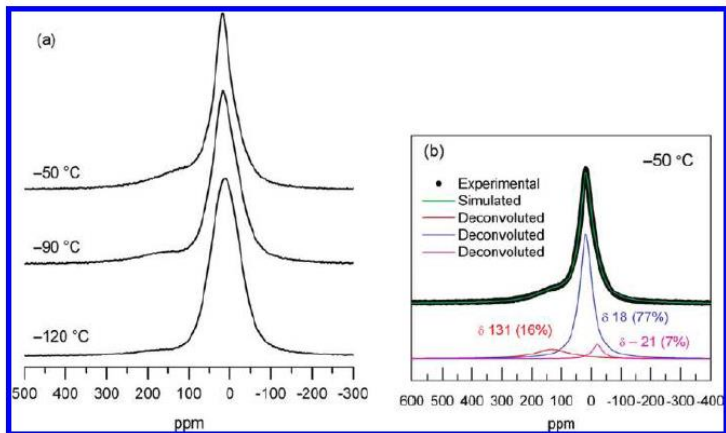


Figure 2.11 Low-temperature ^7Li NMR spectra of SiOC samples at fully lithiated state. (Adapted from Ref. Fukui et al)[25]

The spectrum recorded at low temperature is deconvoluted into three components in the fully lithiated state attributing lithium storage in between carbon layers, but also in the edges of each networks and micropores.

Lithium storage properties of SiOC ceramics are influenced by the temperature and pyrolysis atmosphere during sintering the ceramics. SiOC materials prepared at a temperature above $800\text{ }^\circ\text{C}$ reported to have the maximum lithium storage capability. Formation of different Si-O-C mixed units and free carbon separation in oxycarbide ceramics starts to appear

only above a pyrolysis temperature of 800 °C. Formations of mixed bonds at this temperature are evidenced with the support of NMR studies. This shows the importance of mixed SiOC units in reversible lithium storage. Capacity is found to be larger for 800-900 °C pyrolysed samples, but these samples show significant hysteresis in the lithium insertion / extraction curve leading to a considerable amount of capacity loss. The hysteresis is found to be reduced over 1000 °C pyrolysis temperature. The main reason for this hysteresis is attributed to the presence of residual hydrogen in the final ceramics prepared at 800-900 °C samples. It's already reported by Dahn et al [34,35] that presence of hydrogen attached to edges of disordered carbon networks help to increase the lithium storage capacity and cycling stability. The proposed mechanism is by bonding lithium to the edge carbon atoms having hydrogen attached along with the normal intercalation mechanism. Generally this process results in hysteresis as there occurs a change in hybridization of carbon atom from sp^2 to sp^3 during lithium bonding.

As per the general research outcomes best performance is observed for samples pyrolysed at 1000 °C, at this temperature the formation of mixed bonds is complete with a noticeable reduction in the residual hydrogen content compromising the capacity loss from hysteresis. Even these samples show a hysteresis, which is explained in connections with multiple reasons relating interfacial energy barriers and internal polarization inside the system. The lithium storage capacity starts to diminish with pyrolysis temperature higher than 1000 °C because of phase separation to carbon rich and oxygen rich species along with ordering of free carbon phase at higher temperatures. Ordered carbons are reported to offer reduced capacity and stability compared to the disordered carbon networks. Kaspar et al had reported the variation of lithium storage capacity with increasing pyrolysis temperature. The best performance is observed from

samples prepared at 800-1100 °C and pyrolysis temperature above 1200 °C lead to phase separation of SiC and SiO₂ species with consumption of mixed SiOC units along with ordering of free carbon network resulting in a reduced lithium storage capacity. Reduction of capacity with increasing heat treatment temperature is a well-known phenomenon. Also SiC formed after 1400 °C is proposed to be inactive towards the lithium storage.

Main research on SiOC is currently focused on understanding different electrochemically active sites for the reversible lithium storage. The complete understanding of different structural and electrochemical features is necessary to improve their capacity and performance as potential anode materials with enhanced cycling stability.

References

- [1] R. Reidel, "Advanced ceramics from inorganic polymers, in Processing of ceramics, Part II,; Material science and technology", E. R.J. Brook, Editor. 1996, VCH: Weinheim, Germany. p. 1-50.
- [2] W. Verbeek, "Production of shaped articles of homogeneous mixtures of silicon carbide and nitride", 1973: Germany (Bayer AG).
- [3] S. Yajima, Y. Hasegawa, K. Okamura and T. Matsuzawa, "Development of high tensile strength silicon carbide fibre using an organo silicon polymer precursor", Nature, 273 (1978)
- [4] P. Greil, "Polymer derived engineering ceramics", Advanced Engineering Materials, 2(6)(2000)
- [5] T. Rouxel, G.Massouras and G.D.Soraru., "High Temperature Behavior of a Gel-Derived SiOC Glass: Elasticity and Viscosity", J. Sol-Gel Science and Technology, 14(1999)
- [6] A. Scarmi, G.D. Sorarù and R. Raj, "The role of carbon in unexpected visco(an)elastic behavior of amorphous silicon oxycarbide above 1273K", J. Non-Crystalline Solids, 351(27-29) (2005) 2238-2243
- [7] H. Brequel, J. Parmentier., G.D. Soraru, L. Schiffini and S. Enzo, "Study of the Phase Separation in Amorphous Silicon Oxycarbide Glasses Under Heat Treatment", NanoStructured Materials, 11(6) (1999)
- [8] H. Brequel, J.Parmentier., S. Walter, R. Badheka, G. Trimmel, S. Masse, J. Latournerie, P. Dempsey, C. Turquat, A. Desmartin-

-
- Chomel, L. Le Neindre-Prum, U. A. Jayasooriya, D. Hourlier, H.-J. Kleebe, G. D. Soraru, S. Enzo, and F. Babonneau, "Systematic Structural Characterization of the High-Temperature Behavior of Nearly Stoichiometric Silicon Oxycarbide Glasses", *Chem. Mater.*, 16 (2004)
- [9] G.D. Soraru, S. Modena, E. Guadagnino, P. Colombo, J. Egan and C. Pantano, "Chemical Durability of Silicon Oxycarbide Glasses", *J. Am. Ceram. Soc.*, 85(6) (2002)
- [10] G.D. Soraru and D. Suttor, "High Temperature Stability of Sol-Gel-Derived SiOC Glasses", *J. Sol-Gel Science and Technology*, 14 (1999)
- [11] P. Colombo, et al., "Polymer-Derived Ceramics: 40 Years of Research and Innovation in Advanced Ceramics", *J. Amer. Ceram. Soc.*, 93(7)(2010) 1805-1837.
- [12] R.J.P. Corriu, D. Leclercq., P.H. Mutin and A. Vioux, "Preparation and Structure of Silicon Oxycarbide Glasses Derived from Polysiloxane precursors" *J. Sol-Gel Science and Technology*, 8 (1997) 327-330
- [13] P.H. Mutin, "Control of the Composition and Structure of Silicon Oxycarbide and Oxynitride Glasses Derived from Polysiloxane Precursors", *J. Sol-Gel Science and Technology*, 14 (1) (1999) 27-38
- [14] I.F. Hurwitz and M.A.B. Meador, "Tailoring Silicon Oxycarbide Glasses for Oxidative Stability", *J. Sol-Gel Science and Technology*, 14(1) (1999) 75-86
- [15] C.G. Pantano, A.K. Singh and H. Zhang., "Silicon Oxycarbide Glasses", *J. Sol-Gel Science and Technology*, 14(1)(1999)7-25

-
- [16] J. Latournerie, P. Dempsey, D.H. Bahloul and J.P. Bonnet, "Silicon Oxycarbide Glasses: Part 1-Thermochemical Stability", *J. Amer. Ceram. Soc.*, 89(5) (2006) 1485-1491.
- [17] T.H. Elmer and H.E. MEISSNER, "Increase of annealing point of 96% SiO₂ glass on incorporation of carbon", *J. Amer. Ceram. Soc.*, 59(5-6) (1976)
- [18] G.D. Soraru, L. Pederiva, J. Latournerie and R. Raj, "Pyrolysis Kinetics for the Conversion of a Polymer into an Amorphous Silicon Oxycarbide Ceramic", *J. Amer. Ceram. Soc.*, 85 (2002)
- [19] H.-J. Kleebe and Y.D. Blum, "SiOC ceramic with high excess free carbon", *J. Eur. Ceram. Soc.*, 28(5) (2008) 1037-1042.
- [20] A. Saha, A., R. Raj, and D.L. Williamson, "A Model for the Nanodomains in Polymer-Derived SiCO", *J. Amer. Ceram. Soc.*, 0(0) (2006)
- [21] P. Kroll, "Searching insight into the atomistic structure of SiCO ceramics", *J. Mater. Chem.*, 20(46) (2010) 10528.
- [22] P. Kroll, "Modelling and simulation of amorphous silicon oxycarbide", *J. Materials Chemistry*, 13(7) (2003) 1657
- [23] P. Kroll, "Modelling polymer-derived ceramics", *J. Eur. Ceram. Soc.*, 25(2-3) (2005) 163-174
- [24] P.E. Sanchez-Jimenez and R. Raj, "Lithium Insertion in Polymer-Derived Silicon Oxycarbide Ceramics", *J. Amer. Ceram. Soc.*, 93(4) (2010) 1127-1135.
- [25] H. Fukui, H. Ohsuka, T. Hino and K. Kanamura, "A Si-O-C composite anode: high capability and proposed mechanism of lithium storage associated with microstructural characteristics", *ACS Appl. Mater. Interfaces*, 2(4) (2010) 998-1008

-
- [26] X. Liu, M.-C. Zheng and K. Xie, "Mechanism of lithium storage in Si–O–C composite anodes", *J. Power Sources*, 196(24), 2011 10667-10672
- [27] J. Kaspar, M. Graczyk-Zajac and R. Riedel, "Carbon-rich SiOC anodes for lithium-ion batteries: Part II. Role of thermal cross-linking", *Solid State Ionics*, 225 (2012) 527-531
- [28] M. Graczyk-Zajac, L. Toma, C. Fasel and R. Riedel, "Carbon-rich SiOC anodes for lithium-ion batteries: Part I. Influence of material UV-pre-treatment on high power properties", *Solid State Ionics*, 225 (2012) 522-526.
- [29] H. Fukui, H. Ohsuka, T. Hino and K. Kanamura, "Polysilane/Acenaphthylene Blends Toward Si–O–C Composite Anodes for Rechargeable Lithium-Ion Batteries", *J. Electrochem. Soc.*, 158(5) (2011) A550.
- [30] D. Ahn and R. Raj, "Cyclic stability and C-rate performance of amorphous silicon and carbon based anodes for electrochemical storage of lithium", *J. Power Sources*, 196(4) (2011) 2179-2186.
- [31] W. Xing, A.M.Wilson., K. Eguchi, G. Zank and J. R. Dahn, "Pyrolyzed Polysiloxanes for Use as Anode Materials in Lithium-Ion Batteries", *J. Electrochem. Soc.*, 144(7) (1997)
- [32] S. Wang, H. Matsui, H. Tamamura and Y. Matsumura, "Mechanism of Lithium Insertion in to Disordered Carbon", *Physical Review B*, 58(13) (1998) 8163-8165.
- [33] G.D. Soraru, F. Dalcanale, R. Camprostrini, A. Gaston, Y. Blum, S. Carturan, P.R. Aravind, " Novel polysiloxane and polycarbosilane aerogels via hydrosilylation of preceramic polymers", *J. Mater. Chem.*, 22 (2012) 7676-7680

-
- [34] T. Zheng, "Hysteresis during Lithium Insertion in Hydrogen-Containing Carbons", J. The Electrochem. Soc., 143 (7) (1996) 2137.
- [35] P. Papanek, M.Radosavljevic and J.E.Fischer., "Lithium Insertion in Disordered Carbon-Hydrogen Alloys: Intercalation vs Covalent Bindin", Chem. Mater., 8 (1996) 1519-1526.
- [36] G. Mera, A. Navrotsky, S. Sen, H-J. Kleebe and R. Riedel, " Polymer derived SiCN and SiOC ceramics- Structure and energetics at the nanoscale", J. Mater. Chem. A, 1 (2013) 3826–3836

Chapter 3. Experimental Setup - Synthesis and Characterization of SiOC Glass Networks

3.1 Synthesis of SiOC Ceramics

Different techniques have been implemented successfully to synthesize silicon oxycarbide ceramics with varying O/Si ratios and C/Si ratios. Mainly used synthesis approaches were based on hydrosilylation reactions and sol-gel method. Detailed explanations about various synthesis techniques have given in section 2.3.

The starting precursors are polymers bearing $Si-H$ and $C=C$ moieties (for hydrosilylation) and hybrid alkoxides with terminal organic groups (for sol-gel). The cross linked polymer networks are then pyrolysed in controlled atmospheres to obtain the final SiOC ceramic network. Different cross linking approaches along with used polymer precursors are explained below.

3.1.1 Hydrosilylation

Hydrosilylation process involves the addition of Si-H bonds in poly siloxanes across unsaturated bonds ($C=C$). Different compositions of SiOC samples are prepared by selectiv choosing starting precursors. Selection of suitable precursors is a key step to predesign the structure and properties of final ceramics. The starting precursors used for synthesis of SiOC ceramics by hydrosilylation are polyhydridimethyl siloxane (PHMS), which is having $Si-H$ bonds in the structural network. PHMS is cross linked either with 1,3,5,7 tetramethyl 1,3,5,7 tetravinyl cyclotetrasiloxane (TMTVS) or with divinylbenzene (DVB). TMTVS is a cyclic siloxane used as cross linking agent for the synthesis of SiOC with low carbon content. DVB is used for the synthesis of SiOC with high carbon content.

The main reaction occurs between the $Si-H$ and $C=C$ bonds generating new $Si-C$ bonds. A typical platinum catalyzed hydrosilylation reaction is represented in chapter 2. The starting precursors used for current study are presented in Figure 3.1.

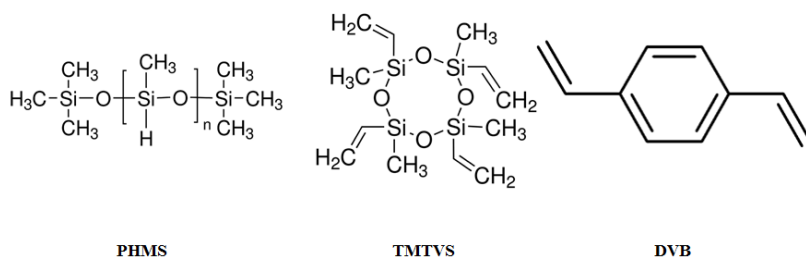


Figure 3.1 Different precursors used for hydrosilylation reaction

Low Carbon SiOCs From PHMS/TMTVS Starting Precursors

The starting precursors used to prepare low carbon SiOCs are polyhydridomethyl siloxane and 1,3,5,7 tetramethyl 1,3,5,7 tetravinyl cyclotetrasiloxane. The final SiOC ceramics are observed to be with low free carbon content.

The cross linking is carried out in the presence of a platinum catalyst to initiate the reaction. The catalyst used for cross linking was platinum divinyltetramethyldisiloxane complex, ~Pt 2% in xylene (Sigma-Aldrich, St. Louis, MO, USA). The composition of final ceramics is tuned by changing the ratio of PHMS/ TMTVS. Different ratios used for starting precursors are given in Table 3.1. Polymers in different ratios are cross linked and the resulting mixture is stirred for few minutes, cast in plastic

tubes, which are then allowed to stand at room temperature for the whole night for setting. Finally samples are left at 60 °C to complete the curing process. The cured materials were hard elastomeric transparent resins. These cross linked resins are then pyrolysed in argon atmosphere at temperatures of 1000-1300 °C to obtain final ceramics.

| Sample name | PHMS | TMTVS |
|-------------|------|-------|
| PT2 | 10g | 1.32g |
| PT5 | 10g | 2.64g |

Table 3.1 Estimated composition of starting precursors

Carbon-rich SiOCs From PHMS/DVB Starting Precursors

PHMS with DVB (divinylbenzene) as cross linking agent results in carbon enriched silicon oxycarbide glasses. Carbon rich SiOC ceramics prepared from this combination have excellent properties towards repeated lithium insertion/extraction. In a typical preparation PHMS is crosslinked with DVB in presence of a platinum catalyst. The mixture is stirred for a while to have a homogeneous mixture. The whole mixing should be done in an ice bath as the cross linking process is highly exothermic. After stirring for 10 minutes the solution is casted in plastic tubes and left in room temperatures for whole night to observe gelation. The gels are then cured at 60 °C for some days to have a hard rubbery material. The dried gels are then pyrolysed at temperatures of 1000-1300 °C to obtain final SiOC ceramics. The composition of final SiOC is varied by changing different proportions of PHMS/ DVB precursors. The used compositions are reported in Table3.2.

| Sample name | PHMS | DVB |
|-------------|------|-----|
| PD1 | 10g | 5g |
| PD2 | 10g | 20g |

Table 3.2 Estimated composition of starting precursors

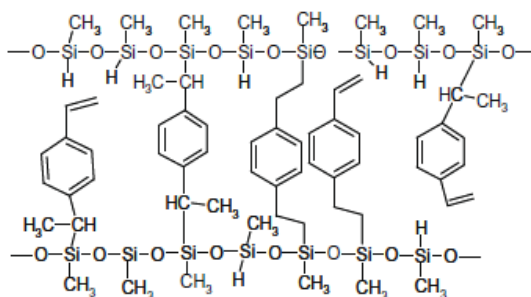


Figure3.2 Typical representation of Cross linked networks using PHMS/DVB system

[5]

3.1.2 Sol-gel

General explanation about sol-gel technique has given in chapter 2. Primary goal of the sol-gel synthesis is to improve the mechanical properties of silica glass by incorporating large amount of carbon in to their networks. Most widely used alkoxides for sol-gel synthesis of silicon oxycarbide ceramics includes, methyltriethoxysilane (MTES), dimethyl diethoxysilane

(DMDES) and phenyl triethoxysilane (PhTES). These precursors are used individually or as combinations to tailor the final composition of SiOC ceramics. The composition of final ceramic varies according to different organic groups attached to the alkoxides. The procedure for synthesis starts with mixing alkoxides in a proper ratio with or without alcoholic solvents and the mixture is then hydrolysed using stoichiometric amount of acidic water followed by condensation reaction to obtain cross linked gel networks.

The alkoxides used for our studies are methyltriethoxysilane and phenyltriethoxysilane. The difference between both lies on different organic groups attached to silicon atom ie, methyl and phenyl groups respectively. General procedure for the synthesis of SiOC remains same for both the alkoxides.

MTES (Methyl triethoxysilane)

Low carbon SiOC samples have been prepared from methyl triethoxysilane cross linked via sol-gel technique using acidic water for hydrolysis and ammonia solution for condensation. In a typical preparation methyltriethoxy silane is hydrolysed by adding stoichiometric amount of acidic water. Molar ratio of Si/H₂O was maintained 1/3 molar ratio to hydrolyse all the three ethoxy groups. The solution is then refluxed for one hour at 70 °C to promote the hydrolysis process. To promote condensation, an ammonia solution (30 wt %) was added to the alkoxide solution (NH₃/MTES=1/5). The mixture is then left for gelation in open plastic tubes. Gels were then dried for one week at 60 °C. Dried gels are then pyrolysed at 1000 and 1400 °C to obtain final SiOC ceramics. Different alkoxides used for this study is represented in **Figure 3.3**. MTES stands for methyltriethoxysilane and PhTES stands for phenyltriethoxysilane.

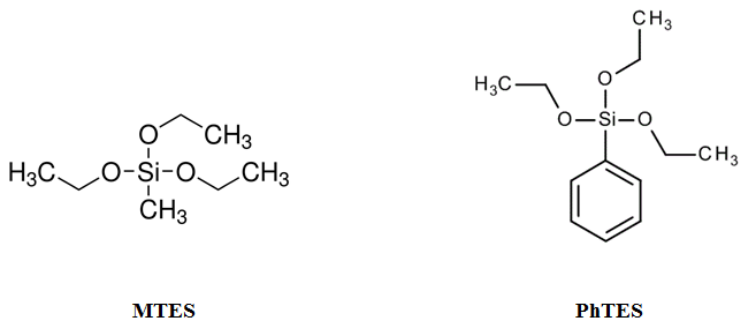


Figure 3.3 Structural representations of alkoxides for sol-gel synthesis of silicon oxycarbide ceramics.

MTES/PhTES (Methyl triethoxysilane/ Phenyl triethoxysilane)

Methyl triethoxysilane (MTES) was mixed with phenyl triethoxysilane (PhTES) in a molar ratio of 2:1. Presence of phenyl groups in the starting precursor will lead to increased carbon content in the final ceramic. The mixture was crosslinked via sol-gel method using acidic water for hydrolysis. Both the alkoxides were first mixed in ethanol solvent to have better homogeneous phase before adding acidic water. The solution is then refluxed after adding acidic water with a molar ratio of Si/H₂O 1:3 at 70 °C for one hour. Then it is cooled down to room temperature and transferred to plastic tubes for gelation. Gelation time is observed to be 4 days at room temperature. Gels are then dried at 60 °C for one week.

The pyrolysis of the crosslinked gels was then carried out in controlled argon atmosphere at different temperatures (1000-1400 °C). A schematic representation of MTES after cross linking is presented in Figure 2.2.

3.1.3 Effect of Heat Treatment

Pyrolysis temperature is a key factor in determining different properties of oxycarbide materials. SiOCs are formed at a pyrolysis temperature of more than 900 °C. At 1000 °C, SiOC structure consists of a mixture of different SiOC units of SiC_xO_{4-x} , $0 \leq x \leq 4$ as evidenced by ^{29}Si MAS NMR measurements. Increasing pyrolysis temperature above 1250°C leads to the phase separation of C-rich and O-rich units with the consumption of mixed SiOC units. Temperature above 1400°C results in separation of nanocrystalline SiC and cristoballite and this can be evidenced by XRD and NMR studies. When the temperature reaches 1500°C carbothermal reduction comes in to action. The SiOC samples for our studies are prepared in the temperature range of 1000-1400°C to have complete understanding of lithium storage properties of different SiOC forms towards repeated lithium storage.

Pyrolysis of all the studied samples was carried out using Lindberg Alumina tubular furnace with a maximum operational temperature of 1700 °C. Cross linked precursors for heat treatment were placed in alumina crucibles. The tubular furnace is fluxed with argon gas for one hour prior to heat treatment to eliminate other gases and then programmed to corresponding temperatures with a maximum heating rate of 5 °C/minute under flowing argon gas atmosphere and holding time of 1hr at maximum.

3.1.4 Effect of Pyrolysis Gas Atmosphere

Pyrolysis of SiOC ceramics requires an inert atmosphere to avoid oxidation. Usually the pyrolysis of polymer precursors was performed under inert atmospheric conditions such as under Ar or N₂ gas flow. Gases used for our studies are pure argon atmosphere and a mixture of Ar/H₂ (5%H₂) gas atmosphere. Main intention behind usage of hydrogen containing atmosphere was to reduce the concentration of dangling bonds in the final SiOC network by terminating the radicals with hydrogen forming C – H bonds. The holding times at maximum temperatures were 1hr for Argon pyrolysed samples and 7hrs for samples pyrolysed under hydrogen containing atmosphere. The gas flow was maintained with a flux rate of 100 mL/min.

3.2 Structural Characterization

3.2.1 Thermogravimetric (TG/DTA) Studies

Thermogravimetric TG/DTA methods are important to understand the thermal evolution of polymer derived ceramics. This technique clearly points out different processes occurring as part of heating with evolution of volatile species at specific temperature range. Thermo gravimetric graph represents the weight loss due to these volatile evolutions as a function of heating temperature. TG graph also helps to understand the final ceramic yield after whole heating and it also predict the onset of decomposition reactions such as carbothermal reduction, which occurs after 1500 °C in case of SiOC ceramics.

DTA measurements in general help to identify different phase separation process including the crystallization and melting of different

phases during entire heating program. The crystallization and melting are associated with an energy consumption or energy release as noticed by an endo and exo peaks respectively.

The thermogravimetric (TGA) experiments were performed using Netzsch equipment (Model STA 409, Netzsch-Geratebau GmbH, Germany). The heat treatment was carried out under an argon atmosphere at a flux of 100 mL/min, with a heating rate of 10 °C/min up to 1500 °C.

3.2.2 Elemental Analysis

Elemental analysis is used to determine the composition of different elements present in the system. In case of silicon based PDC materials, generally the weight % of different elements such as C, H, N, O etc. are determined and then the amount of silicon is calculated as a difference to 100%.

A Leco TC-200 and TC-436 (Leco Corp., USA) are used to determine the carbon and the oxygen content respectively. Hydrogen content is analyzed by Labor Pascher (Remagen-Bandorf, Germany). Silicon content is calculated as a difference to 100 wt%.

3.2.3 X-ray Diffraction Studies

X-ray diffraction studies are an important characterization technique to understand the crystalline/ amorphous nature of ceramic materials. Silicon oxycarbide ceramics pyrolysed at low temperatures (900-1200 °C) are usually X-ray amorphous. Generally SiOC ceramics gives a broad peak corresponding to silica centered around 22 ° along with the peaks of SiC at 35°, 60°, and 72° for high temperature pyrolysed samples. XRD spectra help to find out the crystalline size of different phases present in amorphous SiOC ceramics. Carbon present in SiOC also used to give a peak at $2\theta = 26^\circ$

along with some small peaks at higher 2 theta angle. Ordering of carbon networks and formation of SiC and SiO₂ rich species can be confirmed from XRD spectra.

X-ray diffractograms were collected from Rigaku D-Max diffractometer (Rigaku, Tokyo, Japan) in the Bragg-Brentano configuration using CuK α radiation operating at 40kV and 30mA. The scanning range was 10-80° with a step rate of 0.05° and acquisition time of 5s per point.

3.2.4 NMR

Nuclear magnetic resonance is an important technique to gather different structural information. The existence of nuclear spins and transitions between nuclear spin energy levels give rise to the phenomenon of NMR, the corresponding property of electron spin leads to electron spin resonances. NMR is based on the principle that electrons and certain nuclei possess a magnetic momentum μ associated with an angular orbital momentum l and a spin momentum S . When a magnetic field of strength B is applied in a defined direction, a magnetic moment “ μ ” would have energy

$$U = -\mu * B$$

$$U = -\mu_z * B, \mu_z \text{ is the component of } \mu \text{ in the Z- direction}$$

$$\mu_z = g_n \mu_z m_l = \gamma \hbar m_l / 2\pi \quad (\gamma \text{ is the gyromagnetic ratio, a constant}$$

for each nucleus, m_l is one of the $2I+1$ value that m can assume)

Overall NMR spectroscopy is used to study molecules whose nuclei possess nuclear spin moments different from zero. If B is fixed, the resonant frequency is an intrinsic feature of the nucleus under consideration (Larmor frequency). Information about different structural environments of specific nuclei under investigation could be identified by applying a magnetic field

and observing the frequency of resonant electromagnetic field. A typical NMR spectrometer consists of a magnet that can produce a uniform intense field and an appropriate source of electromagnetic radiofrequency radiation. The resonance frequencies are expressed in terms of an empirical quantity called chemical shift, which is the difference between the resonance frequency ν , of the nucleus in question and that of a reference standard.

$$\delta = \frac{\nu - \nu^\circ}{\nu^\circ} * 10^6$$

Different chemical groups in a compound give peaks at specific chemical shift values corresponding to it. Existence of chemical shift helps to explain several important features of the spectrum.

Solid state NMR is an important technique to identify the mixed bond environments of silicon atoms in SiOC ceramics. Solid state NMR is a powerful technique to determine local molecular environments. In solid-state NMR, such as gels, microcrystalline powders etc.; molecules show a less mobility with respect to solution-phase. The sample rotation averages all the possible orientation assumed by the molecules only to a less extent. Thus the dipolar coupling, electron interaction, scalar and quadrupolar coupling, and a chemical anisotropy, due to all possible molecular orientation lead to a significant line broadening and very long spin-lattice relaxation times. Solid state NMR has been applied to variety of molecular systems such as, organic-inorganic complexes, aluminosilicate minerals, polymers, glasses, ceramics etc.

^{29}Si NMR spectrum is considered as a finger print of SiOC ceramics. ^{29}Si MAS NMR studies on SiOC ceramics shows the formation of

mixed SiOC units, such as SiO₄, SiO₃C, SiO₂C₂, SiC₄ etc in the final ceramic after pyrolysis at higher temperature. The carbon phase can be identified using ¹³C MAS NMR for a low temperature pyrolysed samples (<800 °C) and above this temperature the spectrum lacks clarity due to extremely longer relaxation time and the intrinsic broadening of the electric features of aromatic carbon structures (graphene). In general NMR spectra can be used as a tool to explain the polymer to ceramic conversion.

The ²⁹Si MAS NMR experiments were performed with an AVANCE 300 Bruker using a 4mm probe-head (Bruker Instruments, Karlsruhe, Germany). All the spectra are recorded using single pulse experiments at 45° with a pulse of 2.6 μs with a recycle delay of 100s and 8 kHz of spinning speed.

3.2.5 Electron Paramagnetic Resonance (EPR)

Electron paramagnetic resonance or electron spin resonance (ESR) is used to identify different paramagnetic species, including organic radicals, inorganic radicals, and triplet states having unpaired electrons in their valance shell by observing the magnetic field at which they came in to resonance with monochromatic radiation. The basic principle behind EPR is very similar to the NMR spectroscopy, except that EPR focus on electron spins in a molecule. This is a microwave technique in which the spectrum is determined using radiation falling in the X-band of the microwave region. A lay out of a typical ESR spectrometer is represented in Figure 3.6. ESR spectrometer consists of a microwave source, a sample cavity, microwave detector and electromagnets capable of applying variable fields. EPR spectrum is usually represented as a first derivative of microwave absorption

spectra. The spin magnetic moment interacts with the local magnetic field and the resonance condition is represented as

$$h\nu = g\mu_B B$$

Where g = proportionality factor called g -factor of specific radicals, Bohr magneton (9.274×10^{-24} J/T) and B is the applied magnetic field. Knowledge of g -factor helps to identify the electronic structure of radicals. E.g. g -value of carbon radicals is at 2.0023. Shift in g -factor occurs with changes in electronic environments.

Main application of EPR spectra in SiOC ceramics is to find out different defects in the form of carbon dangling bonds/ silicon dangling bonds, which exists in the form of immobilized radicals carrying an unpaired electron. Generally inorganic networks obtained from polymer pyrolysis have a small part of carbon or silicon atoms having an unpaired electron. These radicals are immobilized with in the amorphous networks. EPR will help to identify the type and concentration of each radical by comparing the spectra with the spectrum of a known internal standard like Cu^{2+} .

EPR analyses were carried out with a Bruker EMX instrument operating in the X band at 9.77G at room temperature with the following parameters: 0.20mW microwave power, 0.2G modulation amplitude, 5E2 receiver gain, 2k points, 1 scan. DPPH was used as external reference for calibrating the spectra. The spin concentration was calculated by using Cu^{2+} compound as internal standard whose number of spins is known.

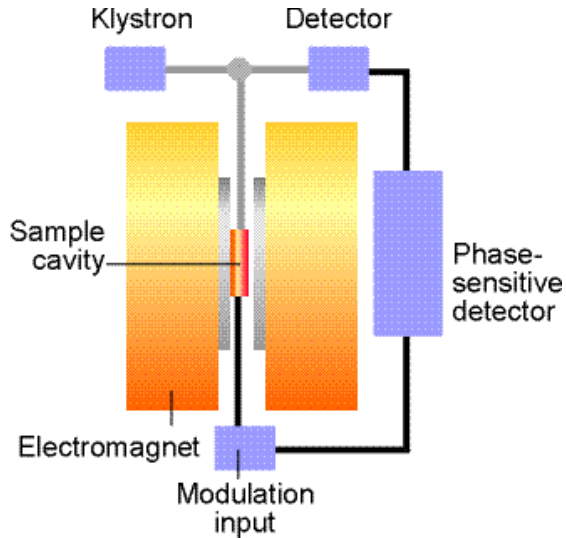


Figure 3.6 Lay out of an EPR spectrometer [1]

3.2.6 Raman Spectra

Raman Spectroscopy is considered as an important tool for the characterization of different modifications of carbonaceous materials. The Raman spectra of disordered carbons generally exhibits two strong peaks named D-band and G-band respectively. The D-band is due to the disorder induced vibrations of 6-fold aromatic rings and G-band represents the in plane bond stretching of sp^2 hybridized carbon pairs. The D and G bands in disordered carbon materials are normally observed at 1340 cm^{-1} and 1580 cm^{-1} respectively. Also at 2700 and 2900 cm^{-1} two peaks are observed in some cases which are called 2D and G+D corresponding to the overtones or combinations of Raman fundamental bands. The development of 2D band indicates the degree of organization. In amorphous carbons the

development of D peak indicates the ordering of carbon network exactly opposite from the case of graphite. The strength of D band is proportional to the probability of finding a 6 fold ring in the cluster. The crystallite size and ordering of carbon networks can be found out from the intensity ratios of D and G bands.

According to the 3-stage model proposed by Ferrari and Robertson the crystallite size is estimated using the intensity ratio of D and G bands. The Ferrari Robertson formula to determine the carbon cluster size is represented as

$$I_D/I_G = C'(\lambda) L_a^2$$

Where C' is a coefficient that depends on the excitation wavelength of laser, $C'(514 \text{ nm}) = 0.0055 \text{ \AA}^\circ$ and L_a is the lattice parameter.

The Raman spectra were collected on a Jobin Yvon Raman spectrometer (Horiba-Jobin Yvon, model T6400) with an excitation wavelength of 514 nm (Ar laser) and spectra were detected by a CCD (256x1024 pixels) cooled by liquid nitrogen.

3.3 Electrochemical Characterization

3.3.1 Electrode Preparation

Electrode preparation is a key step to control the performance of the anode material. Metallic foil, for anode materials typically copper is coated with thin layer of active material. Metallic foil plays a role of current collector, so the material should be uniformly distributed and should adhere

well to the foil. Lithium storage properties depend on parameters such as electrode thickness and uniformity of distribution of active materials. A binder is always used in a specific ratio to ensure good adhesion of active material to the current collector and to its own particles. Carbon black is also used in a very small amount to ensure electronic contact between the grains of the material which is important to facilitate the diffusion of electrons and cations.

Electrodes are made by making homogeneous slurry of the samples with polyvinylidene fluoride (PVdF, SOLEF, Germany) as binder and carbon black as a conducting medium in the weight ratio 85:10:5 using N-methyl pyrrolidone (NMP, BASF, Germany) as the solvent. The slurry is coated with a hand blade on the rough side of a thin copper foil (10 μ m, Copper SE-Cu58, Schlenk Metallfolien GmbH & Co KG) and dried at 80 °C for 12 hours. After drying the electrodes are cut into 7mm size and pressed at a pressure of 20 kN cm⁻². The electrodes are then weighed and dried in a Buchi vacuum oven at 80 °C for 24 hours and directly transferred to the glove box with Argon atmosphere. Picture represented below shows a typical electrode made from SiOC powders in the ratio 85% SiOC +10% PVDF +5% Carbon black.

3.3.2 Cell Assembly

A cell can be assembled in different ways. Main types of cell assembly include coin cells and Swagelok® type cells. Swagelok cell assembly got more interest as it can be cleaned and reused again for multiple times, whereas coin cells have to be dismantled after the experiments. The Swagelok systems are easy to handle and it is just a modified set up using some simple tube fittings. A typical Swagelok cell assembly will have a good sealing against leakage and air intrusion. The inner part of the Swagelok cell assembly is composed of plastic material

which is stable in electrolytes and will be electrically insulating. Metallic fittings with inner plastic coatings are used for high temperature studies.

Electrodes are dried in vacuum to remove any attached impurities. The dried electrodes are then assembled in a two electrode Swagelok® type cell with lithium metal as the counter/reference electrode (99.9% purity, 0.75mm thick, Alfa Aesar, Germany) and SiOC as the working electrode with a Whatman™ quartz microfiber filter (QMA, UK) separator between electrodes, the electrolyte used is a high purity solution of 1M LiPF₆ in ethylene carbonate and diethyl carbonate mixture of weight ratio 1:1 (LP 30, Merck KGaA, Germany). A typical anode contains 3-5 mg cm⁻² of the active material. Cells are assembled in an argon-filled glove box.



Figure 3.7 Swagelok type cell assembly and electrode representation

3.3.3 Galvanostatic Charging/Discharging

Charging/ discharging of a battery represent consecutive lithium insertion / extraction. During galvanostatic technique current remains constant through whole process with variations in potential. The potential for insertion/ extraction is limited to 0 to 3 V range. Potential during charging and discharging should be programmed with a cut off voltage of 0 V and 3 V. The whole process is carried out using a constant current density for charging and discharging. During discharging the polarity of the current will be reversed. The current density is determined in terms of rate of charging

and denoted as C rate. A battery charging in 1C rate means it requires one hour for charging. A slow rate of C/20 means it requires 20 hours to reach complete charging. Generally slow rate of charging is associated with an increased level of lithium storage capacity as it gives enough time to intercalate more lithium ions in the active sites of host matrix. Applications such as hybrid electric vehicles (HEV) require high rates of charging such as 2C, where the battery is recharged in half an hour time. Faster rate generally have a reduction in capacity and have more chances for exfoliation of host structure. Studies are going on to develop electrodes which can function in these faster rates. For the present study the charging/discharging starts with a slower rate of C/20 and after a couple of electrochemical cycling, the rate is gradually increased to C/10 then to C/5 etc. till a very fast rate of 2C. At the end of all these charge/discharge program the cells are again cycled at initial slow rate (C/20 for 2 cycles) to check the stability of the material towards repeated lithiation at different current rates. The C rates were determined by taking graphite as a standard with a theoretical capacity of 372 mAh g⁻¹.

| Charging rate | No. of cycles | Charging rate | No. of cycles |
|----------------------|----------------------|----------------------|----------------------|
| C/20(18mA/g) | 5 | C/2(180mA/g) | 20 |
| C/10(36mA/g) | 5 | C (360mA/g) | 50 |
| C/5 (72mA/g) | 5 | 2C (720mA/g) | 50 |

Table3.3. Different current densities and number of cycles performed at each rate.

3.3.4 Cyclic Voltammetry

Voltammetry is the measurement of current (I) as a function of applied potential (E). In voltammetry techniques current flow is monitored by applying different voltage to the electrodes. Cyclic voltammetry is one of the versatile techniques to understand different electrochemical activities. In cyclic voltammetry, the voltage is swiped between a specific voltage range of V_1 and V_2 at a fixed scan rate and the corresponding current flow at each point is measured. The scan is reversed at each defined cutoff voltage. Cyclic voltammetry is used for getting qualitative information's about different electrochemical reactions occurring in an electrochemical device during its operation. Cyclic voltammetry studies helps to understand clearly different electrochemical activities occurring at a special potential range.

A typical cyclic voltammogram of a lithium ion cell assembly with mesocarbon microbeads (MCMB) anodes and LiCoO_2 cathodes is represented in Figure 3.8. Redox process at the MCMB anode occurs around 0.05V vs. Li and that of the LiCoO_2 cathode evolves at about 4 V vs. Li. The figure shows that the electrolyte domain extends from about 0.8 V vs. Li to 4.5 V vs. Li and that the MCMB anode operates well outside the stability of the electrolyte and the cathode is just at its limit [6] . Cyclic voltammetry studies helps to understand the potential limits for onset of different possible side reactions in an electrochemical system.

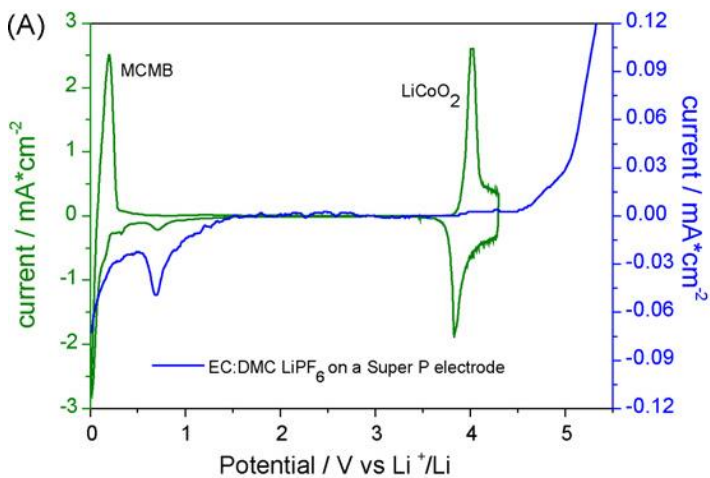


Figure 3.8 Cyclic voltammetry profiles (potential vs. Li/Li⁺) of lithium ion battery components: anode and cathode (green), electrolyte (blue). Counter electrodes: super P carbon; electrolyte: EC–DMC, LiPF₆. Redox process of graphite occurs at a potential of 0.005 V vs. Li and that of LiCoO₂ occurs at 4V vs Li. (B. Scrosati 2010)

References

- [1] Physical Chemistry, Atkins, 6th edition
- [2] Volume 1: Sol-Gel Processing, Hand book of sol-gel processing and technology, Processing characterization and applications, Ed. S. Sakka, Kluwer academic publishers, 2004
- [3] G.D. Soraru, L. Pederiva, J. Latournerie and R. Raj, “ Pyrolysis Kinetics for the Conversion of a Polymer into an Amorphous Silicon Oxycarbide Ceramic” *J. Am. Ceram. Soc.*, **85** [9] 2181–87 (2002)
- [4] P. Dibandjo, S. Diré, F. Babonneau, G.D. Soraru, “Influence of the polymer architecture on the high temperature behavior of SiCO glasses: A comparison between linear- and cyclic-derived precursors”, *J. Non-Cryst. Sol.*, **356** (2010) 132–140.
- [5] G.D. Soraru, F. Dalcanale, R. Campostrini, A. Gaston, Y. Blum, S. Carturan, P.R. Aravind, “ Novel polysiloxane and polycarbosilane aerogels via hydrosilylation of preceramic polymers”, *J. Mater. Chem.*, 22 (2012) 7676-7680
- [6] B. Scrosati, and J. Garche, Lithium batteries: Status, prospects and future. *Journal of Power Sources*, 2010. **195**(9): p. 2419-2430. *Handbook of batteries*
- [7] B. Scrosati, C.A. Vincent, “Modern Batteries”. 1997: Elsevier.
- [8] F. Tuinstra, J.L. Koenig, “Raman spectrum of graphite”, *J. Chem. Phys.* **53** (1970) 1126–30.

-
- [9] A.C. Ferrari and J. Robertson, "Interpretation of Raman spectra of disordered and amorphous carbon", Phys. Rev. B, **61** (2000) 14095-107.
- [10] H.Zhang, C.G. Pantano, " Synthesis and characterisation of silicon oxycarbide glasses" J. Am. Ceram. Soc., 73(1990) 958-963.
- [11] H. Brequel, J. Parmentier, S. Walter, R. Badheka, G. Trimmal, S. Masse, J. Latourmerie, P. Dempsey, C. Turquat, A. Jesmartin, L. Lemeindre, U.A. Jaysurya, D. Hourlier, H.J. Kleebe, G.D. Soraru, S. Enzo and F. Babboneu, " Systematical and structural characterisation of the high temperature behaviour of nearly stoichiometric silicon oxycarbide glasses" Chem. Mater., 16(2004) 2585-2598.
- [12] G. Mera, A. Navrotsky, S. Sen, H.-J. Kleebe, R. Riedel, "Polymer-derived SiCN and SiOC ceramics – structure and energetics at the nanoscale", J. Mater. Chem. A, 1 (2013) 3826-3836.
- [13] G. T. Burns, R. B. Taylor, Y. Xu, A. Zangvil, G. A. Zank, "High-Temperature chemistry of the conversion of Siloxanes to Silicon Carbide", Chem. Mater., **4** (1992) 1313-132.
- [14] M. Narisawa, T. Kawai, S. Watase, K. Matsukawa, T. Dohmaru, K. Okamura, A. Iwase, J. Am. Ceram. Soc. 95 (2012)3935–3940
- [15] G.D. Soraru, F. Babonneau, J.D. Mackenzie, J. Mat. Science, 25 (1990) 3886-93.



Chapter 4. Searching Insights in to the Lithium Storage Mechanism in Polymer Derived SiOC Anode Materials

Part of this chapter has been published in:

“New Insights in to the Lithium Storage Mechanism in Polymer Derived SiOC Anode Materials”, V.S. Pradeep, Magdalena Graczyk-Zajac, R. Riedel, G. D. Soraru , Submitted to Journal of Electrochimica Acta 2013

“Influence of Pyrolysis Atmosphere on the Lithium Storage Properties of Carbon-Rich Polymer Derived SiOC Ceramic Anodes”, V.S. Pradeep, M. Graczyk-Zajac, M. Wilamowska, R. Riedel, G.D. Soraru, Solid State Ionics, 09/2013; DOI:10.1016/j.ssi.2013.08.043

4.1 Understanding Lithium Storage Mechanism in Polymer Derived SiOC Anode Materials

4.1.1 Introduction

For the past two decades polymer-derived silicon oxycarbide (SiOC) ceramics have gained interest as a potential anode material for lithium storage applications [1-10]. The demand for high energy density batteries with excellent multiple recharge performance is increasing with the development of new generation technologies based on portable electronic devices and electric vehicles. Current studies are mainly focusing on the production of thinner, lighter and space effective batteries for the future energy storage applications [11-14]. The SiOC anodes are reported to offer a high reversible lithium storage capacity up to 920 mAh g⁻¹ [1-10], whereas the theoretical capacity of conventional graphite anode is limited to 372 mAh g⁻¹ [12-14]. In spite of these advantages, capacity loss by means of first cycle irreversibility during the first cycle of charging/discharging is a drawback towards the applicability of these materials in future lithium ion batteries. The origin of the high capacity of SiOC anodes has not yet been explained however it is believed that it has to be related to the complex structure of amorphous silicon oxycarbides in which silicon atoms share bonds with oxygen and carbon atoms simultaneously [15-17]. Depending on the chemical composition, maximum pyrolysis temperature, and in particular, from the carbon content, the silicon oxycarbide network may contain graphene layers which can form a continuous free-C network [18,19]. The proposed sites for the reversible Li storage in SiOCs span from the mixed Si-O-C tetrahedra forming the amorphous network [3] to the micropores of the glassy phase [4,5] to the free carbon clusters [5,6], which seems to store more lithium compared to the conventional graphite [6]. Indeed the

maximum storage capacity of graphite leads to the Li_xC_6 with $x=1$ stoichiometry while for the free carbon phase of the SiOC glasses values of $x>1$ have been proposed [6].

The main objective of the presented work is to give a contribution to better understand the mechanism of lithium insertion/extraction process by a comparative study of the structural and electrochemical features of silicon oxycarbide ceramics with different composition and different pyrolysis temperature. The chemical compositions of the studied SiOCs have a constant O/Si atomic ratio, which implies a constant amount of $\text{Si}-\text{O}$ and $\text{Si}-\text{C}$ bonds, while the percentage of the free C phase increases from a value of ca 8 wt% up to almost 50 wt%, thus allowing to investigate the role of these two components, namely the amorphous silicon oxycarbide network and the free C, on the electrochemical behavior of the SiOC anodes.

4.1.2 Experimental Part

4.1.2.1 Materials Synthesis

The siloxanes are purchased from Sigma Aldrich (St. Louis, MO, USA). Two types of siloxane are used: a linear polyhydridomethylsiloxane (PHMS, MW= 1900), which contains Si-H bonds, and a cyclic 1,3,5,7-tetramethyl-1,3,5,7-tetravinyl cyclotetrasiloxane (TMTVS, MW=344) bearing $\text{Si}-\text{C}=\text{C}$ moieties. Divinylbenzene, DVB (technical 80%, mixed isomers) was purchased from Alfa Aesar (Alfa Aesar, Ward Hill, MA, USA). Platinum divinyltetramethyldisiloxane complex, ~Pt 2% in xylene (Sigma-Aldrich, St. Louis, MO, USA) was used as catalyst for the hydrosilylation reaction between the Si-H moieties of the siloxanes and the vinyl groups of the cross linker [20]. All the chemicals were used without any further purification. For the synthesis of C-poor SiOC, PHMS is cross linked with TMTVS while for C-

rich SiOCs PHMS is cross linked with DVB. In a typical preparation the PHMS is mixed with TMTVS or DVB in presence of platinum catalyst (always 5 ppm relative to Si compound). The resulting mixture is stirred for few minutes, cast in plastic tubes, which are then allowed to stand at room temperature for the whole night for setting. Finally samples are left at 60 °C to complete the curing process. The cured materials were hard elastomeric transparent resins. Table 4.1 summarizes the studied compositions.

| Sample | PHMS(g) | TMTVS(g) | DVB(g) |
|--------|---------|----------|--------|
| PT2 | 10 | 1.32 | -- |
| PT5 | 10 | 2.64 | -- |
| PD1 | 10 | -- | 5 |
| PD2 | 10 | -- | 20 |

Table 4.1 Elemental composition of studied SiOC samples, Name PT represents samples derived from PHMS and TMTVS precursors and PD represents the samples from PHMS with DVB.

The cured resins are pyrolysed using an alumina tubular furnace (Lindberg/Blue) under 150 mL/min of flowing argon. The samples are heated at a rate of 5 °C/min up to 1000 and 1300 °C respectively and maintained for 1 hr at the maximum temperature. Cooling down to room temperature is done by turning off the furnace power. The oxycarbide fragments are then milled in an agate mortar and sieved with an 80 µm sieve.

4.1.2.2 Preparation of Electrodes and Cells

SiOC anodes are made by making homogeneous slurry of the samples with polyvinylidene fluoride (PVdF, SOLEF, Germany) as binder and

carbon black as a conducting medium in the weight ratio 85:10:5 using N-methyl pyrrolidone (NMP, BASF, Germany) as the solvent. The slurry is coated with a hand blade on the rough side of a thin copper foil (10 μ m, Copper SE-Cu58, Schlenk Metallfolien GmbH & Co KG) and dried at 80 °C for 12 hours. After drying the electrodes are cut into 7mm size and pressed at a pressure of 20 kN cm⁻². The electrodes are then weighed and dried in a Buchi vacuum oven at 80 °C for 24 hours and directly transferred to the glove box with argon atmosphere. The dried electrodes are then assembled in a two electrode Swagelok® type cell with lithium metal as the counter/reference electrode (99.9% purity, 0.75mm thick, Alfa Aesar, Germany) and SiOC as the working electrode with a Whatman™ quartz microfiber filter (QMA, UK) separator between electrodes, the electrolyte used is a high purity solution of 1M LiPF₆ in ethylene carbonate and diethyl carbonate mixture of weight ratio 1:1 (LP 30, Merck KGaA, Germany). The anode contains 3-5 mg cm⁻² of the active material. Cells are assembled in an argon-filled glove box.

4.1.2.3 Characterization Techniques

Electrochemical testing of the cells is performed using constant current rate of C/20 (18 mA g⁻¹) for the first 5 cycles. After 5 cycles the current rate is increased to C/10, C/5, C/2, C and 2C respectively. The details of current rate and the number of cycles are shown in Table 4.2. Lithium is inserted/extracted within a potential limit of 0 – 3 V. After the series of 135 cycles with increasing current rates the cells are cycled again at initial slow rate to check the recovery of the capacity.

| Charging rate | No. of cycles | Charging rate | No. of cycles |
|---------------|---------------|---------------|---------------|
| C/20(18mA/g) | 5 | C/2(180mA/g) | 20 |
| C/10(36mA/g) | 5 | C (360mA/g) | 50 |
| C/5 (72mA/g) | 5 | 2C (720mA/g) | 50 |

Table 4.2 Different current rates for charging the cells along with number of cycles performed at each rate. Charging and discharging of each cycle are performed at same current rate.

A Leco TC-200 and TC-436 (Leco Corp USA) are used to determine the carbon and the oxygen content respectively. Hydrogen content is analyzed by Labor Pascher (Remagen-Bandorf, Germany). Silicon content is calculated as a difference to 100 wt%. The thermogravimetric (TGA) experiments were done in an argon atmosphere at a flux of 100 mL/min, at a rate of 10 °C/min up to 1500 °C using a Netzsch equipment (Model STA 409, Netzsch-Geratebau GmbH, Germany). The ²⁹Si MAS NMR experiments are performed with an AVANCE 300 Bruker using a 7 nm probe-head (Bruker Instruments, Karlsruhe, Germany). All the spectra are recorded using single pulse experiments at 45 ° with a pulse of 2.6 μs with a recycle delay of 50s and 8 kHz of spinning speed. The Raman spectra were collected on a Jobin Yvon Raman spectrometer (Horiba-Jobin Yvon, model T6400) with an excitation wavelength of 514 nm (Ar laser) and spectra were detected by a CCD (256x1024 pixels) cooled by liquid nitrogen. X-ray diffractograms were collected from Rigaku D-Max diffractometer (Rigaku, Tokyo, Japan) in the Bragg-Brentano configuration using CuKα radiation

operating at 40kV and 30mA. The scanning range was 10-80 °with a step rate of 0.05 ° and acquisition time of 5s per point.

4.1.3 Results and Discussion

4.1.3.1 Structural Characterization

The chemical analysis results of the studied SiOC compositions pyrolysed at 1000 °C are reported in Table 4.3. The thermogravimetric measurements between 1000 and 1300 °C indicated a mass loss < 0.2 wt.%, which is within the elemental measurement errors. Therefore, the chemical compositions of the glasses pyrolysed at 1300 °C were considered the same as those of the samples pyrolysed at 1000 °C. The raw data are presented according to the general formula consisting of a stoichiometric silicon oxycarbide network, $\text{SiC}_x\text{O}_{2(1-x)}$ and a C_{free} phase [21]. The hydrogen, being always well below 1%, has been neglected.

| Sample | Si | C | O | H | Oxycarbide Stoichiometry $\text{SiC}_x\text{O}_{2(1-x)} + y\text{C}_{\text{free}}$ | $\text{SiC}_x\text{O}_{2(1-x)}$ (Wt. %) | $y\text{C}_{\text{free}}$ (Wt. %) |
|--------|-------|-------|-------|------|--|--|--------------------------------------|
| PT2 | 50.55 | 18.34 | 30.99 | 0.12 | $\text{SiC}_{0.46}\text{O}_{1.08} + 0.38\text{C}_{\text{free}}$ | 92 | 8 |
| PT5 | 45.67 | 27.69 | 26.45 | 0.19 | $\text{SiC}_{0.49}\text{O}_{1.02} + 0.92\text{C}_{\text{free}}$ | 82 | 18 |
| PD1 | 38.09 | 40.33 | 21.30 | 0.28 | $\text{SiC}_{0.51}\text{O}_{0.98} + 1.96\text{C}_{\text{free}}$ | 68 | 32 |
| PD2 | 29.24 | 55.15 | 14.99 | 0.62 | $\text{SiC}_{0.55}\text{O}_{0.90} + 3.85\text{C}_{\text{free}}$ | 51 | 49 |

Table 4.3 Elemental analysis results showing different SiOC compositions along with weight percent of mixed SiOC phase and free carbon phase.

The compositions are also shown in the Si-O-C ternary phase diagram: the experimental points fell on a straight line originating from the C apex and having a constant atomic ratio $O/Si=1$. Samples obtained from PHMS/TMTVS (PT2 and PT5) show lower carbon content compared to the PHMS/DVB series (samples PD1 and PD2). In particular chemical composition of PT2 sample falls very close to the stoichiometric tie line between SiC and SiO₂ and therefore can be regarded as an almost “pure” silicon oxycarbide network with a C_{free} content lower than 10 wt%. The electrochemical characterization has been performed on all the samples while for the structural characterization we decided to focus our attention on the two compositions with the lowest (PT2) and highest (PD2) carbon content.

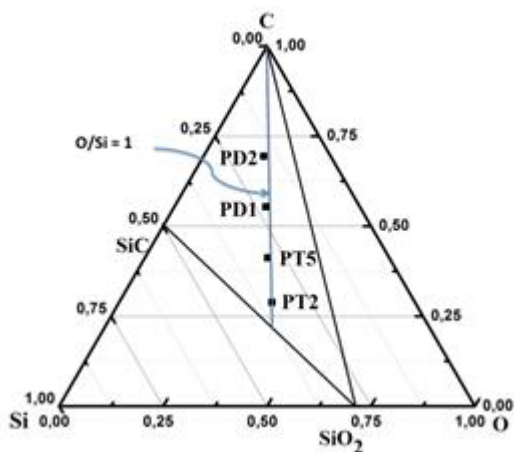


Figure 4.1 Ternary representations of studied Si-O-C samples

TGA analysis reveals the typical decomposition pattern of siloxane resins transforming into SiOC ceramics with a main weight loss step between 400 and 900 °C [22]. The ceramic yield at 900°C decreases from PT2 (ca 80 wt %) to PD2 (ca 60 wt. %) composition.

Thermogravimetric behavior of studied samples is presented in Figure 4.2. High carbon PD2 samples have maximum weight loss of about 40% and the main weight loss step is observed from 450 °C to 800 °C corresponding to the release of hydrogen and organic moieties during polymer to ceramic conversion.

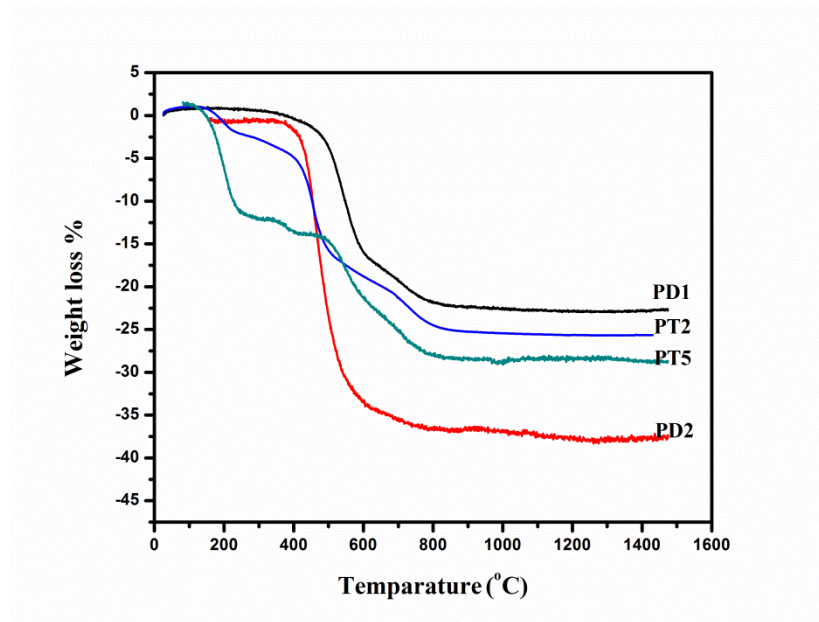


Figure 4.2 TG graphs of studied compositions

The higher ceramic yield is noted for PD1 samples with minimum weight loss during heating. Low carbon SiOCs from PHMS-TMTVS compositions do also have a better ceramic yield with maximum weight loss reaching only around 20-25%. Weight loss patterns of both PT and PD compositions are slightly different with more intermediate weight loss steps for PT samples starting first at 200 °C then at 400- 600 °C then the final weight loss from 600-800 °C. This difference in weight loss pattern is because of multiple reasons, including difference in structural arrangement of starting precursors, the moisture trapped during cross linking and also to different degree of cross linking in these polymers.

Amorphous nature of the SiOC samples has been checked by X-ray diffraction analysis. XRD spectra recorded on the sample with the lowest (PT2) and highest (PD2) carbon content pyrolyzed at 1000 and 1300 °C are reported in Figure 4.3. At 1000 °C both samples show an amorphous spectrum while at 1300 °C the broad hump at $2\theta \approx 22^\circ$ is due to the SiO₂-based network and the broad reflections at $2\theta \approx 35, 60$ and 72° reveal the nucleation of cubic SiC nanocrystals. The spectrum of the high-C composition (PD2) has narrower and more intense SiC reflections suggesting the formation of larger SiC nanocrystals and an increased fraction of crystallized phase.

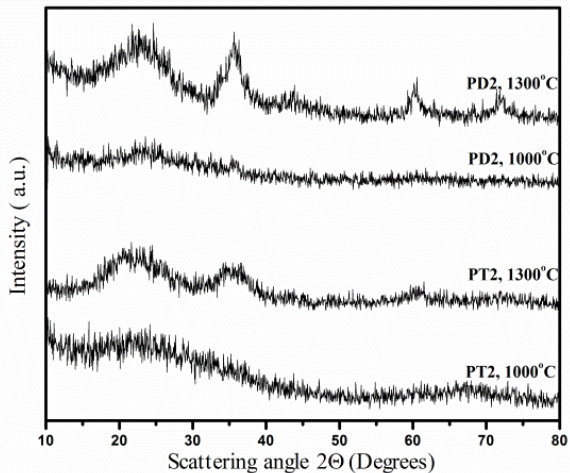


Figure 4.3 XRD spectrum of samples pyrolysed at 1000 and 1300 °C respectively

Raman spectroscopy is considered as an important tool for the characterization of different modifications of carbon clusters in carbonaceous materials. The Raman spectra of the studied compositions are shown in Figure 4.3. The spectra show features similar to graphitic carbons with two strong peaks named D-band (at $\approx 1350 \text{ cm}^{-1}$) and G-band (at $\approx 1600 \text{ cm}^{-1}$) respectively. The D-band is due to the disorder induced vibrations of 6-fold aromatic rings and G-band represents the in plane bond stretching of sp^2 hybridized carbon atoms within the chain structure. The strength of D band is proportional to the probability of finding a 6 fold rings in the cluster [23,24].

According to the model proposed by Ferrari and Robertson [24] the crystallite size is estimated using the intensity ratio of D and G bands. The formula to determine the carbon cluster size is represented as

$$I_D/I_G = C'(\lambda) L_a^2$$

Where C' is a coefficient that depends on the excitation wavelength of the laser, $C'_{(514 \text{ nm})} = 0.0055 \text{ \AA}^{-2}$ and L_a is the lattice parameter. The detailed calculation of the integrated intensity ratios, lattice parameter and FWHM of all the peaks are reported in Table 4.4.

| Sample Name | D (cm⁻¹) | G (cm⁻¹) | I_D/I_G | L_a (Å⁰) | FWHM_D (cm⁻¹) | FWHM_G (cm⁻¹) |
|--------------------|----------------------------|----------------------------|------------------------------------|--------------------------------------|---|---|
| PT2 1000 | 1329 | 1604 | 0.88 | 12.6 | 111 | 66 |
| PT2 1300 | 1350 | 1603 | 1.25 | 15.1 | 101 | 58 |
| PD2 1000 | 1349 | 1594 | 0.68 | 11.2 | 154 | 74 |
| PD2 1300 | 1343 | 1589 | 0.95 | 13.1 | 111 | 68 |

Table 4.4 Raman spectra measurements with position and intensity ratio of D and G bands representing free carbon networks along with crystallite size of carbon network and full width half maximum.

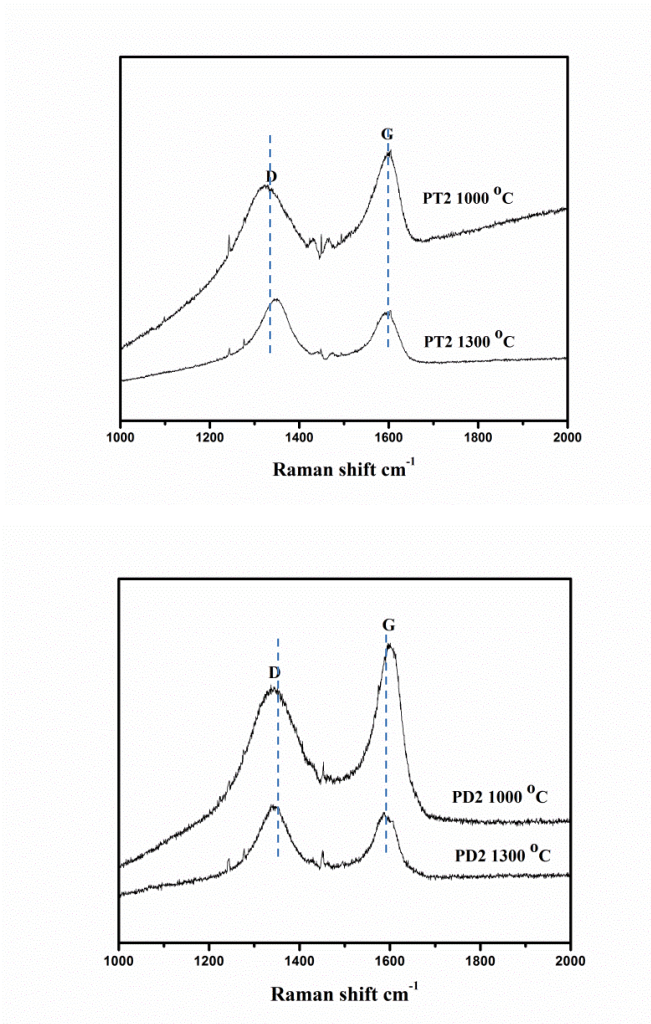


Figure 4.4 Raman spectra of studied compositions showing D and G bands associated with carbon content.

Both PT2 and PD2 samples, with low and high carbon contents respectively, show the same trend in Raman spectra with increasing pyrolysis temperature: the bands becomes more narrow with a decrease of the FWHM and the I_D/I_G ratio increases indicating an ordering and a size growth of the graphite crystals. At each temperature, the crystallite size is found to be smaller for the PD2 samples compared to the low carbon PT2 series.

^{29}Si MAS NMR studies are regarded as the most convenient tool to characterize the formation of the amorphous silicon oxycarbide network [16,17]. The ^{29}Si MAS-NMR spectra are shown in Figure 4.4.

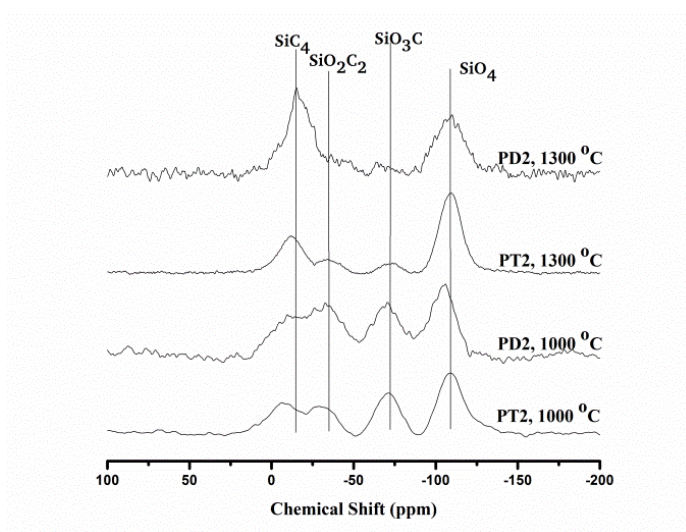


Figure 4.5 ^{29}Si MAS NMR spectra of studied compositions showing mixed SiOC units

The spectra are simulated with 4 Gaussian peaks with isotropic chemical shifts of around -108, -70, -34, and -14 ppm corresponding to the

SiO_4 , SiO_3C , SiO_2C_2 , SiC_4 sites present in silicon oxycarbides. These units, following the classical Si notation are also labeled as Q, T, D, and X respectively. The deconvolution details are reported in Table 4.5

| Sample | Pyrolysis Temp. (°C) | Si site (%) | | | |
|--------|-------------------------|-------------|----------|------------|---------|
| | | SiO_4 | SiO_3C | SiO_2C_2 | SiC_4 |
| PT2 | 1000 | 38 | 23 | 15 | 24 |
| PT2 | 1300 | 59 | 5 | 7 | 29 |
| PD2 | 1000 | 29 | 24 | 20 | 27 |
| PD2 | 1300 | 41 | 2 | 1 | 56 |

Table 4.5 NMR deconvoluted spectrum showing compositions of different mixed SiOC units

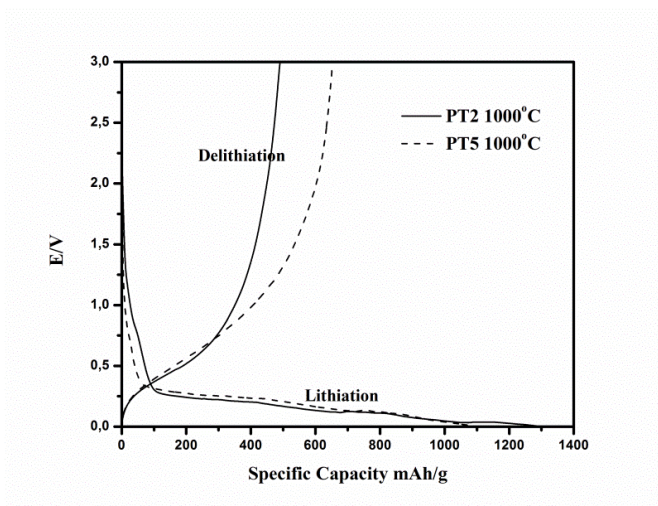
The ^{29}Si MAS-NMR spectroscopic studies confirm the presence, at 1000°C, of different Si sites with silicon sharing bonds with oxygen and carbon simultaneously. With increasing pyrolysis temperature a redistribution reaction between Si-C and Si-O bonds occurs, leading to a phase separation and to the formation of carbon rich, SiC_4 , and oxygen rich, SiO_4 , species with the consumption of mixed-bond Si sites[25]. Indeed, the NMR spectra at 1300°C are dominated by the peaks at around -108, and -14 ppm due to Q and X units with a consumption of mixed T and D units (peaks at around -70 and -34 ppm respectively) The quantitative data obtained from the deconvolution of the experimental spectra are reported in Table 4.5. The phase separation occurring at 1300°C seems more effective in C-rich SiOC indeed, for PD2 sample at 1300°C, the presence of mixed T and D units is

negligible while for the PT2 composition at the same temperature 12% of the Si atoms are still present in mixed silicon oxycarbide units.

4.1.3.2 Electrochemical Characterization

4.1.3.2.1 First insertion/extraction Behavior

The first insertion/extraction curves (potential vs. capacity) for the samples with the lowest (PT2) and highest (PD2) carbon content are shown in Figure 4.5. When comparing the shape of the curves in Figure 4.5, solid-electrolyte-interface (SEI) formation is seen between 1.5 and 0.6 V during the first Li-insertion. During the first extraction a significant amount of charge is continuously recovered between 0.005 and 1.5 V, as reported for disordered soft and hydrogen-containing carbon [26, 27] with a smaller hysteresis for the sample with higher carbon content (PD2).



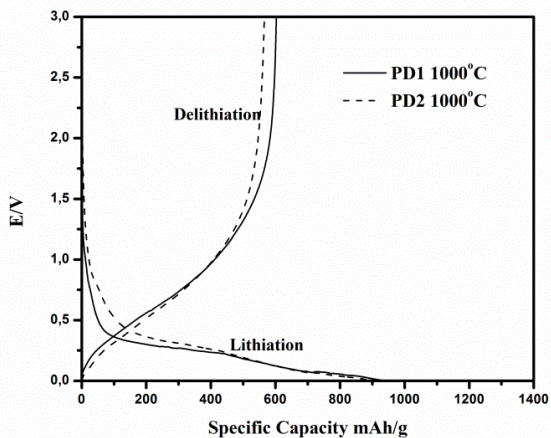
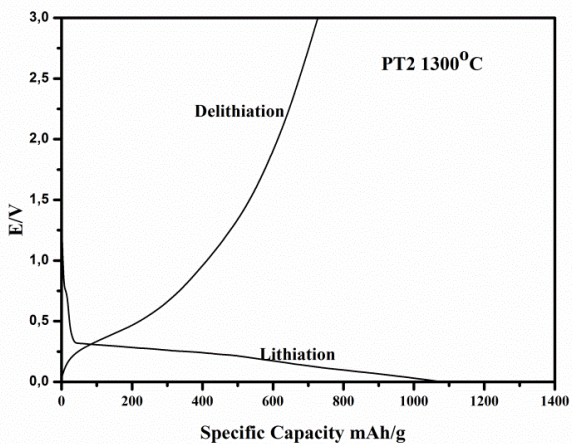


Figure 4.6 First cycle lithium insertion/ extraction pattern of both low carbon and high carbon compositions pyrolysed at 1000°C.



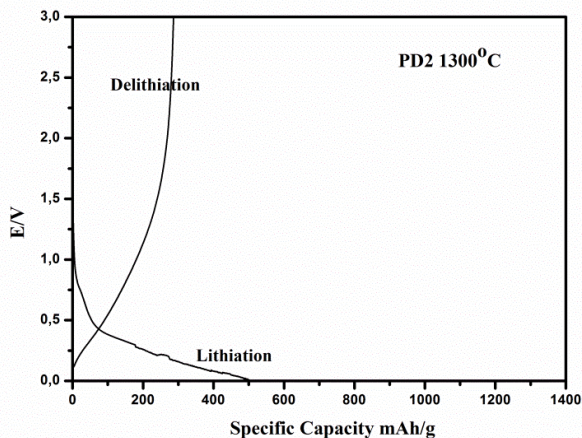


Figure 4.7 First cycle lithium insertion/ extraction pattern of both low carbon and high carbon compositions pyrolysed at 1300°C.

Note that the highest hysteresis is registered for the samples PT2 1300 °C, with lithium extracted over the whole potential range (0 to 3 V). The insertion profiles for low carbon samples are quite similar for both investigated temperatures and characterized by quasi-plateau at ~ 0,2 V. The shape of the insertion curves of high carbon content samples is different; at both pyrolysis temperatures no plateau is observed.

The first cycle charging/discharging and irreversible capacities along with the coulombic efficiency of all the investigated samples are listed in Table 4.6. The efficiency η is calculated as the ratio of discharge capacity to the first charging capacity, using the following equation

$$\eta = (C_{\text{discharge}}/C_{\text{charge}})*100$$

| Sample | Pyrolysis Temp. (°C) | Q _{insertion} (mAh/g) | Q _{extraction} (mAh/g) | Q _{irreversible} (mAh/g) | Efficiency (%) |
|----------|----------------------|--------------------------------|---------------------------------|-----------------------------------|----------------|
| PT2 | 1000 | 1287 | 493 | 794 | 38 |
| PT5 | 1000 | 1097 | 656 | 441 | 59 |
| PD1 | 1000 | 930 | 605 | 325 | 65 |
| PD2 | 1000 | 898 | 568 | 330 | 63 |
| PT2 | 1300 | 1070 | 728 | 342 | 68 |
| PD2 | 1300 | 512 | 293 | 219 | 57 |
| Graphite | | 468 | 400 | 68 | 83 |

Table 4.6 First cycle lithium insertion/ extraction datas of studied compositions along with coulombic efficiency and amount of irreversible capacity. Datas of graphite electrode is also shown as a bench mark.

At 1000 °C the first charge capacity decreases with increasing the C content from a maximum value of 1287 mAh g⁻¹ down to 898 mAh g⁻¹ for the PT2 and PD2 samples respectively. The charge irreversible trapped during the first cycle follows a similar trend with the highest value (794 mAh g⁻¹) for the PT2 composition down to 325-330 mAh g⁻¹ for the PD1 and PD2 samples. The coulombic efficiency displays a complementary evolution: the lowest values are recorded for the C-poor SiOC samples and the highest efficiency for the C-rich compositions.

The influence of the pyrolysis temperature on the electrochemical performance of the SiOC ceramics can be evaluated by comparing the data measured for the PT2 and PD2 samples. The insertion capacity decreases

for both samples but the PD2 composition at 1300 °C loses more than 50% of the insertion capacity measured at 1000°C. On the other hand, the extraction capacity at 1300 °C show a decrease for the high-C sample (PD2) but an increase for the low-C material (PT2). The coulombic efficiency of the PT2 composition at 1300 °C, 68%, reaches the highest value among all the studied samples. The temperature dependence of the reversible capacity of the PT2 sample is unusual since it is typically reported that the reversible capacity of SiOC materials decreases when the pyrolysis temperature is increased above 1100 °C[9, 29].

There is still an open debate in the literature on the active sites for the Li storage in silicon oxycarbides. Fukui et al.[4-5], based on ⁷Li NMR studies, proposes the presence of three different electrochemically active sites in SiOCs: intercalation between and at the edges of graphene layers, micro pores and the mixed silicon oxycarbide phase. Raj et al.[3], based on a detailed analysis of the electrochemical data published by Dahn et al.[1] focuses on the storage capacity of the mixed silicon oxycarbide units, i.e. the Si atoms which share bonds with C and O simultaneously and form the glassy SiC_xO_{2(1-x)} network. The experimental data reported in Table 4.6 very clearly suggest a relation between the first insertion capacity and the C content of the SiOC samples reported in Table 4.3. However, the trend does not point toward an increase of insertion capacity with the amount of free carbon present in the SiOC but rather with the amount of silicon oxycarbide (SiC_xO_{2(1-x)}), which is the phase that contains the mixed silicon oxycarbide units. Accordingly, the idea which seems to emerge from our data is that the main storage sites for lithium are indeed in the mixed silicon oxycarbide units rather than the disordered carbon of the free C phase. This result can be immediately appreciated from the plot of Figure 4.6 which reports the first cycle insertion capacity of the samples pyrolysed at 1000 °C as a function of

the amount (wt%) of the $\text{SiC}_x\text{O}_{2(1-x)}$ phase. The data reported in Figure 4.8 unveil a clear linear dependence of the insertion capacity from the amount of silicon oxycarbide phase, in good agreement with the model proposed by Raj et al.[3]. Moreover, the extrapolation of the linear fit down to zero, which means a sample of pure free carbon, indicates a capacity of 350 mAh g^{-1} , in good match with the theoretical capacity of graphite (372 mAh g^{-1}). These results suggest that SiOC anodes behaves, from the electrochemical point of view, as a composite materials formed by a mixture of pure silicon oxycarbide, $\text{SiC}_x\text{O}_{2(1-x)}$, and free carbon phases. Interestingly, the insertion capacity of pure $\text{SiC}_x\text{O}_{2(1-x)}$ phase, which can be obtained by extrapolating the linear fit up to 100% is 1300 mAh g^{-1} . In Ref. 3, the lithium insertion capacity for the mixed silicon oxycarbide phase has been estimated to fall in the range $45000\text{-}75000 \text{ mAh g-atom}^{-1}$. Recalling that the average composition of the silicon oxycarbide phase in our samples is $\text{SiC}_{0.5}\text{O}_1$, which corresponds to a MW of 50 amu, the insertion capacity of 1300 mAh g^{-1} becomes $26000 \text{ mAh g-atom}^{-1}$. This value is between 2 and 3 times smaller than that reported in Ref. 3.

Electrochemical data reported in Table 4.6 show a similar relation for the irreversible capacity which is maximum for the sample with the highest amount of mixed silicon oxycarbide units. This observation suggests that the main sites for lithium trapping must reside in the amorphous $\text{SiC}_x\text{O}_{2(1-x)}$ network more than in the free carbon phase. Moreover, the previously published results [7,8] match very well the tendency presented in Figure 4.6. However, one should keep in mind that the theoretical $\sim 1300 \text{ mAh g}^{-1}$ capacity of pure $\text{SiC}_x\text{O}_{2(1-x)}$ phase is hardly achievable. According to our preliminary experiments phase pure SiOC materials with less than 0.5%wt of free carbon show no electrochemical activity, i.e. the first insertion capacity of is $\sim 20\text{-}30 \text{ mAh g}^{-1}$.

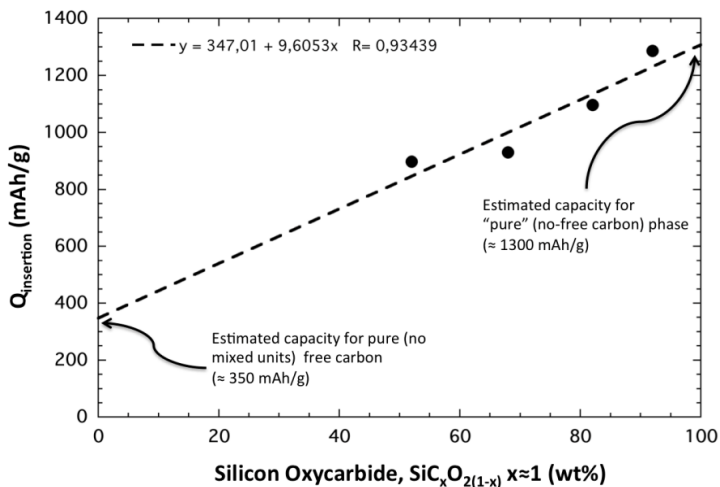


Figure 4.8. Weight % of SiOC stoichiometric composition vs. first insertion capacity. The plot represents a linear dependence of first cycle charging capacity towards composition of mixed bonds in the network.

This result seems to suggest that a certain amount of free carbon phase is necessary to insure the basic electronic conductivity of the ceramic phase and to exploit to the utmost the Li storage capacity of SiOC anodes.

The increase of the pyrolysis temperature up to 1300 °C reduces the insertion capacity for both the low-C and high-C SiOC glasses, however PD2 composition shows a higher reduction compared to PT2 sample. This evidence can be rationalized based on the structural evolution of these two samples as revealed by the XRD, Raman and, in particular, by the ²⁹Si MAS NMR data. At 1300 °C the high-C sample (PD2) undergoes a strong structural transformation with the crystallization of cubic SiC (cnf Figure 4.2)

and the complete partitioning of the mixed silicon oxycarbide network into SiC_4 and SiO_4 sites (cnf Figure 4.4 and Table 4.5). On the other hand, at 1300 °C, the structural evolution of the low-C composition (PT2) is not so advanced: XRD spectra show broader and less defined crystallization peaks and the ^{29}Si NMR study still indicates the presence of mixed T and D units, even if in lesser amount compared to 1000 °C. Accordingly, in the PD2 composition, the disappearance at 1300 °C of the $\text{SiC}_x\text{O}_{2(1-x)}$ network, which is the component of the SiOC glasses having the highest Li insertion capacity and the higher organization of the carbon phase with increasing pyrolysis temperature -what is also confirmed by increasing carbon crystallite size calculated from Raman spectra- leads to a clear reduction of the total Li storage capacity. Indeed, organized carbon offers less space for reversible lithium storage [29] and a similar evolution of electrochemical properties with increasing pyrolysis temperature has been already observed for other PDC-derived carbon-rich SiOC materials [28]. On the other hand, for the low-C composition (PT2), at 1300 °C the mixed silicon oxycarbide units are still present in the material and the reduction of the first cycle insertion capacity is less pronounced.

Interestingly, the first cycle extraction capacity of the PT2 sample at 1300 °C increases and reaches a very high value of 728 mAh g⁻¹. Recalling that this sample is mainly constituted by the $\text{SiC}_x\text{O}_{2(1-x)}$ network with a low amount of free C then these results imply that a higher fraction of Li atoms inserted into the silicon oxycarbide structure is not irreversibly trapped but can be reversibly extracted. These results may be related with the higher thermodynamic stability of the SiOC glasses pyrolysed at temperature above 1000 °C which we have recently observed [30]. Accordingly, the silicon oxycarbide network at 1000 °C being less stable is also more susceptible to react with Li ions forming irreversible structures such as Li_2O while the

structure of the SiOC glass at 1300 °C has been relaxed into a lower free energy state and it is therefore less available to irreversibly react with the inserted lithium ions.

4.1.3.2.2 Rate Capability Studies

The charge/discharge behavior of the studied compositions for multiple galvanostatic cycling is presented in Figure 4.9 and Figure 4.10. The detailed description of the charging/discharging procedure can be found in Experimental Part (Table 4.2).

The cycles start with a slow charging/discharging rate of 18 mA g⁻¹ (C/20) and then the current density is gradually increased up to a fast charging rate of 720 mA g⁻¹ (2C). After the first cycle, the cycling efficiency is about 99%. C-poor samples, PT2 1000 °C and PT2 1300 °C show very rapid capacity fading upon cycling, in both cases the stabilization is observed at the rate C/5 - C/2 (72 - 180 mA h g⁻¹). Although the capacity recovered at C/2 rate by PT2 1300 °C is a bit higher than that for PT2 1000 °C, namely 80 vs 45 mA h g⁻¹, respectively, these values are still very low if considering possible application of the material in Li-ion battery. On the other hand, samples PD2 1000 °C and PD2 1300 °C present a stable performance towards multiple charge/discharge cycles. PD2 1000 °C delivers a capacity of around 200 mA h g⁻¹ at 2C rate and it recovers its initial capacity at a slower rate of C/20 (18 mA g⁻¹) after the series of charging/discharging with various currents.

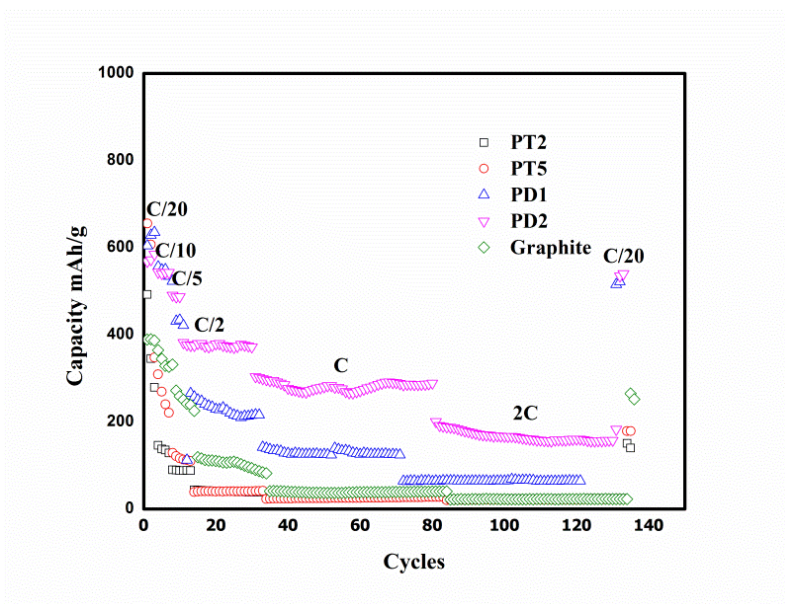
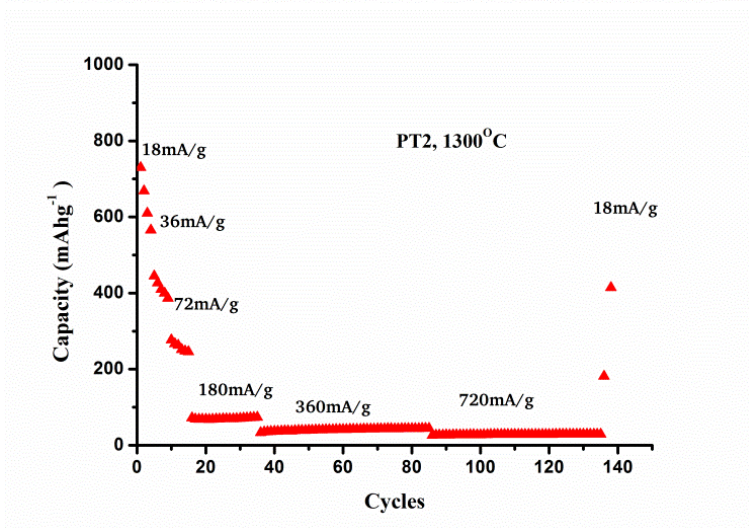
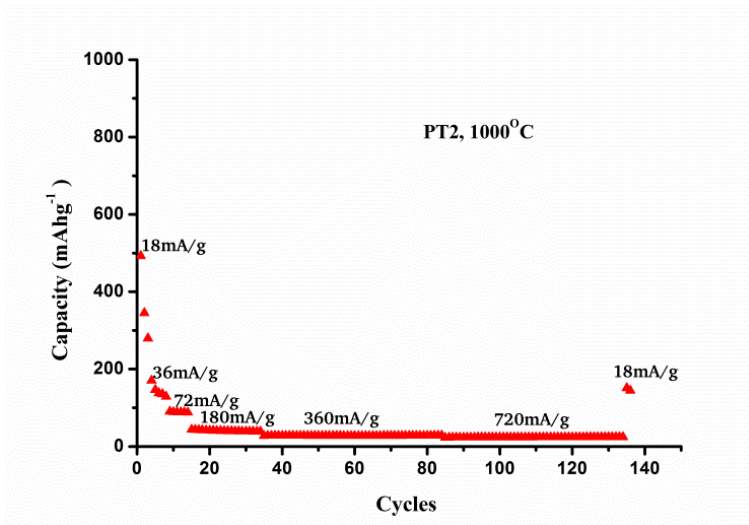


Figure 4.9. Electrochemical cycling with increasing current rate for studied SiOC compositions pyrolysed at 1000 °C with varying free carbon content. Graphite electrode is used as bench mark

The charging/discharging capacity of the C-poor samples degrades faster than the C-rich SiOC. From this point of view, C-rich SiOCs, having a higher volumetric fraction of free carbon, should display a lower elastic modulus and consequently should accommodate easier the breathing of the structure compared to the C-poor material.



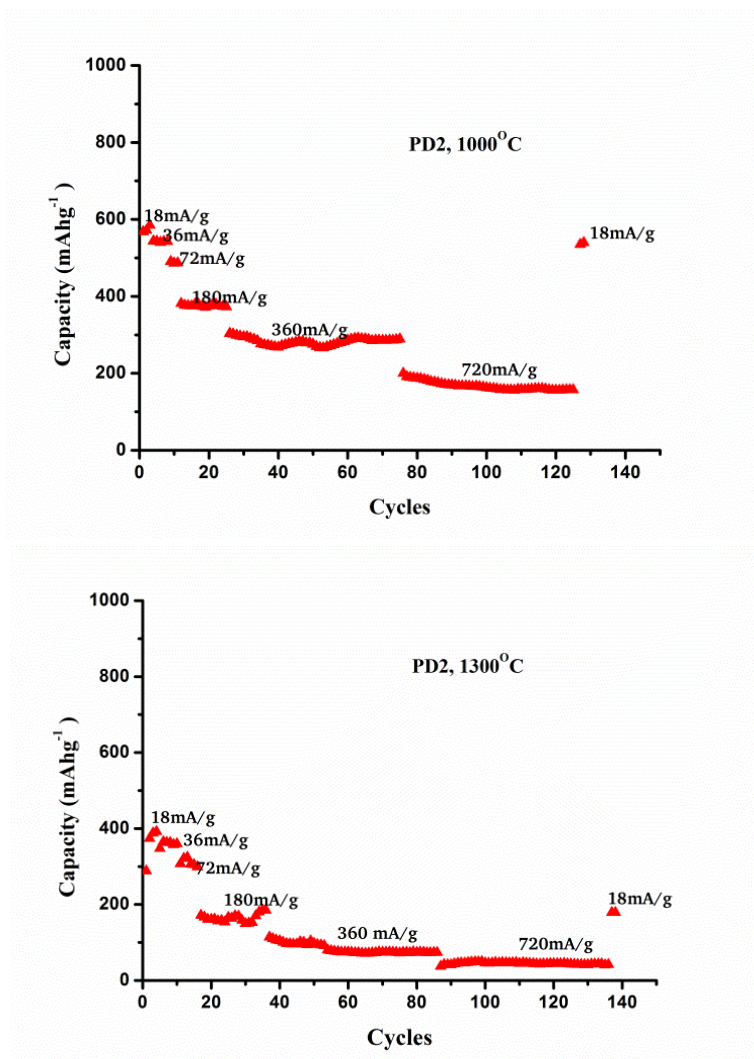


Figure 4.10. Electrochemical cycling with increasing current rate for low carbon PT2 and high carbon PD2 samples pyrolysed at 1000 and 1300 °C.

From these studies it is clear that both the silicon oxycarbide network and the free carbon phase play an important role in repeated lithiation/delithiation experiments and both must be taken into account towards reversible lithium storage. SiOC phases works towards increasing first cycle insertion capacity, while carbon phase determines the reversibility and cyclability. The sample PD2 1000 °C, is capable to recover high specific capacity of about 600 mAh g⁻¹ at low rates and 200 mAh g⁻¹ at a fast charging rate of 2C (720mA g⁻¹), whereas the low carbon PT2 sample accommodate more than 1000 mAh g⁻¹ during the first cycle, however it shows a poor cycling stability.

4.1.4 Conclusions

SiOC glasses formed by an amorphous silicon oxycarbide network and increasing amounts of a free-C phase have been synthesized and characterized, both from the structural and electrochemical point of view. For all the investigated samples the amorphous silicon oxycarbide network has the same chemical composition of SiC_xO_{2(1-x)} with x≈1. The amount of free C varies from a minimum of 8wt% up to 49wt%. SiOC anodes behave like a composite material: the silicon oxycarbide phase has the highest first cycle insertion capacity up to 1300 mAh g⁻¹ while the reversibility and cyclability comes primarily from the free C phase. Accordingly, the highest reversible capacity for samples treated at 1000 °C and the best cyclability has been measured for the SiOC anode materials with 51wt% of amorphous phase and 49wt% of free carbon (PD2 sample). This material is able to deliver up to 200 mAh g⁻¹ of charge at a 2C rate and, after more than 130 cycles it recovers its initial capacity if charged at a low rate (C/20).

Anodes treated at higher temperature (1300 °C) behave differently: the high-C sample (PD2) follows the known trend of decreasing both the reversible capacity and the cyclability while the low-C SiOC showed an opposite evolution with an increase of the first cycle reversible capacity up to 728 mAh g⁻¹. The latter result has been explained observing that for the low-C material, pyrolysis at 1300 °C does not completely consume the amorphous silicon oxycarbide phase as in the high-C SiOC; moreover the remaining silicon oxycarbide network treated at 1300 °C is most probably energetically more stable and less prone to react with the inserted lithium forming irreversible compounds therefore increasing the charge that can be reversible discharged compared to its 1000 °C counterpart.

4.2 Influence of Pyrolysis Atmosphere on the Lithium Storage Properties of Carbon-Rich SiOC Anodes

4.2.1 Introduction

High energy storage materials are vital to meet the requirements of modern consumer electronics. A great deal of work has been devoted to the development of suitable Li insertion materials to obtain high energy density batteries. Many forms of disordered carbons have been studied as active insertion material for lithium ion batteries [11, 31, 32]. Silicon oxycarbide ceramic (SiOC) has emerged as a good anode material candidate due to its higher reversible capacities up to 700 mAh g⁻¹ compared to the theoretical capacity of conventional graphite electrode which is limited to 372 mAh g⁻¹[3, 5,7-9, 29, 33]. Silicon oxycarbides are amorphous materials with silicon bonded to oxygen and carbon simultaneously; moreover they usually contain a fraction of free carbon dispersed in the amorphous SiOC matrix [34-37]. The lithium storage properties of SiOC anodes depend on a number of features including the pyrolysis temperature, amount of disordered free carbon, etc. However, the nature of the active sites for Li storage in SiOC ceramics is still a matter of debate. It has been proposed that Li can be stored either on the mixed Si-O-C units[3] or in the free-C phase either in between the carbon layers and also at the edges of each layer[5, 33, 38].

Pioneering work of Dahn et al.[27] followed by the study of Hu et al.[38] showed that the presence of a small amount of hydrogen bonded to carbon enhances the lithium storage capacity of disordered carbonaceous

materials. Accordingly, beside the “usual” intercalation between graphene layers, lithium is supposed to reversibly interact with hydrogen bonded to carbon.

SiOC ceramics investigated within this work are synthesised under pure argon and under argon containing 5% of hydrogen gas. The main focus of this work is to study the influence of the pyrolysis atmosphere on the electrochemical properties of the final SiOC phase with respect to its microstructure and elemental composition.

4.2.2 Experimental Part

4.2.2.1 Sample Preparation

All the chemicals were purchased from Sigma–Aldrich and used as received. In a typical preparation a linear polyhydridomethylsiloxane (PHMS, MW= 1900) was crosslinked with 200 weight % of divinylbenzene using platinum catalyzed hydrosilylation reaction as reported in our previous work [6]. The resulting mixture was cast in plastic tubes, allowed to gel and left for aging at 60 °C. The gels were then pyrolyzed using an alumina tubular furnace (Lindberg/Blue) in different gas atmospheres, namely under pure argon and also under an Ar/H₂ (5% H₂) gas mixture. The samples were heated at a rate of 5 °C/min up to 1000 °C and maintained at the maximum temperature for 1 h (pure Ar) and 7 hrs (Ar/H₂). Cooling down to room temperature was done by turning off the furnace power. The pyrolysed material was then milled in an agate mortar and sieved to a particle size less than 80 µm. The samples are denoted as PD21 for the Ar pyrolysed sample and PD21_H2 for the sample pyrolysed under Ar/H₂ atmosphere.

4.2.2.2 Characterization

C and O elemental analysis were performed using a C-analyzer, LecoTC-200 (Leco Corp USA) to determine the carbon content and an O-analyzer, Leco TC-436 (Leco Corp USA) to quantify the oxygen content. The hydrogen content was analyzed by Mikroanalytisches Labor Pascher (Germany). The amount of silicon is calculated as the difference to 100 wt% of the sum of the C, O & H contents. The defects (dangling bonds) in the structure were thoroughly studied using the ESR technique. The ESR analysis was carried out with a Bruker EMX instrument operating in the X band at 9.77 G at room temperature, 0.20 mW microwave power and 0.2 G modulation amplitude. Diphenylpicrylhydrazyl (DPPH) was used as an external reference. The ^{29}Si MAS NMR experiments are performed with an AVANCE 300 Bruker using a 7 mm probe-head (Bruker Instruments, Karlsruhe, Germany). All the spectra are recorded using single pulse experiments at 45° with a pulse of 2.6 μs with a recycle delay of 50s and 8 kHz of spinning speed. The Raman spectra were collected on a Jobin Yvon Raman spectrometer (Horiba-Jobin Yvon, model T6400) with an excitation wavelength of 514 nm (Ar laser) and spectra were detected by a CCD (256x1024 pixels) cooled by liquid nitrogen.

For the electrochemical characterization, Swagelok® type, two-electrodes, half cells were assembled in an argon-filled glove box (MBraun, Germany), as described elsewhere¹⁶. The following current rates were applied for lithium insertion/extraction: 2x C/20 (18.6 mA g⁻¹), 5x C/10 (37.2 mA g⁻¹), 5x C/5 = (74.4 mA g⁻¹), 20x C/2 (186 mA g⁻¹), 50x C (372 mA g⁻¹) and 50x 2C (744mA g⁻¹).The same rate was used for charge (C) and discharge (D) studies and the measured capacities were recalculated to the

initial amount of active mass for data analysis. The potential was limited to 0 and 3 V for insertion and extraction, respectively.

4.2.3 Results and Discussion

The chemical compositions of the studied SiOC ceramics are reported in Table 4.7. The amount of free carbon is calculated from the experimental O/Si ratio using the stoichiometric formula $\text{SiC}_x\text{O}_{2(1-x)}$.

| Sample | Si | C | O | H | Oxycarbide | H/C _{To} | H/C _{free} | SiC _x O _{2(1-x)} | C _{free} |
|---------|-------|-------|-------|------|--|-------------------|---------------------|--------------------------------------|-------------------|
| | | | | | Stoichiometry | tal | | x) | |
| (Wt. %) | | | | | SiC _x O _{2(1-x)} +yC _{free} | (at/at) | | Wt% | |
| PD21 | 29.24 | 55.15 | 14.99 | 0.62 | SiC _{0.55} O _{0.90} +3.85C _{free} | 0.13 | 0.15 | 51 | 49 |
| PD21_H2 | 34.18 | 46.37 | 18.97 | 0.48 | SiC _{0.52} O _{0.97} +2.73C _{free} | 0.12 | 0.15 | 61 | 39 |

Table 4.7. Chemical compositions of the studied SiOC glasses with respective stoichiometric formulae, H/C ratios and weight % of corresponding SiOC and Free carbon phases.

The elemental analysis data reported in Table 4.7 show a significant decrease in the free carbon content for the samples pyrolysed in Ar/H₂ gas atmosphere. This result is due to the more efficient removal of excess C as CH₄ in the presence of H₂ during pyrolysis [50]. Furthermore, the PD21_H2 sample is characterised by a comparatively lower amount of hydrogen. This finding suggests that the amount of hydrogen in the SiOC ceramic is mainly related to the total amount of C present in the sample and is less dependent on the pyrolysis atmosphere. Indeed, the chemical

analysis reveals an almost constant H/C atomic ratio in both compositions, namely 0.12-0.13 and 0.15 for the total and free carbon content, respectively.

The ESR spectra, reported in Figure 4.11 exhibit a single isotropic signal centered at $g = 2.0026$, with a line width of 0.44 and 0.61 G for the PD21 and PD21_H2 samples, respectively. The g value corresponds to carbon dangling bonds [40]. The intensity of the ESR spectrum recorded on the Ar/H₂-treated SiOC sample is lower compared to that pyrolyzed in pure Ar indicating (since the ESR study was performed on the same weight of samples) that pyrolysis in H₂-rich atmosphere leads to a reduction of the defect concentration in the final SiOC ceramic. Thus, a possible mechanism to explain this defect reduction is the transformation of the C dangling bonds into C-H groups.

The Quantitative ESR data are reported in Table 4.8. The spectrum shows a decrease in spin concentration for the hydrogen pyrolysed sample. Number of spins varies from 10^{21} to 10^{20} due to termination of C \cdot with C-H bonds.

| Sample | g value | line width | Spins/g |
|---------|---------|------------|----------|
| PD21 | 2.0017 | 0.79 | 1.27E+18 |
| PD21_H2 | 2.0016 | 0.78 | 1.12E+19 |

Table 4.8 Quantitative ESR data of samples including g-values, line width and spin density. g-values of lies closer to the g-factor of carbon radicals, which have a g-value of 2.0023.

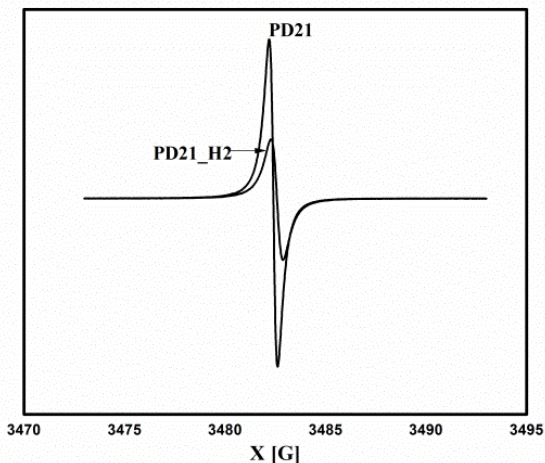


Figure 4.11 ESR spectrum of PD21 and PD21_H₂ samples. A decreased intensity is observed for PD21_H₂ sample corresponding to a decreased spin density in these samples.

NMR spectra of hydrogen treated samples are represented in Figure 4.12. The spectra show peaks corresponding to different mixed species along with SiO₄ and SiC₄ peaks. The peaks are observed in same position with same chemical shifts. Deconvolution of spectra shows an increased SiO₄ concentration for the hydrogen pyrolysed samples. This can be explained by connecting many reasons. The presence of hydrogen in the pyrolysis atmosphere terminated carbon dangling bonds with formation of C-H bonding and this may reduce the attack of SiO₄ units with carbon. There is a noticeable reduction in the SiC₄ concentration from ca. 27% to 16 % for hydrogen pyrolysed samples. The detailed deconvolution datas are reported

in Table 4.9 showing concentration of different mixed species in the spectrum.

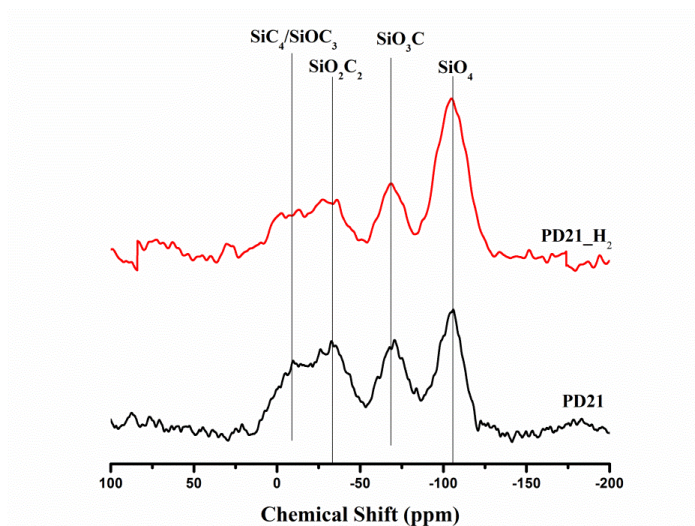


Figure 4.12 ^{29}Si MAS NMR spectra of studied compositions showing mixed SiOC units in both samples.

| Sample | Pyrolysis Temp. (°C) | Si site (%) | | | |
|---------------------|----------------------------|----------------|------------------------|--------------------------|----------------|
| | | SiO_4 | SiO_3C | SiO_2C_2 | SiC_4 |
| PD21 | 1000 | 29 | 24 | 20 | 27 |
| PD21_H ₂ | 1000 | 47 | 18 | 19 | 16 |

Table 4.9 NMR deconvoluted spectrum showing compositions of different mixed SiOC units.

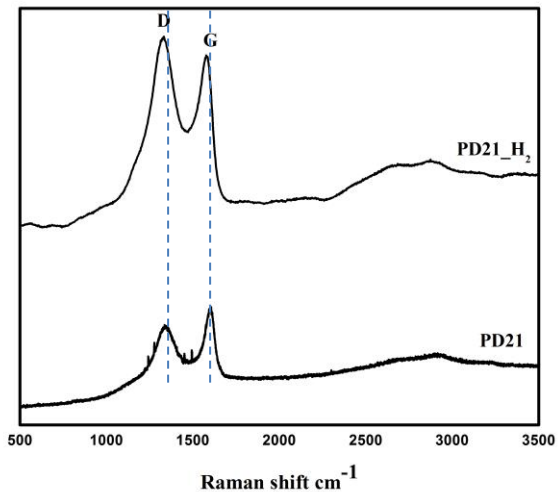


Figure 4.13 Raman spectra of studied compositions with appearance of D band at 1350 cm^{-1} and G band at 1600 cm^{-1} .

The carbon phase in both the composition is characterized in detail using Raman spectra. Raman spectra of the studied samples reveal the nature and crystallinity of the carbon phase. Spectra show typical D and G bands corresponding to the disordered induced vibrations and of stretching of sp^2 carbon pairs. The crystallite size data and FWHM of respective peaks are reported in Table 4.10. The crystallite size is larger for the hydrogen pyrolysed sample showing increased ordering of carbon networks in hydrogen pyrolysed samples.

| Sample Name | D (cm ⁻¹) | G (cm ⁻¹) | I _D /I _G | La (Å ⁰¹) | FWHM _D (cm ⁻¹) | FWHM _G (cm ⁻¹) |
|-------------|-----------------------|-----------------------|--------------------------------|-----------------------|---------------------------------------|---------------------------------------|
| PD21 | 1349 | 1594 | 0.68 | 11.2 | 154 | 74 |
| PD21_H2 | 1332 | 1567 | 0.95 | 14.2 | 198 | 99 |

Table 4.10 Raman spectra deconvolution data showing intensity ratios and calculated lattice parameters along with respective D and G peak positions.

The first charge/discharge profiles and cycling performance of the studied SiOC compositions are presented in Figure 4.14. The charging profiles (Figure 2a) of the two samples are very similar to each other: There is a solid electrolyte interface (SEI) formation between 1.4 – 0.7 V [12] followed by a fading quasi-plateau which starts at 0.5 V related to lithium intercalation into SiOC ceramics [36]. The voltage profiles of the lithium extraction of PD21 and PD21_H₂ are also similar, demonstrating no pronounced plateau. Almost the whole capacity is recovered under 1.5 V, while e.g. the materials produced by Ahn et al.[40] reveal a significantly stronger hysteresis with a capacity recovered in the broad 0 to 3V potential range.

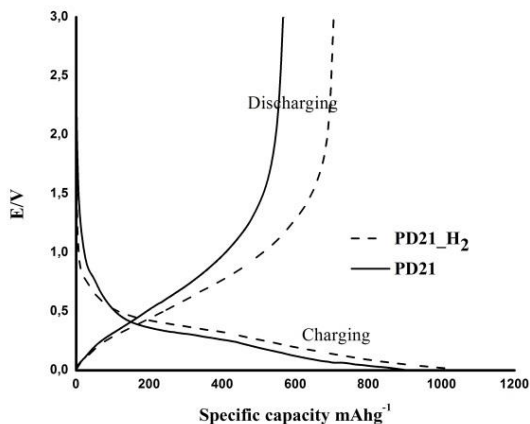


Figure 4.14 First cycle charging/discharging profiles of argon and argon/hydrogen pyrolysed samples with potential V vs specific capacity (mAh g^{-1}). Solid lines represents the charge/discharge profiles of argon pyrolysed samples and dashed lines represents the hydrogen treated sample.

The sample treated under H_2 shows higher charging and discharging capacities. The capacity values together with the efficiency of the first cycle are summarized in Table 4.11. The coulombic efficiency is the quantity of charge captured irreversibly within the first cycle and is estimated by the ratio $Q_{1st, \text{ extraction}}/Q_{1st, \text{ insertion}} \times 100 \%$. The sample treated under H_2 reveals increased insertion (1049 mAhg^{-1} vs 898 mAhg^{-1}) and extraction (704 vs 568 mAh g^{-1}) capacities. There is a significant improvement of the first cycle efficiency for the samples pyrolysed in Ar/H_2 mixture, namely 67 vs 63 % compared to that of SiOC pyrolysed in pure Ar .

Increased capacity during initial cycling can be explained in connection with increased mixed bond%. The H₂ pyrolysis leads to reduction in excess carbon and the mixed bond composition raise to 58% from 51%. This explanation is in agreement with our findings on previous section with significantly larger first cycle capacity for these samples. The removal of excess carbon in turn also helps to improve their cycling behaviour and capacity. The samples maintain its initial capacity gain throughout the cycling procedure with an excellent rate capability.

| Sample | Pyrolysis Atmosphere | Q_{insertion} (mAh/g) | Q_{extraction} (mAh/g) | Efficiency (%) |
|----------------|-----------------------------|--------------------------------------|---------------------------------------|-----------------------|
| PD21 | Ar | 898 | 568 | 63 |
| PD21_H2 | Ar/H ₂ | 1049 | 704 | 67 |

Table 4.11 Electrochemical first cycle data of the studied SiOC ceramics.

Figure 4.15 presents the extended cycling performance of PD21 and PD21_H₂, registered for increasing current applied to insertion/extraction of lithium. The charging/discharging procedure was described in detail in the experimental part. Both samples present stable cycling behavior; the small oscillations of the recovered capacity (rate C for PD21) are attributed to the changes of the external temperature.

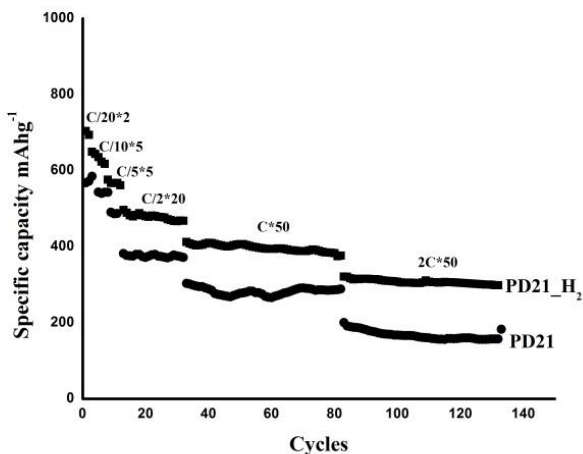


Figure 4.15 Galvanostatic cycling experiments at different current densities from an initial rate of C/20 to a very fast rate of 2C. Charging and discharging has been done at same current rates by changing the polarity of the current. Both the samples

The capacity of the material synthesized under the Ar/H₂ mixture is significantly higher and the losses are lower when switched to higher current compared to that of the material pyrolysed in pure argon. The stable reversible capacity of the SiOC pyrolysed in H₂ at 2C rate is close to 372 mAh g⁻¹, similar to that of the theoretical capacity of graphite when charged with low currents. When 2C/2D rates are applied for pure commercial graphite, a capacity below 100 mAh g⁻¹ is recovered [41].

The explanation why the SiOC ceramic pyrolyzed in an Ar/H₂ mixture shows a better performance in terms of reversible capacity, first cycle efficiency and cyclic stability is not straightforward. Indeed, as reported in the introduction, the active sites for the Li storage in silicon oxycarbides

are still not well defined and comprise the free carbon phase –with lithium intercalated in the graphite structure and bonded at the edge of the C planes - and the mixed Si-C-O units forming the silicon oxycarbide network. Assuming that the main Li storage site is the free C of the SiOC ceramics, we should have measured a corresponding decrease of the recovered capacity for the PD21_H₂ sample, since the pyrolysis in H₂ atmosphere leads to a decrease of the free C content, unless we postulate that the free C phase of the H₂-treated sample has an increased capacity to store Li compared with the one obtained in pure Ar. This could be the case if we follow the observation of Dahn [27] on the role of the H/C molar ratio in the Li storage capacity of carbonaceous materials. Unfortunately our experimental H/C ratio is constant around 0.12 -0.15 (either considering the total C or the C present in the C_{free} phase) for the two set of samples, so we cannot correlate the electrochemical properties with the increasing amount of hydrogen.

Accordingly, our experimental results seem to point towards a modification of the silicon oxycarbide network leading to a corresponding increase of Li storage capacity. The most relevant structural modification induced by the H₂ treatment is the quenching (decrease) of the defect concentration, more specifically a decrease of the C dangling bonds as revealed by the ESR study. We could then assume that C radicals deactivate some potential Li storage sites. The measured difference in the Li charging (or discharging) capacity is ca 150 mAh g⁻¹ which translates into a difference of ca 10²¹-10²² Li atoms/cc (we consider a density of SiOC of 2 g/cc). Knowing that the typical spin concentration (C dangling bonds) in these PDC materials spans in the range between 10¹⁹ and 10²⁰ spins/cc[40], then we can think that 1 C radical can deactivate 10¹ – 10² potential Li storage sites.

4.2.4 Conclusions

The electrochemical behavior of a SiOC ceramic pyrolyzed in an Ar/H₂ atmosphere has been studied and compared with the same material pyrolysed in pure Ar. The presence of hydrogen in the pyrolysis atmosphere significantly affects the lithium insertion behavior leading to an improved first cycle capacity, efficiency and enhanced rate capability. ESR study showed that the presence of hydrogen reduced the concentration of C dangling bonds in the oxycarbide structure. It has been proposed that C radicals can de-activate potential Li storage sites degrading the electrochemical performance of SiOC anode materials.

References

- [1] W. Xing, A.M. Wilson, K. Eguchi, G. Zank and J.R. Dahn, "Pyrolysed polysiloxanes for use as anode materials in lithium-ion batteries", *J. Electrochem. Soc.*, **144** (1997) 2410-2416.
- [2] A.M. Wilson, G. Zank, K. Eguchi, W. Xing, J.R. Dahn " Pyrolysed silicon-containing polymers as high capacity anodes for lithium-ion batteries", *J. Power Sources*, **68** (1997) 195-200.
- [3] E. Sanches-Jimenez, R. Raj, "Lithium insertion in polymer-derived silicon oxycarbide ceramics", *J. Am. Ceram. Soc.*, **93** [4] (2010) 1127–1135.
- [4] H. Fukui, H. Ohsuka, T. Hino, K. Kanamura, "Preparation of microporous Si-O-C composite material and its lithium storage capability". *Chem. Lett.*, **38** (2009) 86-87.
- [5] H. Fukui, H. Ohsuka, T. Hino and K. Kanamura, " A Si-O-C composite anode: High capability and proposed mechanism of lithium storage associated with microstructural characteristics", *Appl. Mater. Interf.*, **2** (2010) 998-1008.
- [6] P. Dibandjo, M. Graczyk-Zajac, R. Riedel, V.S. Pradeep, G. D. Soraru, "Lithium insertion into dense and porous carbon-rich polymer-derived SiOC ceramics", *J. Eur. Ceram. Soc.*, **32** [10] (2012) 2495–2503.
- [7] M. Graczyk-Zajac, L. Toma, C. Fasel, R. Riedel, "Carbon-rich SiOC anodes for lithium-ion batteries: Part I. Influence of material UV-pre-

-
- treatment on high power properties”, *Sol. State Ion.*, 225, (2012) 522–526.
- [8] J. Kaspar, M. Graczyk-Zajac, R. Riedel, “Carbon-rich SiOC anodes for lithium-ion batteries: Part II. Role of thermal cross-linking”, *Sol. State Ion.*, 225 (2012) 527–531.
- [9] D. Ahn, R. Raj “Cyclic stability and C-rate performance of amorphous silicon and carbon based anodes for electrochemical storage of lithium”, *J. Power Sources*, 196 (2011) 2179–2186.
- [10] D. Ahn, R. Raj, “Thermodynamic measurements pertaining to the hysteretic intercalation of lithium in polymer-derived silicon oxycarbide”, *J. Power Sources*, 195 (2010) 3900–3906.
- [11] J.M. Tarascon, M. Armand “Issues and challenges facing rechargeable lithium batteries” *Nature*, 414, (2001) 359-367.
- [12] M. Winter, J.O. Besenhard, M.E. Spahr, P. Novak, “ Insertion electrode materials for rechargeable lithium bateries” *Adv. Mater.*, 10 (1998) 725-763.
- [13] B. Scrosati, J. Garche, “ Lithium batteries: Status, prospectus and future”, *J. power sources*, 195 (2010) 2419-2430.
- [14] R. Marom, S. F. Amalraj, N. Leifer, D. Jacoba and D. Aurbach, “A review of advanced and practical lithium battery materials”, *J. Mater. Chem.*, 21(2011)9938-9954.
- [15] H.Zhang, C.G. Pantano, “ Synthesis and characterisation of silicon oxycarbide glasses” *J. Am. Ceram. Soc.*, 73(1990) 958-963.

-
- [16] H. Brequel, J. Parmentier, S. Walter, R. Badheka, G. Trimmal, S. Masse, J. Latourmerie, P. Dempsey, C. Turquat, A. Jesmartin, L. Lemeindre, U.A. Jaysurya, D. Hourlier, H.J. Kleebe, G.D. Soraru, S. Enzo and F. Babboneu, “ Systematical and structural characterisation of the high temperature behaviour of nearly stoichiometric silicon oxycarbide glasses” *Chem. Mater.*, **16**(2004) 2585-2598.
- [17] G. Mera, A. Navrotsky, S. Sen, H.-J. Kleebe, R. Riedel, “Polymer-derived SiCN and SiOC ceramics – structure and energetics at the nanoscale”, *J. Mater. Chem. A*, **1** (2013) 3826-3836.
- [18] G. D. Sorarù, R. Pena-Alonso, H.-J. Kleebe, “The effect of annealing at 1400 °C on the structural evolution of porous C-rich silicon (boron)oxycarbide glass”, *J. Eur. Ceram. Soc.*, **32** (2012) 1751–1757.
- [19] H.-J. Kleebe, Y. D. Blum, “SiOC ceramic with high excess free carbon”, *J. Eur. Ceram. Soc.*, **28** (2008) 1037–1042.
- [20] G. D. Sorarù, F. Dalcanale, R. Campostrini, Amélie Gaston, Y. Blum, S. Carturan, P. R. Aravind, “Novel polysiloxane and polycarbosilane aerogels via hydrosilylation of preceramic polymers”, *J. Mater. Chem.*, **22** (2012) 7676-7680.
- [21] G.D. Soraru, S. Modena, E. Guadagnino, P. Colombo, J. Egan and C. Pantano, “Chemical durability of silicon-oxycarbide glasses,” *J. Am. Ceram. Soc.*, **85** [6] (2002) 1529-36.

-
- [22] P. Dibandjo, S. Diré, F. Babonneau, G.D. Soraru, "Influence of the polymer architecture on the high temperature behavior of SiCO glasses: A comparison between linear- and cyclic-derived precursors", *J. Non-Cryst. Sol.*, **356** (2010) 132–140.
- [23] F. Tuinstra, J.L. Koenig, "Raman spectrum of graphite", *J. Chem. Phys.* **53** (1970) 1126–30.
- [24] A.C. Ferrari and J. Robertson, "Interpretation of Raman spectra of disordered and amorphous carbon", *Phys. Rev. B*, **61** (2000) 14095-107.
- [25] G. T. Burns, R. B. Taylor, Y. Xu, A. Zangvil, G. A. Zank, "High-Temperature chemistry of the conversion of Siloxanes to Silicon Carbide", *Chem. Mater.*, **4** (1992) 1313-132.
- [26] J.R. Dahn, T. Zheng, Y. Liu, J.S. Xue, "Mechanisms for lithium insertion in carbonaceous materials", *Science* **270** (1995) 590–593;
- [27] T. Zheng, W.R. McKinnon, J.R. Dahn, "Hysteresis during lithium insertion in hydrogen-containing carbons", *J. Electrochem. Soc.*, **143** (1996) 2137–2145.
- [28] J. Kaspar, M. Graczyk-Zajac, R. Riedel, "Lithium insertion into carbon-rich SiOC ceramics: Influence of pyrolysis temperature on electrochemical properties", *J. Power Sources*, **225** (2012) 527-531.

-
- [29] H. Azuma, H. Imoto, S. Yamada, K. Sekai, "Advanced carbon anode materials for lithium ion cells" *J. Power Sources*, 81–82 (1999) 1–7.
- [30] A. H. Tavakoli, R. Campostrini, C. Gervais, F. Babonneau, J. Bill, G. D. Sorarù, A. Navrotsky, "Energetics and structure of polymer derived Si-(B-)O-C Glasses: Effect of the boron content and pyrolysis temperature", *J. Am. Ceram. Soc.*, (2013) Submitted.
- [31] M. Armand and J.-M. Tarascon, "Building better batteries", *Nature*, 451, (2008) 652–657
- [32] H. Azuma, H. Imoto, S. Yamada, and K. Sekai, "Advanced carbon anode materials for lithium ion cells", *J. Power Sources*, 81-82, 1–7 (1999)
- [33] H. Fukui, H. Ohsuka, T. Hino, and K. Kanamura, "Polysilane/Acenaphthylene Blends Toward Si–O–C Composite Anodes for Rechargeable Lithium-Ion Batteries", *J. Electrochem. Soc.* 158, (2011)A550
- [34] P. Colombo, G. Mera, R. Riedel, and G. D. Sorarù, "Polymer-Derived Ceramics: 40 Years of Research and Innovation in Advanced Ceramics", *J. Am. Ceram. Soc.* 93 [7] (2010)1805-1837
- [35] C. Pantano, A. Singh, and H. Zhang, "Silicon Oxycarbide Glasses", *J. Sol-Gel Sci. Technol.*, 25, (1999)7–25
- [36] A. Saha, R. Raj and D. L. Williamson, "A Model for the Nanodomains in Polymer-Derived SiCO", *J. Am. Ceram. Soc.*, 89[7] (2006) 2188-2195
- [37] G. Gregori, H.-J. Kleebe, Y. D. Blum and F. Babonneau, "Evolution of C-rich SiOC ceramics – Part II. Characterization by high lateral

-
- resolution techniques: electron energy-loss spectroscopy, high-resolution TEM and energy-filtered TEM”, *Int. J. Mater. Res.*, 97 [6] (2006) 710-720
- [38] Y.-S. Hu, P. Adelheim, B. M. Smarsly, S. Hore, M. Antonietti, J. Maier, “Synthesis of Hierarchically Porous Carbon Monoliths with Highly Ordered Microstructure and Their Application in Rechargeable Lithium Batteries with High-Rate Capability”, *Adv. Funct. Mater.* 17, (2007) 1873-1878
- [39] M. Narisawa, T. Kawai, S. Watase, K. Matsukawa, T. Dohmaru, K. Okamura, A. Iwase, “Long-Lived Photoluminescence in Amorphous Si–O–C(–H) Ceramics Derived from Polysiloxanes”, *J. Am. Ceram. Soc.* 95 (2012)3935–3940
- [40] G.D. Sorarù, F. Babonneau, J.D. Mackenzie, “Structural evolutions from polycarbosilane to SiC ceramic”, *J. Mat. Science*, 25 (1990) 3886-93.
- [41] S.R. Sivakumar, J.Y. Nerkar, A.G. Pandolfo, “Rate capability of graphite materials as negative electrodes in lithium-ion capacitors”, *Electrochim. Acta* 55 (2010) 3330–3335.

Chapter 5. Li Storage Properties of Dense and Porous SiOC ceramics

Part of this chapter has been published in:

“Lithium Insertion into Dense and Porous Carbon-Rich Polymer-Derived SiOC Ceramics”, P. Dibandjo, M. Graczyk-Zajac, R. Riedel, V.S. Pradeep, G.D. Soraru, *Journal of the European Ceramic Society*, 03/2012; 32(10):2495–2503. DOI:10.1016/j.jeurceramsoc.2012.03.010

5.1 Introduction

The increase in energy density and power density requirements for lithium-ion batteries leads to continuous research for new electrode materials. Currently mostly graphitic materials are used as anode material in lithium ion batteries due to low price and high reversibility despite relatively low capacity (372 mAh g^{-1}), instability during long-time cycling and inadequacy for high power applications [1,2]. In consequence there is still a need of new materials, which could be economically advantageous but would demonstrate higher capacity, longer life time and better high rate capability. Carbon-containing silicon oxycarbide electrodes for Li-ion batteries have been widely studied by Dahn et al. in the middle of the nineties [3–7]. Nevertheless, there is presently an interest in these ceramic-based materials due to the recently announced commercialization of SiOC ceramic based anodes (by Dow Corning [8]) and the increased availability/lower price of commercial ceramic polymer precursors (PDC's). Recently various SiCN [9–13] and SiOC [14–21] systems of high carbon content have been reported to exhibit a good electrochemical performance in terms of lithium insertion/extraction. Some of the SiOC compositions show high reversible capacities above 600 mAh g^{-1} [17, 19, 20]. However, there is still no clear understanding of the type of active sites responsible for such high values of Li storage. Moreover, a basic research on the mechanism of lithium storage in polymer-derived SiOC materials is still required as the final electrochemical properties of the material depend significantly on the chemical composition of the preceramic polymer and pyrolysis temperature. The work of Sanchez and Raj [16] proposes that the unusually high reversible capacity of silicon oxycarbide is due to the presence of silicon sites in which Si atoms share bonds with O and C atoms, the so called

mixed silicon oxycarbide units or mixed bonds. On the other hand Fukui et al., working on a microporous silicon oxycarbide glass [18,19] suggested that lithium atoms could also be stored in the glass micropores, besides being stored in the interstitial spaces or edges of graphene layers formed in situ during the SiOC synthesis procedure. In the recent years we gained experience in producing porous silicon oxycarbide glasses by etching of dense SiOC materials [22–25]. In particular we have studied how the feature of the porous material correlates with the composition and pyrolysis treatment of the parent dense SiOC glass. Accordingly, we decided to take advantage of our experience and to investigate the electrochemical behavior of dense/porous SiOC glasses with the aim of shedding some light on the role of porosity on the storage capacity of SiOC glasses. We studied two polymer- derived SiOC compositions with different amount of carbon. The porous SiOCs have been obtained by HF etching of the silica phase present in the silicon oxycarbide network; following a reported procedure [22] In order to promote the formation of porosity through HF etching the SiOC glasses have been pyrolyzed at 1400°C to increase the phase separation of the silicon oxycarbide network. It is worth saying that the highest Li capacity is usually measured for SiOC glasses pyrolyzed at lower temperature (ca 1000–1100 °C) [17–21]. However, since in this study we are not aiming for high Li insertion capacities but indeed, for comparing the electrochemical behavior of dense and porous materials, we deliberately decided to use the samples treated at high temperatures. The starting preceramic network was obtained by crosslinking a linear polysiloxane containing Si-H groups with different amount of divinylbenzene (DVB) [26]. The silicon oxycarbide materials, either in their dense or porous form, have been structurally characterized using X-ray diffraction, Raman and ²⁹Si solid-state NMR spectroscopies, N₂ adsorption and HR-TEM imaging. Finally the Li-

intercalation process has been studied by electrochemical methods. Comparison of the electrochemical behavior among the four sets of samples contributes to understand the type of lithium intercalation mechanism in SiOC ceramics.

5.2. Experimental

5.2.1. Materials Synthesis

All the chemicals were purchased from Sigma–Aldrich and used as received. As siloxane polymer we used a linear polyhydridomethylsiloxane (PHMS, MW = 1900). In a typical preparation the catalyst (platinum divinyltetramethyldisiloxane always 5 ppm relative to the Si compound) and 10, 200 wt% (calculated on the siloxane weight) of divinylbenzene (DVB) were mixed together and then added to the siloxane to prepare the carbon-enriched SiOC preceramic polymers without any addition of solvent. The resulting low-viscous mixture was placed in a test tube which was covered. The cast solution was allowed to stand at room temperature (RT) and complete setting was achieved overnight. After RT setting, the solutions become hard rubbery materials. All the samples were pyrolyzed using an alumina tubular furnace (Lindberg/Blue) under 150 mL/min of flowing argon. The samples were heated at 5 °C/min and maintained for one hour at a temperature of 1400 °C. The obtained silicon oxycarbide products were milled in an agate mortar and sieved to a particle size smaller than 80 µm. The specimens are denoted as SiOC-*X* where *X* represents the amount of DVB used for the synthesis (10, 200). Etching of the silicon oxycarbide was performed using a 20 vol% HF solution in H₂O. 0.5 g of the powdered sample was placed in a polypropylene container with the appropriate hydrofluoric acid (HF) solution. The solution was gently stirred at room

temperature for 6 h and then filtered and rinsed off with distilled water to remove any residual HF. The sample was then kept inside an oven at 100 °C for one day to dry. Hereafter, the specimen is denoted as SiOC-X-HF (10, 200).

5.2.2. Preparation of Electrodes and Cells

The electrodes from SiOC-10, SiOC-200, SiOC-10-HF and SiOC-200-HF materials were prepared by mixing the material with 10 wt% polyvinylidene fluoride (PVdF, SOLEF) solution in *N*-methyl-2-pyrrolidone (NMP, BASF). The ratio carbonaceous material/PVdF was 9:1 and was constant for all the samples. NMP was added in order to form homogeneous slurry (about 0.8 g of solvent for 1 g of solution). The slurry was spread on the rough side of copper foil (10 μm, Copper SE-Cu58 (C103), Schlenk Metallfolien GmbH & Co. KG) using hand blade coating technique and dried at 80 °C for 24 h. The active material loading was always between 6 and 8 mg/cm². After drying, the circles (electrodes) of 10 mm in diameter were cut. The electrodes were pressed with 40 kN cm⁻² for 3 min. The weight of electrodes was measured, and then the electrodes were dried under vacuum at 90°C for 48 h in Buchi oven and transferred directly to the glove box (MBraun Glove Box Systems, H₂O, O₂ < 1 ppm) without contact with air. All the electrochemical measurements were performed in two-electrodes of Swagelok® type cells with SiOC as the working electrode and lithium foil (99.9% purity, 0.75 mm thick, Alfa Aesar) as counter/reference electrode. High purity solution of 1 M LiPF₆ in ethylene carbonate (EC) and dimethyl carbonate of weight ratio 1:1 (LP30, Merck KGaA) was used as electrolyte. Porous polypropylene membrane (Celgard 2500) was used as separator.

5.2.3. Characterization Techniques

Hermetically closed cells were electrochemically tested by means of galvanostatic and cyclic voltammetry methods using VMP multipotentiostat (BioLogic Science Instruments). For galvanostatic charges the cut-off voltages of 0 and 3 V were applied. A constant voltage float was used when the cell reached the cut-off voltage for slow charging regime (18 mA g^{-1}). The SiOC-X and the SiOC-X-HF samples were characterized by X-ray diffraction (XRD) with a synchrotron radiation with a wavelength of 4.562 nm. The Raman spectra were collected using a system inVia Raman microprobe (Renishaw) employing an Ar-ion laser with a wavelength of 514.5 nm. The ^{29}Si MAS NMR was performed with a MSL300 Bruker with 7 mm probe-head at a spinning rate of 4 kHz. All the ^{29}Si NMR spectra were recorded using one pulse experiments with 90° pulses and 100 s as recycle delays, conditions that allow a quantitative assessment of the spectra. The experimental spectra were simulated using dmfit modeling software developed, as described in Massiot et al.[26] The analyzed signals arising from the different pyrolyzed samples are labeled as Q (SiO_4), D (SiC_2O_2), T (SiOC_3) and X (SiC_4). Spectra were referenced externally to TMS at 0 ppm. The specific surface area (SSA) and pore size distributions (PSD) of the resulting porous SiOC ceramics were measured by nitrogen gas adsorption at 77 K using an ASAP 2010 (Micromeritics) instrument. SSA was determined from a BET (Brunauer, Emmet and Teller) analysis in the P/P_0 range of 0.05–0.30 using a molecular cross-sectional area for N_2 of 0.163 nm^2 and a minimum of 5 data points. The pore size distributions were obtained from the adsorption branch of the isotherm through the BJH (Barret, Joyner and Halenda) analysis. The HR-TEM images were taken with

a TOPCON EM002B transmission electron microscope operated at 200 kV. For the studies, the powder was dispersed in *n*-butanol using an ultrasonic bath and transferred on a carbon-coated grid for measurement.

5.3. Results

5.3.1. Structural Characterization

5.3.1.1. Chemical Analysis

Chemical analysis results of the as pyrolyzed SiOCs as well as that of the HF etched samples are reported in Table 5.1. Increasing the amount of DVB in the starting precursor results into an increase of the C content in the pyrolyzed SiOC from 18.6 up to 44.2 wt%. The HF treatment dissolves SiO₂ with a corresponding decrease of the O content in the HF-treated samples. In Table 5.1 the composition of the silicon oxycarbide materials is also represented considering the general formula: $x\text{SiC} + (1-x)\text{SiO}_2 + y\text{C}_{\text{free}}$ [27]. The main difference between the SiOC-10 and the SiOC-200 lies in the amount of C_{free} which ranges from ~14 wt% up ~40 wt%, respectively. On the other hand the relative amounts of SiC and SiO₂ are similar for the two studied compositions: ~0.30 moles of SiC and ~0.70 moles of SiO₂.

| Sample Name | Element content* | | | $x\text{SiC} + (1-x)\text{SiO}_2 + y\text{C}_{\text{free}}$ | | | C_{free} |
|-----------------|------------------|------|------|---|------------------|-------------------|--------------------------|
| | (wt%) | | | (mol) | | | (wt%) |
| | C | O | Si | SiC | SiO ₂ | C _{free} | |
| SiOC-10 | 18.6 | 34.4 | 42.2 | 0.29 | 0.71 | 0.74 | 14.1 |
| SiOC-200 | 44.2 | 23.4 | 31.1 | 0.34 | 0.66 | 2.97 | 40.2 |
| SiOC-10- HF | 39.3 | 17.6 | 33 | 0.53 | 0.47 | 2.25 | 35.3 |
| SiOC-200- HF | 66 | 8 | 19 | 0.63 | 0.37 | 7.47 | 65.4 |

Table 5.1 Elemental analysis results of the studied silicon oxycarbide samples.

5.3.1.2. Powder XRD and Raman Spectroscopy Analysis of the Studied Silicon Oxycarbide Materials

Before etching, the diffraction pattern presented two broad peaks at $2\theta = 6.4^\circ$ and 10.4° (Figure 5.1) attributed to amorphous SiO_2 and SiC phase respectively. It is well known that silicon oxycarbide undergoes, at high temperature, a phase separation with formation of SiO_2 -rich nanodomains and nanocrystalline SiC [28]. The two compositions follow this regular evolution. For both compositions, after HF etching, the XRD pattern show a decrease of the halo of the amorphous silica at $2\theta = 6.4^\circ$, which allows the reflection corresponding to the (0 0 2) plane of graphite at $2\theta = 7.1^\circ$ to emerge from the background. At the same time, reflections corresponding to (1 0 1) planes of graphite at $2\theta = 12.5^\circ$, and the diffraction peaks of SiC become more evident (Figure 5.1). We also find an increase of the intensity of the peak at $2\theta = 10.4^\circ$. The d value of peak at $2\theta = 7.1^\circ$ can be attributed to the (0 0 2) reflection of graphitic, disordered carbon. Finally,

a new peak at $2\theta = 5.4^\circ$ ($d = 4.86^\circ \text{ \AA}$) is assigned to the formation of F-intercalated graphite [29]. Raman spectroscopy is extensively used for the characterization of graphitic carbon materials [30]

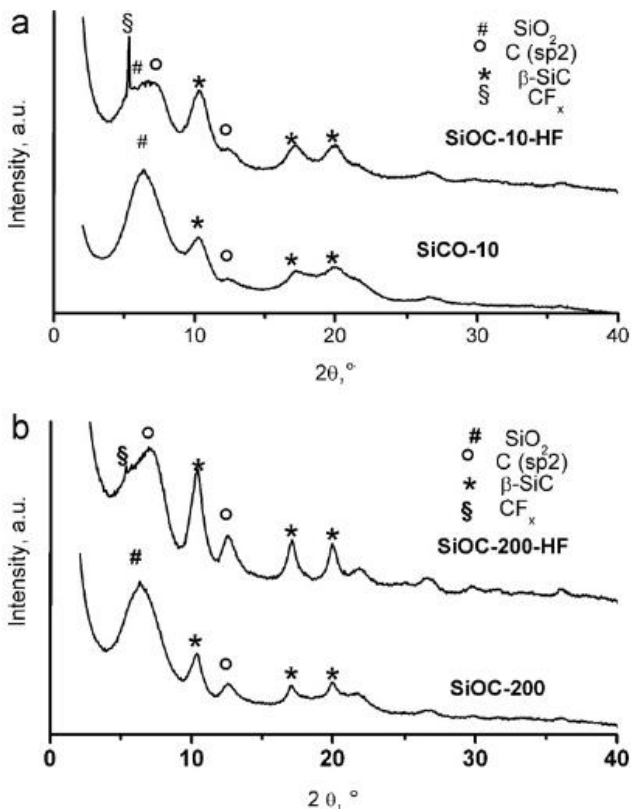


Figure 5.1. XRD diffraction patterns of (a) SiOC-10, SiOC-10-HF and (b) SiOC- 200, SiOC-200-HF. CF_x denotes fluorine-intercalated graphite

Raman allows distinguishing between low, medium and high structural organization in all types of carbon materials. Figure 5.2a and b shows the Raman spectra of the SiOC samples before and after etching. The nature of the Raman spectra is identical in both unetched compositions and is characterized by two bands, with similar intensity, at $\sim 1340\text{ cm}^{-1}$ and $\sim 1600\text{ cm}^{-1}$ which are attributed to the D and G bands of carbon, respectively [31]. Before etching the intensity ratio of the $I(D)/I(G)$ bands is higher for both, the SiOC-10 and SiOC-200 samples than that of the corresponding etched samples. A high $I(D)/I(G)$ ratio indicates ordering of carbon clusters into nanocrystalline form and has been already discussed elsewhere [10,31]. After etching, the principal change is a consistent narrowing of the G band, which suggests a higher degree of order of the graphitic carbon structures [22].

5.3.1.3. N₂ Adsorption Analysis

The porous structure of the SiOC samples prepared from PHMS and DVB was characterized by nitrogen sorption method, the obtained results are reported in Table 5.2. The N₂ adsorption isotherms are characteristic of highly microporous materials with a small hysteresis loop suggesting also the presence of mesopores [32,33] (Figure 5.3). The specific surface area (BET) increases from 460 to 640 m²/g with the increase of the DVB content. Regarding the mesoporous volume fraction the value did not change with the increase of the DVB, while the microporosity shows a net increase in volume from 0.05 to 0.20 cm³ g⁻¹. The pore size distribution does not change with the amount of DVB, having an average value of 2.5 nm. It is important to note that the non-etched SiOC-10 and SiOC-200 samples do not present any measurable porosity.

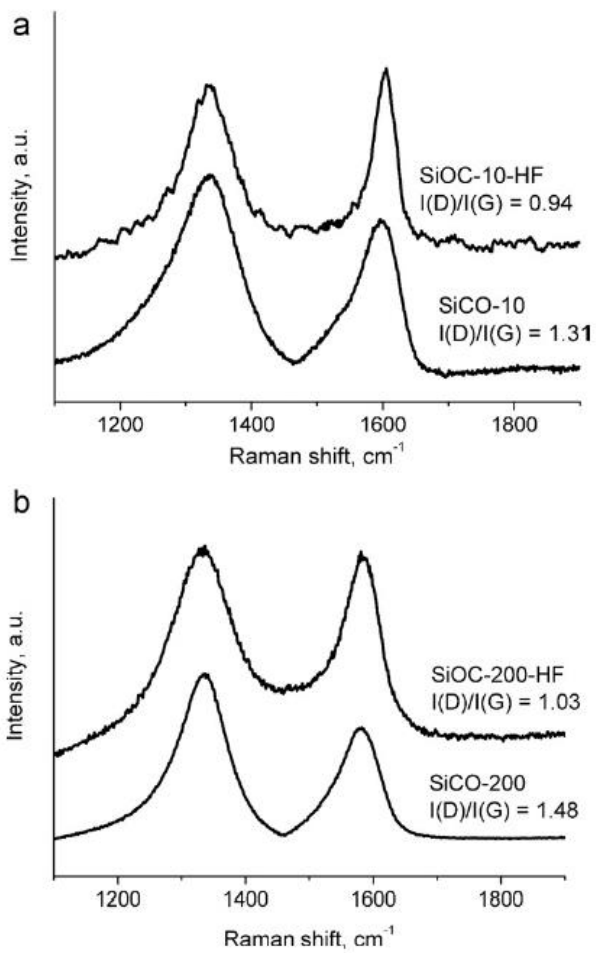


Figure 5.2. Raman spectra of (a) SiOC-10, SiOC-10–HF and (b) SiOC-200, SiOC-200–HF samples.

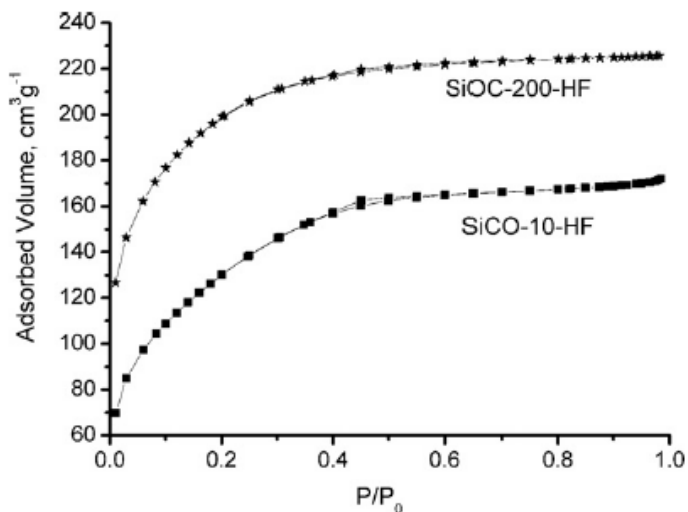


Figure 5.3. Nitrogen adsorption/desorption of SiOC-10-HF and SiOC-200-HF.

| Samples | SSA (m ² /g) ±1% | Mesopore volume (cm ³ /g) ^a ±0.01 | Micropore volume (cm ³ /g) ^c ±0.01 | Average pore size (nm) ^b ±0.1 |
|-----------------|-----------------------------------|---|--|--|
| SiOC-10- HF | 460 | 0.17 | 0.05 | 2.6 |
| SiOC- 200-HF | 640 | 0.13 | 0.20 | 2.4 |

^a Mesopore range ≈ 2-50nm. Micropore range <2nm

^b As obtained from the BJH mesopore distribution using the adsorption data of isotherm

^c Calculated from the t-plot analysis

Table 5.2. SSA, Mesopore, and micropore volumes and pore size (BJH) of carbon based materials

5.3.1.4. Transmission Electron Microscopy (TEM)

Characterization

The overall microstructure of the SiOC samples produced upon pyrolysis at 1400 °C is similar to those of other carbon-rich SiOC materials³⁴ with fringes of turbostratic carbon, and SiC nanocrystals embedded in an amorphous SiOC matrix. The HR-TEM study does not allow us to clearly differentiate SiOC-10 and SiOC-200 materials as they show a similar microstructure. Accordingly we discuss here the features of both samples based on the HR-TEM images of SiOC-10 composition (Figure 5.4a–c). Before and after etching turbostratic carbon features and SiC nanocrystals can be clearly seen (Figure 5.4a and b). Moreover, for the HF-etched samples nanopores, which according to the N₂ adsorption analysis have a dimension below 2.5 nm, can be seen. Interestingly, few large graphitic structures have also been observed (Figure 5.4c) consisting of extended graphite nano-ropes formed by several sp² carbon planes which reach several tenth of nanometers. Moreover, close to these larger structures, pores extending up to 5–10 nm have also been detected. In conclusion, the HR-TEM investigation confirms the formation of silicon oxycarbide glasses consisting of a mixture of free carbon in the form of turbostratic carbon and SiC nanocrystals dispersed into a mostly amorphous matrix. In the etched samples predominantly fine pores, in agreement with the N₂ adsorption studies, have been observed with few larger voids (5–10 nm) located close to extended graphite nano-ropes.

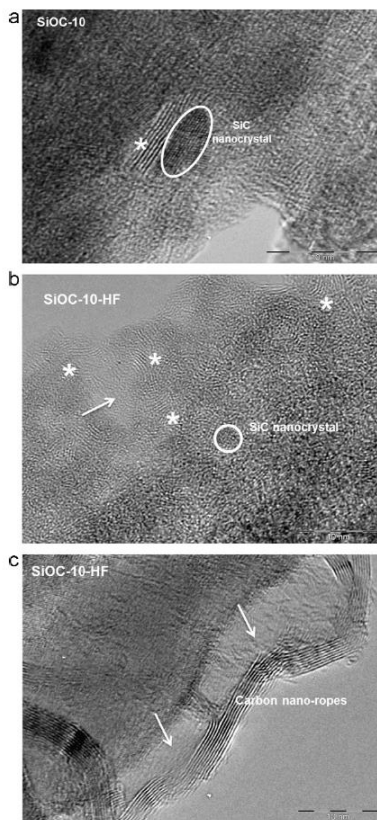


Figure 5.4. HR-TEM images of: SiOC-10 (a), and SiOC-10-HF (b and c). Stars indicate turbostratic carbon features while arrows indicate the pores present in the structure.

5.3.2. Electrochemical Investigation

In Figure 5.5 the first lithium insertion/extraction cycles are presented and the electrochemical data are summarized in Table 5.3. Figure 5.5(a) shows the first charge/discharge cycle registered for the SiOC samples before HF etching. A high first charge capacity of 380 and 611 mAh g⁻¹ is followed by significantly lower discharge capacities of 102 and 241 mAh g⁻¹ for SiOC-10 and SiOC-200, respectively. After etching, the capacities of the SiOC-10–HF and SiOC-200–HF samples (Figure 5b) are analyzed to 457 and 648 mAh g⁻¹ for charging and 272 mAh g⁻¹ and 268 mAh g⁻¹ for discharging. The lithium insertion into the SiOC-10 sample takes place at the potential < 0.1 V with a long quasi-plateau close to the lithium plating, while the extraction starts at the potential of ~0.5 V. The shape of the intercalation/extraction curves is quite similar for all the other samples besides that of the SiOC-10 material. The lithium intercalation into the SiOC-200 sample starts at about 0.7 V vs. Li. There are also no significant charge losses related to solid electrolyte interphase (SEI) formation and very small hysteresis, i.e. there is a relatively small difference in the potential range between lithium insertion and extraction. Moreover, most of the capacity is recovered up to 1.5 V, which is beneficial regarding possible material application in complete lithium ion batteries.

Both samples, SiOC-10 and SiOC-200, do not present any porosity, which results in low amount of SEI formation and hence small capacity losses. For the etched materials the electrochemical process starts at ~1 V for SiOC-10–HF and at ~2 V for SiOC-200–HF. This electro-activity is related to a pronounced SEI formation due to the higher amount of interface of the porous HF etched samples. Correspondingly, the registered capacity losses related to the SEI formation are much higher for the samples with

higher DVB content. Following, a quasi-plateau at 0.3–0.5 V is registered. This plateau and the significant hysteresis (almost 30% of the capacity is recovered over 1.5 V) seem to be typical features of high-capacity SiOC compositions, as already reported by Wilson et al. [5]

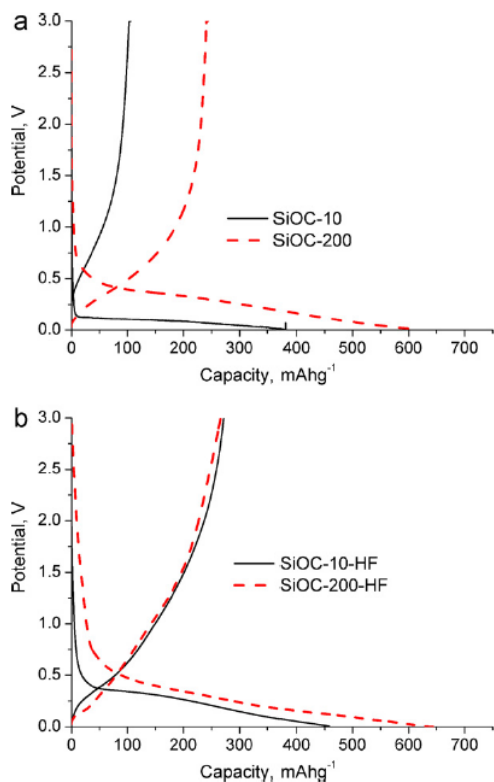


Figure 5.5. First lithium intercalation/extraction cycle for SiOC-10 and SiOC-200 electrodes (a), SiOC-10-HF and SiOC-200-HF (b). Charging/discharging rate 18 mA g⁻¹. Solid black line SiOC-10/SiOC-10-HF, dashed red line SiOC-200/SiOC-200-HF.

| Sample | C _{Insertion} (mAhg ⁻¹) | C _{Extraction} (mAhg ⁻¹) | C _{irr} (mAhg ⁻¹) | η ₁ (%) | η ₁₀ (%) | C _{discharge} / g C _{free} (mAhg ⁻¹) | x value in LiC _x |
|-------------|---|--|---|-----------------------|------------------------|--|-----------------------------------|
| SiOC-10 | 380 | 102 | 278 | 27 | 3 | 723 | 3.1 |
| SiOC-200 | 611 | 241 | 370 | 40 | 9 | 600 | 3.7 |
| SiOC-10-HF | 457 | 272 | 185 | 59 | 35 | 771 | 2.9 |
| SiOC-200-HF | 648 | 268 | 380 | 42 | 32 | 410 | 5.4 |
| Graphite | 434 | 395 | 39 | 91 | 88 | 395 | 5.9 |

Table 5.3 Capacity values and electrode efficiency of first galvanostatic lithium intercalation/de-intercalation (data from **Figure 5**). The efficiency calculated after the 10th cycle is also reported.

The extended charging/discharging behavior of all investigated samples is presented in Figure 5.6a–d. For the initial cycles a slow charging/discharging rate of 18 mA g⁻¹ was used. After 10 cycles the charging/discharging current was increased up to 36 mA g⁻¹. The comparison of electrode capacities, the irreversible losses measured during the first cycle ($C_{irr} = C_{charge} - C_{discharge}$) and electrode efficiency η is presented in Table 5.3. The efficiency, η , is calculated as the ratio of the n -cycle discharge (deintercalation) capacity to the first charge (intercalation) capacity, using the following equation:

$$\eta_n (\%) = C_{n\text{-discharge}} / C_{1\text{st-charge}} \times 100$$

This value enables an estimation of the quantity of charge captured irreversibly during the n -cycle.

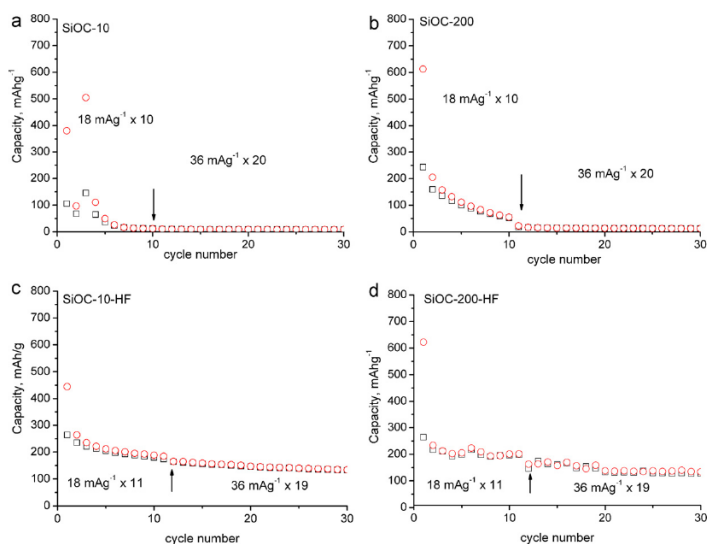


Figure 5. 6. Cycling behavior (capacity vs cycle number) of samples SiOC-10 (a), SiOC-200 (b), SiOC-10–HF (c) SiOC-200–HF (d) in two-electrode cells. The number of complete charging/discharging cycles and applied current is indicated inside each figure, i.e. 18 mA g⁻¹ × 10 means that the cell was ten times charged and discharged with 18 mA/g of active material used. Arrow indicates the cycle with increasing current, charge (squares), discharge (circle).

5.4. Discussion

In spite of the fact that the first charge capacity is higher than that of graphite, the first cycle demonstrates quite high irreversibility for all the studied materials. The first cycle efficiency ranges between 27% and 59%. Irreversibility in these materials is usually accounted for a combination of two processes: (i) for mation of poorly reversible structures similar to Li_2O_3 and (ii) to SEI formation [35]. The former should be related to the amount of oxygen present in the SiOC while the latter to the specific surface area. Accordingly, between the two dense materials, the SiOC-10 sample shows a lower efficiency (27%) as compared to that of the SiOC-200 sample (40%) with significantly lower oxygen content. The high oxygen content in SiOC based materials is considered as a source for high irreversible capacity and significant hysteresis [36, 37]. It was found that excessive oxygen works as a trap for lithium ions during the first lithium insertion [37]. On the other hand, the first cycle efficiency of the two porous oxycarbides seems to be more related to their high surface area than to the oxygen content. For these materials the lower efficiency is determined for the SiOC-200–HF sample which has lower oxygen content but a higher specific surface area and pore volume compared to that of the porous SiOC-10–HF sample. The first cycle reversible capacities recorded for the SiOC samples ranges from 102 up to 272 mAh g^{-1} . These values are between ca. 27 and 73% of the benchmark for lithium intercalation in graphite (372 mAh g^{-1}) even though the amount of carbon in these materials amounts only 14.1 and 65.4 wt%. In the literature two models have been proposed to explain the lithium storage mechanism in polymer-derived SiOC ceramics. The first one proposed by Raj's group [16] suggests that the mixed Si-C-O tetrahedra are the active sites for Li storage while the second one, proposed in the work of Fukui et al.[19] indicates the

interstitial spaces or edges between the graphene layers as the major storing sites. In order to prove these concepts we decided to perform ^{29}Si MAS solid state NMR spectroscopy on the four samples in order to learn more about the structural features of the samples. The results of the solid state NMR studies are presented in Figure 5.7 and the corresponding quantitative analysis of the various silicon sites obtained from the simulation of the spectra are reported in Table 5.4.

| Samples 1400⁰C | X (%) δ (ppm) | D₂ (%) δ (ppm) | T₃ (%) δ (ppm) | Q₄ (%) δ (ppm) |
|----------------------------------|--|--|--|--|
| SiOC-10 | 27 (-14.8) | 9 (-35.9) | 8 (72.7) | 56 (-108.8) |
| SiOC-10-HF | 61 (-11.5) | - | 2 (-69.3) | 37 (-108.6) |
| SiOC-200 | 48 (-18.4) | - | - | 52 (-107.7) |
| SiOC-200-HF | 83 (-16.7) | - | - | 17 (-107.2) |

Table 5.4. Quantitative analysis of the various silicon sites obtained from the simulation of the spectra from **Figure 5.7**.

The spectra of the two as pyrolyzed samples before HF etching show the presence of two major contributions from Q, SiO_4 , ($\delta \approx -108$ ppm) and X, SiC_4 , ($\delta \approx -16$ ppm) sites. For the low-C content SiOC-10 few mixed

T, SiO_3C , ($\delta \approx -72$ ppm) and D, SiO_2C_2 , ($\delta \approx -36$ ppm) units are also observed while for the high-C sample, SiOC-200, no mixed silicon oxycarbide units are revealed by this technique. These results agree well with the known high temperature phase separation of the silicon oxycarbide network into SiO_4 -rich and SiC_4 -rich clusters.

Indeed, our samples were pyrolyzed up to 1400 °C for 1 h and, at this temperature; we expect that this type of partitioning of the SiOC matrix has taken place. The NMR spectra of the HF-etched samples show the expected decrease of the SiO_4 units and a corresponding relative increase of the SiC_4 sites. Both samples do not contain mixed Si-O-C units in significant amounts. Based on the NMR data we believe that, in our SiOC samples pyrolyzed at 1400 °C, storage of Li atoms in mixed silicon oxycarbide tetrahedral sites should not play a major role since the samples which contain the highest amount of mixed bonded Si units is the one which shows the smallest first cycle reversible capacity of 102 mAh g^{-1} and the samples which show higher reversible capacities between 241 and 272 mAh g^{-1} contain negligible amounts of mixed tetrahedral SiOC units. Following the suggestion of Fukui et al [19], the reversible capacity measured during the first discharge has been ascribed to the free carbon phase and the values have been normalized to the amount of free carbon present in the SiOC ceramics.

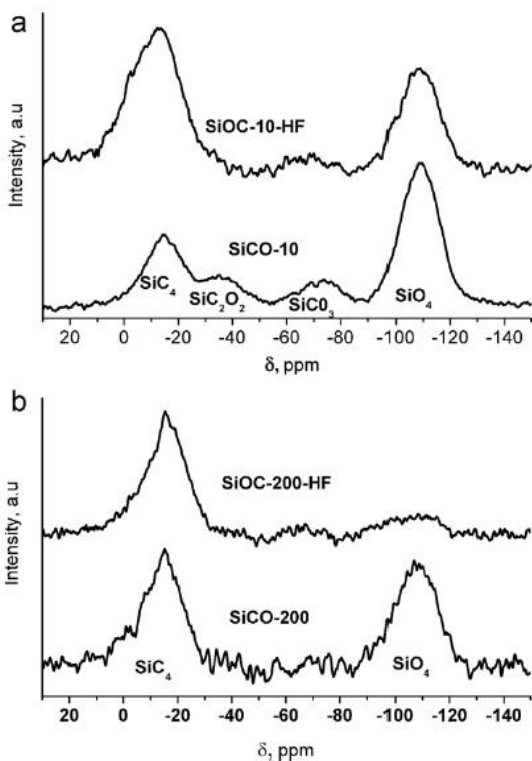


Figure 5.7. ^{29}Si MAS NMR spectra of the investigated SiOC samples.

The results, reported in the last two columns of Table 5.3 reveal that the carbon phase present in the non-etched silicon oxycarbide matrix can reversibly store almost double the amount of lithium compared to that of commercial graphite, i.e. up to 723 mAh g^{-1} compared to 371 mAh g^{-1} . The same values can be used to get the x value of the LiC_x formula. Accordingly, for commercial carbon anode the x value is 6 (LiC_6) while for silicon

oxycarbide glasses x can go down to ≈ 3 . The higher amount of Li atoms that can be reversibly stored in the in situ formed carbon phase in the SiOC matrix could be related to the nano-sized dimensions of the carbon clusters which can store lithium not only in the interstitial spaces of the graphite-like sp^2 -carbon structure but also at the edges of the graphene layers. After etching the amount of lithium which can be stored in the free carbon phase remains un-changed for the SiOC-10 composition, with an x value around 3, LiC_3 , while for the C-rich sample, SiOC-200, it increases from $x = 3.7$ in the non-etched sample up to 5.4 after etching approaching almost the amount of Li stored by commercial graphite, $x = 6$. The reason why for the low-C SiOC the etching of the silica phase does not change the storage capacity of free carbon while for the high-C sample it does is not clear at the moment. It is known that the HF etching of SiOC not only dissolves silica but can also modify the structure, for example releasing residual stresses [23] or by intercalating F atoms into the graphene layers. These modifications could significantly influence the Li storage and it is likely that the SiOC-200 sample could be more seriously affected by the etching procedure with HF than it is the case for the SiOC-10 ceramic containing much less free carbon. Another interesting feature of the studied samples emerges from the analysis of the cycling behavior. Etched porous SiOC samples show much better efficiency of about 30% after 10 cycles compared to the dense, un-etched SiOCs. The best first and tenth cycle efficiency is registered for SiOC-10–HF. It should also be noted that cycling has a detrimental effect on the Li-insertion of both dense samples. The charging/discharging capacities vanish and the efficiency drops to almost zero. The good cycling behavior of the porous SiOC compared to the dense material could be due to the different stiffness of the two types of materials. Dense SiOC materials have a high modulus silicon oxycarbide matrix built up by Si-O and Si-C bonds in which the

carbon phase is embedded [38]. Even if the volume change of the graphite-like clusters during the lithiation/delithiation process is known to be small (about 6% [39]) such a high stiffness network could constrain the free expansion/contraction of the carbon nanocrystals leading to a rapid failure of the storage capacity. On the contrary, in the porous samples the silica phase has been partially removed leading to a less stiff and more compliant structure which improves the cycling stability by increasing tolerance to stress cracking.

5.5. Conclusions

Dense and porous polymer-derived SiOC samples with different amount of carbon have been processed through pyrolysis at 1400 °C of a linear polysiloxane, PMHS, cross linked with DVB via hydrosilylation reactions. The dense SiOCs show a phase separated nanostructure consisting of SiO₂-rich clusters, nanocrystalline SiC and nanocrystalline carbon phase. The corresponding porous materials were obtained by etching the dense SiOC with 20% aqueous HF solution. The SiOC materials show a high first charge capacity between 380 and 648 mAh g⁻¹ followed by significantly lower discharge capacities between 102 and 272 mAh g⁻¹. The high first cycle irreversibility found for the dense SiOC has been associated to different the oxygen content of the two compositions while for the porous ones the Li charge loss seems more related to the pore volume and the specific surface area of the two samples. Interestingly, considering that the active phase for Li storage would be the free carbon of the SiOC ceramics, the first cycle reversible capacity, normalized to the amount of this phase, shows that the carbon phase present in the silicon oxycarbide structure can reversibly store almost double the amount of lithium as compared to

commercial graphite, i.e. up to 723 mAh g^{-1} . This higher amount of Li atoms that can be stored reversibly in the present carbon phase is related to the nano-sized dimensions of the carbon clusters which can store lithium not only in the interstitial spaces of the sheet-like carbon structure but also at the edges of the graphene layers. Finally the porous samples, being more compliant show a stable electrochemical response up to 30 cycles while for the dense materials the charging/discharging capacities vanish and the efficiency drops to almost zero already after 10 cycles.

References

- [1] N. Takami, A. Satoh, M. Hara and T. Ohsaki, "Structural and kinetic characterization of lithium intercalation into carbon anodes for secondary lithium batteries", *J. Electrochem. Soc.* 142 (1995) 371–9.
- [2] J.O. Besenhard, M. Winter, J. Yang and W. Biberacher, "Filming mechanism of lithium–carbon anodes in organic and inorganic electrolytes", *J. Power Sources*, 54 (1995) 228–31.
- [3] W. Xing, A.M. Wilson, K. Eguchi, G. Zank and J.R. Dahn, "Pyrolyzed polysiloxanes for use as anode materials in lithium-ion batteries", *J. Electrochem. Soc.* 144 (1997) 2410-6.
- [4] A.M.Wilson, J.N. Reimers, E.W. Fuller, J.R. Dahn and "Lithium insertion in pyrolysed siloxane polymers" *Solid State Ionics*, 74 (1994)249–54.
- [5] A.M. Wilson, G. Zank, K. Eguchi, W. Xing and J.R. Dahn, "Pyrolysed silicon-containing polymers as high capacity anodes for lithium-ion batteries", *J. Power Sources*, 68 (1997) 195–200.
- [6] J.R. Dahn, A.M. Wilson, W. Xing and G. Zank, inventors; Dow Corning Corp., assignee. "Electrodes for lithium ion batteries using polysilanes" United States Patent US 6306541(B1); 23 October 2001.
- [7] J.R. Dahn, K. Eguchi, A.M. Wilson, W. Xing and G. Zank, inventors; Dow Corning Corp., assignee. "Electrodes for lithium ion batteries using polysiloxanes" United States Patent US 5824280(A); 20 October 1998.
- [8] P.Kroll, private communication.
- [9] R. Kolb, C. Fasel, V. Liebau-Kunzmann and R. Riedel, "SiCN/C–ceramic composite as anode material for lithium ion batteries", *J. Eur. Ceram. Soc.* 26 (2006) 3903–8.

-
- [10] M. Graczyk-Zajac, C. Fasel, R. Riedel and “Polymer-derived-SiCN ceramic/graphite composite as anode material with enhanced rate capability for lithium ion batteries” *J. Power Sources*, 196 (2011) 6412–8.
- [11] J.R. Dahn, A.M. Wilson, W. Xing and G. Zank, inventors; Dow Corning Corp., assignee. “Electrodes for lithium ion batteries using polysilazanes ceramic with lithium”, United States Patent US 5631106(A); 20 May 1997.
- [12] M. Graczyk-Zajac, G. Mera, J. Kaspar and R. Riedel, “Electrochemical studies of carbon-rich polymer-derived SiCN ceramics as anode materials for lithium-ion batteries”, *J. Eur. Ceram. Soc.* 30(2010) 3235–43.
- [13] J. Kaspar, G. Mera, A. Nowak, M. Graczyk-Zajac and R. Riedel “Electrochemical study of lithium insertion into carbon-rich polymer-derived SiCN ceramics” *Electrochim. Acta*, 56 (2010) 174–82.
- [14] L.J. Ning, Y.P. Wu, L.Z. Wang, S.B. Fang and R. Holze, “Carbon anode materials from polysiloxanes for lithium ion batteries”, *J. Solid State Electrochem.* 9 (2005) 520–3.
- [15] D. Ahn and R. Raj, “Thermodynamic measurements pertaining to the hysteretic intercalation of lithium in polymer-derived silicon oxycarbide”, *J. Power Sources*, 195 (2010)3900–6.
- [16] P.E. Sanchez-Jimenez and R. Raj, “Lithium insertion in polymer-derived silicon oxycarbide ceramics”, *J. Am. Ceram. Soc.* 93 (2010) 1127–35.
- [17] D. Ahn and R. Raj “Cyclic stability and C-rate performance of amorphous silicon and carbon based anodes for electrochemical storage of lithium”, *J. Power Sources*, 196 (2011) 2179–86.
- [18] H. Fukui, H. Ohsuka, T. Hino and K. Kanamura, “Preparation of microporous Si–O–C composite material and its lithium storage capability”, *Chem. Lett.* 38 (2009) 86–7.

-
- [19] H. Fukui, H. Ohsuka, T. Hino and K. Kanamura, "A Si–O–C composite anode: high capability and proposed mechanism of lithium storage associated with microstructural characteristics", *ACS App. Mater. Interfaces*, 2 (2010) 998–1008.
- [20] M. Graczyk-Zajac, L. Toma, C. Fasel and R. Riedel, "Carbon-rich SiOC anodes for lithium-ion batteries: Part I. Influence of material UV-pre-treatment on high power properties", *Solid States Ionics*, <http://dx.doi.org/10.1016/j.ssi.2011.12.007>, in press.
- [21] J. Kaspar, M. Graczyk-Zajac and R. Riedel, "Carbon-rich SiOC anodes for lithium ion batteries. Part II. Role of thermal crosslinking", *Solid State Ionics*, <http://dx.doi.org/10.1016/j.ssi.2012.01.026>, in press.
- [22] R. Pena-Alonso, G.D. Soraru and R. Raj, "Preparation of ultrathin-walled carbon-based nanoporous structures by etching pseudo-amorphous silicon oxycarbide ceramics", *J. Am. Ceram. Soc.* 89 (2006) 2473–80.
- [23] R. Pena-Alonso, G. Mariotto, C. Gervais, F. Babonneau and G.D. Soraru, "New insights on the high temperature nanostructure evolution of SiOC and B-doped SiBOC polymer-derived glasses", *Chem. Mater.* 19 (2007) 5694–702.
- [24] P. Dibandjo, S. Diré, F. Babonneau and G.D. Soraru, "Influence of the polymer architecture on the high temperature behavior of SiCO glasses: a comparison between linear- and cyclic-derived precursors", *J. NonCryst. Solids*, 356 (2010)132–40.
- [25] G.D. Soraru, R. Pena-Alonso and H.J. Kleebe, "The effect of annealing at 1400⁰C on the structural evolution of porous C-rich silicon (boron) oxycarbide glass", *J. Eur. Ceram. Soc.* 32 (2012) 1751–7.
- [26] D. Massiot, F. Fayon, M. Capron, I. King, S. Le Calvé, B. Alonso et al. "Modelling one- and two-dimensional solid-state NMR spectra" *Magn. Reson. Chem.* 40 (2002) 70–6.

-
- [27] G.D. Soraru, G. D'Andrea, R. Camprostrini, F. Babonneau and G. Mariotto, "Structural characterization and high-temperature behavior of silicon oxycarbide glasses prepared from sol-gel precursors containing Si-H bonds" *J. Am. Ceram. Soc.* 78 (1995) 379-87.
- [28] H. Bréquel, J. Parmentier, S. Walter, R. Badheka, G. Trimmel, S. Masse et al. "Systematic structural characterization of the high-temperature behavior of nearly stoichiometric silicon oxycarbide glasses", *Chem. Mater.* 16 (2004) 2585-98.
- [29] A. Hamwi, "Fluorine reactivity with graphite and fullerenes. Fluoride derivatives and some practical electrochemical applications", *J. Phys. Chem. Solids*, 57 (1996) 677-88.
- [30] P.C. Eklund, J.M. Holden and R.A. Jishi "Vibrational modes of carbon nanotubes; spectroscopy and theory" *Carbon*, 33 (1999) 959-72.
- [31] F. Tuinstra and J.L. Koenig, "Raman spectrum of graphite," *J. Chem. Phys.* 53 (1970) 1126-30.
- [32] J. Rouquerol, D. Avnir, C.W. Fairbridge, D.H. Everett, J.H. Haynes, N. Pernicone et al. "Recommendations for the characterization of porous solids", *Pure Appl. Chem.* 66 (1994) 1739-58.
- [33] K.S.W. Sing, D.H. Everett, J.H. Haynes, R.A.W. Hall, L. Moscou, J. Rouquerol et al. "Reporting physisorption data for gas/solid systems with special reference to the determination of surface area and porosity" *Pure Appl. Chem.* 57 (1985) 603-19.
- [34] H.J. Kleebe and Y.D. Blum "SiOC ceramic with excess free carbon", *J. Eur. Ceram. Soc.* 28 (2008) 1037-42.
- [35] M. Winter, K.C. Moeller and J.O. Besenhard, "Carbonaceous and graphitic anodes" In: Nazri FA, Pistoia G, Nazri G-A, Pistoia G, editors. *Lithium batteries. Science and technology.* Kluwer Academic Publisher; 2004. p. 144-80.

-
- [36] A.M. Wilson, W. Xing, G. Zank, B. Yates and J.R. Dahn, "Pyrolysed pitch-polysilane blends for use as anode materials in lithium ion batteries II: the effect of oxygen" *Solid State Ionics*, 100 (1997) 259–66.
- [37] D. Larcher, C. Mudalige, A.E. George, V. Porter, M. Gharghoury and J.R. Dahn, "Si-containing disordered carbons prepared by pyrolysis of pitch/polysilane blends: effect of oxygen and sulfur", *Solid State Ionics* 122, (1999) 71–83.
- [38] G.D. Sorarù, E. Dallapiccola and G. D'Andrea, "Mechanical characterization of sol-gel derived silicon oxycarbide glasses", *J. Am. Ceram. Soc.* 79 (1996) 2074–80.
- [39] M. Winter and J.O., Besenhard, "Electrochemical lithiation of tin and tin-based intermetallics and composites", *Electrochim. Acta*, 45 (1999) 31.
-

Chapter 6. Thesis Conclusions

In the present thesis, SiOC ceramics were investigated as anode materials for lithium storage applications. The motivation of this thesis work was to evaluate the electrochemical properties of the SiOC ceramics in terms of their capacity and cyclability and understand in detail the lithium intercalation and storage mechanism.

Silicon oxycarbide glasses of controlled compositions have been synthesized from polymer precursors using different crosslinking approaches, pyrolysis atmospheres and pyrolysis temperatures. The obtained final ceramics were structurally characterized by NMR, XRD, elemental analysis (EA), Raman spectra, EPR spectroscopy, TEM, N₂ adsorption techniques and electrochemical characterization by means of galvanostatic charging/discharging and cyclic voltammetry experiments.

The present investigation has unveiled that the promising electrochemical properties of SiOC ceramics were connected with their complex amorphous nanostructure comprising SiC_xO_{4-x} (0 ≤ x ≤ 4) mixed SiOC units along with a network of disordered free carbon. Pyrolysis temperature also has an important role in controlling the structure formation and corresponding lithium storage properties. The increase of the pyrolysis temperature (≥1000 °C) led to the separation of SiOC in to O-rich and C-rich species with consumption of mixed SiOC units. This phase changes results in a poor electrochemical performance. The best electrochemical properties are observed for samples pyrolysed at 1000 °C. It was found that lithium storage capacity faded with increasing pyrolysis temperature. The Li storage

properties of SiOC ceramics were related to: (1) mixed SiOC composition (2) amount and nature of free carbon content (3) thermodynamic stability of the SiOC structure (4) role of defects in the Li storage properties. SiOC anodes revealed the behavior of a composite material: the silicon oxycarbide phase led to high first cycle insertion capacity up to 1300 mAh g^{-1} while the reversibility and cyclability came primarily from the free C phase. The best electrochemical performance in terms of excellent cyclability and rate capability has been measured for the SiOC anode materials with 51wt% of amorphous phase and 49wt% of free carbon (PD2 1000°C sample). This material is able to deliver up to 200 mAh g^{-1} of charge at a 2C rate and, after more than 130 cycles it recovers its initial capacity if charged at a low rate (C/20).

The pyrolysis atmosphere was also found to have a key role in improving the lithium storage properties. C-rich samples were pyrolysed in argon (Ar) and in argon/hydrogen (Ar/H₂) atmosphere. ESR study revealed that the presence of hydrogen in the pyrolysis atmosphere reduces the concentration of C-dangling bonds in the oxycarbide structure and it helps to improve the lithium storage properties of SiOC samples. C-radicals may deactivate some potential Li storage sites bringing about fading of electrochemical performance.

The role of porosity was investigated by making a comparative study with dense and porous ceramics as lithium host material. The porous ceramics were created by HF etching of carbon rich SiOC ceramics. Removal of SiO₂ with HF etching leaves a porous network and this structure was able to host larger amount of lithium than the dense SiOC ceramics. Also during extended cycling investigation porous SiOC networks with surface area of $640 \text{ m}^2 \text{ g}^{-1}$ delivered higher capacity and better stability compared to the dense analogues.

As a summary, the main outcomes of the present thesis points out that SiOC ceramics are promising anode materials for Li-ion battery applications. Structural composition and pyrolysis conditions are important parameters determining lithium storage properties. In order to reach an excellent electrochemical performance, the final composition should be controlled to optimize the ratio between SiOC phase and free carbon networks.

Future Outlook

The present thesis reports lithium storage properties of SiOC ceramics of different structural and electrochemical features. The results of this proposed research activity explains different Li intercalation mechanisms in SiOC anodes.

Detailed structural analysis of anodes after lithiation with the help of techniques such as ^7Li NMR, ^{29}Si MAS NMR etc. may shed some more light in to understanding of electrochemically active sites. A clear understanding of the intercalation mechanism is necessary to rectify the draw backs of SiOC anodes. It will be also interesting to have a study of mechanical properties of these ceramics and correlating with electrochemical properties to know the response of structural networks towards repeated volume changes during repeated lithiation.

It is already clear from our preliminary experiments that changing pyrolysis atmosphere to a hydrogen containing atmosphere have a clear advantage by improving the specific capacity and also it offer an improved cycling stability. More detailed studies focusing on role of defects/dangling bonds in different SiOC compositions are important to realize the commercial applications of these electrodes.

The role of porosity in supporting repeated lithiation can be investigated in more detail by preparing Si-O-C networks of controlled porosity using aerogel approach and applying this as anode materials for lithium storage applications. The porosity is believed to help in adapting the volume changes during lithium intake maintaining the structural stability to have an extended cycling stability and longer life time.

Acknowledgements

Foremost, I would like to express my sincere gratitude to my advisor Prof. Gian Domenico Soraru for his continuous support during my PhD program. His patience, constant motivation and encouragements had helped me to make progress in my research career. His guidance helped me in all the time of research and writing of this thesis.

Thanks to Dr. P.R. Aravind for his encouragements and advices to develop my research career. It was a great pleasure for me to work with him. I would like to extend my thanks to Prof. Claudio Dellavolpe and Dr. Caterina Zanella for helping me to start my initial experiments on electrochemistry. I will keep on record my sincere thanks to all the Professors and colleagues in Ceramic laboratory for all their help and support during my stay.

I would like to thank Prof. R. Riedel for offering me a chance to work as a part of his research group in TU Darmstadt. The period which I spend in Darmstadt had helped me to improve my experimental skills and also got the chance to work with different scientific experts. I would like to express my sincere thanks to Dr. Magdalena Graczyk-Zajack for her valuable advice during my entire PhD program. I am grateful to acknowledge her care and support to carry out different experiments on Li-ion batteries and also to understand the general concepts of electrochemistry. I would like to express my sincere thanks to my friends and colleagues in Technical University Darmstadt for their help and consideration during my stay in Germany.

I would like to acknowledge Prof. Gino Mariotto, University of Verona for the Raman spectra measurements and Dr. Emanuela Callone, University of Trento for the NMR and EPR measurements.

I would like to express my sincere thanks to my friends in Trento, especially, Kiran, Pradnyesh, Anshu, Tinku, Jinu, Rahul, Sajid, Meera, Rajesh, Shine, Van lam, Dr. John Downs, Emanuele, Michele and so on for making my 4 year stay wonderful with lots of fun and adventures.

Finally, I am especially grateful to my family for their wholehearted support and encouragement during my entire life to achieve my dreams.

Without the help and assistance from all these special people, this thesis would not have been completed.

Curriculum Vitae

Educational Background

PhD: Department of Industrial Engineering, University of Trento, Trento, Italy (2009-2013)

Dissertation: "Study of Silicon Oxycarbide as Anodes for Li-ion Batteries"

MSc. General Chemistry, Mahatma Gandhi University, Kottayam, India (2006-2008)

Thesis: "Study of Oscillator strength of Lycopene and Beta Carotene"

BSc. General Chemistry, Calicut University, Calicut, India (2003-2006)

Research Experience

Early Stage Researcher (ESR) in Marie Curie Research Training Network on Tailored Multifunctional Polymer-Derived Nano ceramics (PolyCerNet), Trento, Italy (July 2009-December 2009)

- Structural characterisation of porous silicon oxycarbide (SiOC) glass ceramics

SFB Research Fellow, FB Material- und Geowissenschaften, Technical University Darmstadt, Darmstadt Germany, (April 2011- June 2011)

-
- Electrochemical characterization of polymer derived ceramic anodes for lithium ion batteries

SFB Research Fellow, FB Material- und Geowissenschaften, Technical University Darmstadt, Darmstadt Germany, (October 2012- December 2012)

- Electrochemical characterization of polymer derived ceramic anodes for lithium ion batteries

Publications

- P. Dibandjo, M. Graczyk-Zajac, R. Riedel, V.S. Pradeep, G. D. Soraru, "Lithium Insertion into Dense and Porous Carbon-Rich Polymer-Derived SiOC Ceramics", *J. Eur. Ceramic Soc.* 32(10) (2012) 2495–2503.
- V.S. Pradeep, M. Graczyk-Zajac, M. Wilamowska, R. Riedel, G.D. Soraru "Influence of Pyrolysis Atmosphere on the Lithium Storage Properties of Carbon-rich Polymer Derived SiOC Ceramic Anodes" Article accepted in *Solid State Ionics*. DOI: 10.1016/j.ssi.2013.08.043
- V.S. Pradeep, M. Graczyk-Zajac, R. Riedel, G.D. Soraru "New insights in to the lithium intercalation mechanism of polymer derives SiOC anode materials" Article under communication with *Electrochimica Acta*-2013.
- N. Kumar, P. Bettotti, S. Gennaro, V.S. Pradeep, G.D. Soraru "High quality free-standing double layer for layer transfer process on medium doped n-type silicon" Article under communication

Conferences

- V.S. Pradeep, M. Graczyk-Zajac, R. Riedel, G.D. Soraru, "Searching insights in to the lithium intercalation mechanism of SiOC anodes". Oral presentation

in 10th CMCEE conference 2012, May20, Dresden, Germany.

- V.S. Pradeep, G.D. Soraru, M. Graczyk-Zajac, R. Riedel" Influence of Pyrolysis Atmosphere on the Lithium Storage Properties of Carbon-rich Polymer Derived SiOC Ceramic Anodes ", Poster presentation in the 19th Solid State Ionics Conference, June 02-08, 2013, Kyoto, Japan.
- M. Wilamowska, V. S. Pradeep, M. Graczyk-Zajac, R. Riedel, G. D. Soraru, " Silicon Oxycarbide (SiOC) Ceramic Materials as Anodes for Lithium Ion Batteries", Smart Energy Conversion and Storage, IV Polish forum, 1-4 October, Krynica, Poland.
- V.S. Pradeep, G.D. Soraru, M. Graczyk-Zajac, R. Riedel"Polymer derived SiOC ceramic as anode material for lithium-ion batteries", Poster presentation in the 12th European Ceramic Society Conference-June 19-23, 2011, Stockholm, Sweden.
- V.S. Pradeep, G.D. Soraru, M. Graczyk-Zajac, R. Riedel"New insights into the Li-Storage mechanism of polymer derived SiOC anodes", Poster presentation in TICME - 2011,Trento Innovation Conferences on Materials Engineering, December 12-14,Trento, Italy.
- Different Summer schools and workshops organized by University of Trento